

2023

Gnetin C for chemoprevention and therapy of prostate cancer

Gisella Campanelli
Long Island University

Follow this and additional works at: https://digitalcommons.liu.edu/brooklyn_fulltext_dis



Part of the [Pharmacy and Pharmaceutical Sciences Commons](#)

Recommended Citation

Campanelli, Gisella, "Gnetin C for chemoprevention and therapy of prostate cancer" (2023). *Selected Full-Text Dissertations 2020-*. 6.

https://digitalcommons.liu.edu/brooklyn_fulltext_dis/6

This Dissertation is brought to you for free and open access by the LIU Brooklyn at Digital Commons @ LIU. It has been accepted for inclusion in Selected Full-Text Dissertations 2020- by an authorized administrator of Digital Commons @ LIU. For more information, please contact natalia.tomlin@liu.edu.

GNETIN C FOR CHEMOPREVENTION AND THERAPY OF PROSTATE CANCER

A DISSERTATION SUBMITTED
IN PARTIAL FULFILLMENT OF THE REQUIREMENTS
FOR THE DEGREE OF
DOCTOR OF PHILOSOPHY
WITH SPECIALIZATION IN PHARMACEUTICAL SCIENCES
(PHARMACOLOGY AND TOXICOLOGY)
TO THE FACULTY OF THE ARNOLD & MARIE SCHWARTZ COLLEGE
OF PHARMACY AND HEALTH SCIENCES
LONG ISLAND UNIVERSITY
BROOKLYN, NEW YORK
DECEMBER 16TH 2022
BY
GISELLA CAMPANELLI

SPONSORING COMMITTEE

Avinash Kumar, Ph.D., Co-Chair

Anait S. Levenson, M.D., Ph.D., Co-Chair

Eun Jung Park, Ph.D., Committee Member

Grazia Stagni, Ph.D., Committee Member

Yan Dong, Ph.D., External Committee Member

David R. Taft, Ph.D., Division Chair

Joseph J. Bova, M.S., Vice Dean of Academic Affairs

In loving memory of my father

PREFACE

The concept for this dissertation was the vision and intellectual property of Dr. Anait S. Levenson. Our laboratory has had a long history investigating naturally derived stilbene compounds as therapeutic agents against prostate cancer. While resveratrol, pterostilbene and other similar analogs have been the focus of earlier studies, today, the laboratory has directed its attention towards a compound known as Gnetin C, a resveratrol dimer.

This dissertation builds upon preceding *in vitro* experiments, which demonstrated that Gnetin C has superior pharmacodynamic and pharmacokinetic properties compared to resveratrol and pterostilbene, thus justifying further investigation. For this research, we delved deeper by revealing the pharmacological activity of Gnetin C in diverse *in vivo* murine models of prostate cancer at varying stages of the disease. The outcome of this study is expected to provide a better understanding of the potential of Gnetin C as an anti-cancer agent for the prevention and treatment of prostate cancer: a disease which remains highly prevalent amongst men worldwide.

With minor exceptions, all data presented in this dissertation was obtained, analyzed, and interpreted by myself. Wherever data was collected as a collaborative effort, the respective lab members were duly credited in figure captions.

All animal protocols were approved in advance by the Institutional Animal Care and Use Committee (IACUC) at Long Island University in accordance with the NIH Guidelines for the Care and Use of Laboratory Animals.

This dissertation has been supported by NCI/NIH #R15CA216970 grant awarded to Dr. AS Levenson.

ACKNOWLEDGEMENTS

For their guidance, encouragement, and relentless support, I wish to express my heartfelt gratitude to my co-advisors, Dr. Avinash Kumar and Dr. Anait S. Levenson. I cannot thank them enough for having given me this invaluable learning opportunity and promising start to a new career. The time and effort that they invested in me will not be forgotten.

To my fellow laboratory team members, Prashanth Parupathi, Lakshmisirisha Devarakonda, Ameer Adhvaryu, Anand Paur, and Rabab Al Deabel, I extend my deepest thanks for their assistance, collaboration, and enduring friendship.

I wish to offer my sincere thanks to Dr. Grazia Stagni for her guidance and support in helping me achieve my pharmacokinetic goals for this dissertation. I am especially grateful to Dr. Eun-Jung Park for her professional advice, words of encouragement, and unwavering generosity. And, I offer my utmost gratitude to Dr. Yan Dong, from Tulane University, for her expertise and unique insight into prostate cancer. Furthermore, I wish to thank Dr. Stagni, Dr. Park, and Dr. Dong for taking part in my dissertation as much valued committee members.

I wish to acknowledge Dr. Qing Cai, Dr. Joseph Morin, Ms. Rena Azayev, and Dr. Bhaskar Das for their assistance with our studies. I also extend my deepest thanks to Ms. Aruna Kissoon, Dr. Christopher Surratt, Dr. David R. Taft, and Mr. Steve Chin for their administrative support throughout my time at Long Island University.

Lastly, but by no means least, I wish to thank my family and friends for their loving support. I offer a special word of thanks to my father, Vincenzo Campanelli, for teaching me that empowerment comes from learning, hard work, and self-reliance. To the man that I owe all that I have in this life, I am more grateful to you than you will ever know.

ABSTRACT

Prostate cancer is common among aging men. Despite current management, it continues to be associated with a high mortality rate. A need, therefore, exists for improved treatment approaches that target every stage of the disease. In this study, we investigated the efficacy of Gnetin C, a resveratrol dimer found abundantly in melinjo (*Gnetum gnemon*) seeds, across three different treatment modalities. The first involved a Gnetin C-supplemented diet as a chemopreventive strategy in a high-risk transgenic mouse model which overexpresses MTA1 on a background of Pten heterozygosity ($R26^{MTA1}; Pten^{+/f}$). The second involved the administration of Gnetin C by intraperitoneal (i.p.) injection as a therapeutic strategy in a more aggressive transgenic mouse model which overexpresses MTA1 on a background of Pten loss ($R26^{MTA1}; Pten^{ff}$). The third involved i.p. Gnetin C administered as monotherapy and combination therapy (with enzalutamide) in a xenograft-generated model for highly aggressive castrate-resistant prostate cancer. Our chemopreventive studies demonstrated that mice fed Gnetin C diets exhibited significantly less PIN foci, cellular proliferation, angiogenesis, and systemic inflammation. Gnetin C-fed mice also exhibited reduced expression of MTA1 with an upregulation of PTEN. We found that mice injected with Gnetin C as a therapeutic strategy exhibited favorable histopathology with fewer PIN foci, reduced proliferation and angiogenesis, and an increase in apoptosis. Serum from these mice showed a reduction in pro-inflammatory cytokines, and prostate tissue expressed less MTA1. The CRPC xenograft study demonstrated that Gnetin C treatment was associated with favorable histopathology, reduced expression of MTA1, full-length AR, and truncated AR-V7. Results also showed that combination with enzalutamide could offer benefits over monotherapy. Finally, from our pharmacokinetic studies of Gnetin C, we were able to estimate parameters, such as systemic exposure or AUC (809 mcg.h/L), half-life (1.7 h), and clearance (30.9 L/h/kg). Altogether, this data provides evidence for the use of Gnetin C as a novel anticancer agent that can target different stages of prostate cancer in different modes of administration.

TABLE OF CONTENTS

PREFACE.....	iii
ACKNOWLEDGEMENTS	iv
ABSTRACT	v
LIST OF FIGURES.....	viii
LIST OF TABLES	x
CHAPTER I. INTRODUCTION	- 11 -
<i>The Prostate</i>	- 11 -
<i>Prostate Cancer</i>	- 12 -
<i>Key Molecular Players of Prostate Cancer</i>	- 14 -
<i>Pharmacological Inhibition of Prostate Cancer</i>	- 17 -
<i>Prostate Cancer Cell Lines</i>	- 25 -
<i>Preclinical Animal Models of Prostate Cancer</i>	- 26 -
<i>Pharmacokinetic Profiling</i>	- 29 -
CHAPTER II. RESEARCH GOALS.....	- 32 -
<i>The Knowledge Gap</i>	- 32 -
<i>Rationale and Justification</i>	- 33 -
<i>Hypothesis</i>	- 34 -
<i>Specific Research Aims</i>	- 36 -
CHAPTER III. MATERIALS AND METHODS.....	- 37 -
<i>Treatment Compounds</i>	- 37 -
<i>In Vitro Studies</i>	- 37 -
(i) Cell Culture	- 37 -
(ii) Generation of Stable 22Rv1 Cells with MTA1 Knockdown	- 38 -
(iii) Generation of Stable 22Rv1 Cells Tagged with Luciferase.....	- 39 -
(iv) Cell Viability Assay	- 40 -
(v) Treatments (for protein and RNA isolation).....	- 41 -
<i>In Vivo Studies</i>	- 42 -
(i) Generation of Transgenic Prostate-Specific MTA1 knock-in Mice	- 42 -
(ii) Generation of Transgenic Prostate-Specific Pten Knockdown Mice	- 43 -
(iii) Genotyping	- 44 -
(iv) Experiment Design – Chemoprevention Study	- 45 -
(v) Experiment Design – Chemotherapeutic Study	- 47 -
(vi) Generation of Subcutaneous Xenografts.....	- 48 -

(vii) Experiment Design – CRPC Study	- 49 -
<i>Western Blot Analysis</i>	- 50 -
<i>qRT-PCR</i>	- 54 -
<i>Immunohistochemistry (IHC)</i>	- 56 -
<i>ELISA (Enzyme-Linked immunosorbent Assay)</i>	- 58 -
<i>Pharmacokinetic Studies</i>	- 59 -
<i>Statistical Analysis</i>	- 62 -
CHAPTER IV. RESULTS	- 63 -
<i>Preliminary In Vitro Investigations</i>	- 63 -
<i>Aim 1: Gnetin C as a Chemopreventive Agent in High-Risk PCa Model</i>	- 67 -
<i>Aim 2: Gnetin C as a Therapeutic Agent in Advanced PCa Model</i>	- 78 -
<i>Aim 3: Gnetin C as a Therapeutic Agent in a CRPC Model</i>	- 85 -
<i>Aim 4: Gnetin C – Pharmacokinetic Single-Dose Study</i>	- 107 -
CHAPTER V. DISCUSSION AND CONCLUSIONS	- 114 -
<i>Dissertation Findings</i>	- 114 -
<i>Limitations</i>	- 119 -
<i>Future Direction</i>	- 119 -
<i>Closing Statement</i>	- 121 -
CHAPTER VII. REFERENCES	- 123 -
CHAPTER VIII. APPENDICES	- 131 -
<i>APPENDIX A: Publications</i>	- 131 -
<i>APPENDIX B: Posters and Presentations</i>	- 132 -

LIST OF FIGURES

Figure 1. Schematic representation of the male urogenital system.....	11 -
Figure 2. H&E staining of normal human prostate tissue.....	11 -
Figure 3. Schematic representation of the progression of prostate cancer.	13 -
Figure 4. Schematic diagram showing the role of MTA1 in prostate cancer.	15 -
Figure 5. Schematic presentation of AR-signaling in PCa.....	16 -
Figure 6. Schematic representation of prostate cancer timeline.....	17 -
Figure 7. Polyphenolic chemical structure of resveratrol and pterostilbene.....	19 -
Figure 8. Chemical structure of Gnetin C, a dimer of trans-resveratrol.	20 -
Figure 9. Representative western blot comparing Gnetin C, Res, Pter, and antiandrogens.....	21 -
Figure 10. Chemical structure of enzalutamide.....	22 -
Figure 11. Mechanism of action of enzalutamide.....	22 -
Figure 12. Gnetin C IC ₅₀ value compared to enzalutamide	23 -
Figure 13. Western blot Gnetin C monotherapy and Gnetin C + enzalutamide combination.....	25 -
Figure 14. Schematic representation of ADME.....	30 -
Figure 15. Breeding strategy for transgenic mice.....	43 -
Figure 16. Experimental design for chemopreventive study in high-risk model of PCa.	46 -
Figure 17. Experimental design for therapeutic study in high-grade PIN model of PCa.....	48 -
Figure 18. Gel-membrane transfer sandwich	52 -
Figure 19. MTT assays in PC3 and 22Rv1 after treating with Res, Pter, and Gnetin C	64 -
Figure 20. MTT assays in PC3, PC3M, and 22Rv1 after treating with Gnetin C, D1 and D2.....	66 -
Figure 21. Experimental design for investigating Gnetin C chemoprevention	68 -
Figure 22. Effects of diets on food intake and body weight.....	69 -
Figure 23. Representative images of UGS of mice from each diet group.	70 -
Figure 24. Representative H&E and IHC staining.....	72 -
Figure 25. Quantitation for H&E and IHC	73 -
Figure 26. Western blot of MTA1 and PTEN protein levels in prostate tissues	75 -
Figure 27. Effects of diets on the levels of circulating inflammatory cytokines	77 -
Figure 28. Experimental design for investigating Gnetin C therapy.....	79 -
Figure 29. Representative H&E and IHC staining.....	81 -
Figure 30. Quantitation of H&E and IHC	82 -
Figure 31. Western blot of MTA1 in prostate tissues.	83 -
Figure 32. Effect of Gnetin C on the levels of circulating IL-2 levels.....	84 -
Figure 33. GFP expression in knockdowns by fluorescence microscopy	87 -
Figure 34. Western blot of MTA1 protein levels and qRT-PCR of MTA1 mRNA expression.....	88 -
Figure 35. Reaction of luciferin to oxyluciferin catalyzed by the luciferase enzyme.....	89 -

Figure 36. Image of 22Rv1-Luc cells and BLI validates luciferase activity in 22Rv1-Luc cells...	91 -
Figure 37. BLI confirms equal luciferase activity in 22Rv1-Luc MTA1 knockdown cells	92 -
Figure 38. Experimental design investigating Gnetin C in CRPC.....	93 -
Figure 39. Effects of treatment on body weight	95 -
Figure 40. Tumor volumes.....	95 -
Figure 41. Representative images of tumors from each study group.	97 -
Figure 42. Tumor weights.....	97 -
Figure 43. BLI for each study group taken at days 0, 1, 7, 10, and 14	100 -
Figure 44. Representative H&E and IHC staining	103 -
Figure 45. Quantitation of H&E and IHC.	104 -
Figure 46. Western blot comparing monotherapy and combination therapy.....	106 -
Figure 47. Timeline depicting dosing and blood collection	108 -
Figure 48. UPLC chromatograms for Gnetin C quantitation.....	109 -
Figure 49. Calibration curve for Gnetin C quantitation by UPLC.....	110 -
Figure 50. Plot for Gnetin C serum concentration vs. time.....	111 -
Figure 51. Semi-log plot of serum concentration of Gnetin C vs. time	111 -
Figure 52. Terminal phase data.....	112 -

LIST OF TABLES

Table 1. Number of cells seeded per well for MTT assay.....	40 -
Table 2. PCR primers used for genotyping.....	45 -
Table 3. Antibodies used for western blot and their dilution ratios	53 -
Table 4. Sequence of qPCR primer pairs used in this study	56 -
Table 5. Antibodies used for IHC and their dilution ratios.....	57 -
Table 6. Gnetin C pharmacokinetic parameters	113 -

CHAPTER I. INTRODUCTION

The Prostate

The prostate is a walnut-sized gland of the male urogenital system (UGS). Its primary role is in the secretion of seminal fluid, which nourishes sperm and aids in its transport¹. The gland is positioned immediately below the bladder, and envelopes the ejaculatory ducts and the urethra (Figure 1).

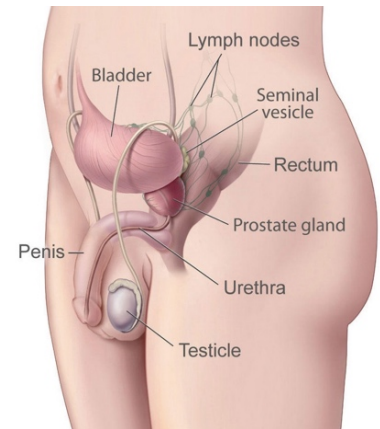


Figure 1. Schematic representation of the male urogenital system¹.

Histologically, the human prostate is composed of epithelial and stromal cells. Secretory luminal cells, basal cells, and a small population of neuroendocrine cells form the glandular epithelium^{2,3}. These epithelial cells are surrounded by supportive stroma which consists of smooth muscle cells, fibroblasts, vascular endothelial cells, nerve cells, and inflammatory cells^{4,5} (Figure 2).

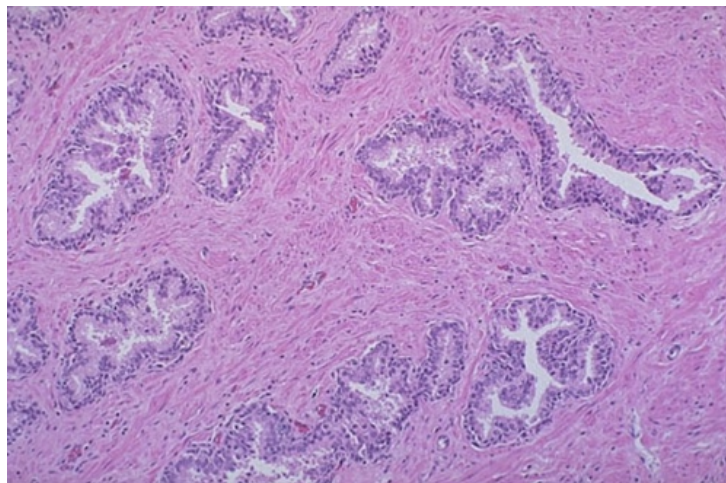


Figure 2. H&E staining of normal human prostate tissue⁵.

Prostate Cancer

The most common diseases affecting the prostate include prostatitis, benign prostatic hypertrophy, and cancer. Of these illnesses, prostate cancer (PCa) is the most deadly. While age is considered the biggest risk factor, other determinants include family history, race, and diet⁶. Despite current therapies, it remains one of the most common causes of cancer-related death in the United States. A need, therefore, exists for novel pharmacological therapies that have greater efficacy.

PCa begins when normal epithelial cells mutate to become proliferative and abnormal in function and morphology. While the basement membrane prevails, these abnormal cells remain confined to the glandular lumen. This stage is commonly referred to as prostatic intraepithelial neoplasia (PIN), which is a well-known precursor to PCa⁷. It is during this time that the tumor is largely dependent on endogenous androgens for growth and survival, among other key molecular drivers⁸.

Over time, the cancer cells undergo genetic alterations and begin to gain invasive properties. The basement membrane degrades and the tumor invades the surrounding stromal tissue. With further genetic alterations, the tumor becomes increasingly aggressive as it proliferates further, undergoes angiogenesis, becomes resistant to apoptotic processes, and gains further migratory properties where it invades local tissue and later metastasizes to distant sites.

When PCa continues to grow in spite of a downregulation in androgens caused by androgen-deprivation therapy (ADT), the disease is said to have progressed to a stage known as castrate-resistant prostate cancer (CRPC). CRPC is often associated with the emergence of an androgen receptor (AR) mutation, known as AR-V7, which is an androgen-independent receptor variant^{9,10}.

AR-V7 no longer expresses a ligand-binding domain through which it would normally bind to androgens for activation. Instead, this truncated AR-V7 remains constitutively active, allowing tumor cells to thrive irrespective of androgens or ADT¹⁰. CRPC is a very aggressive form of PCa, with 90 % of patients eventually developing bone metastasis¹¹ (Figure 3). Having now developed resistance to ADT, CRPC poses a challenge for ongoing treatment.

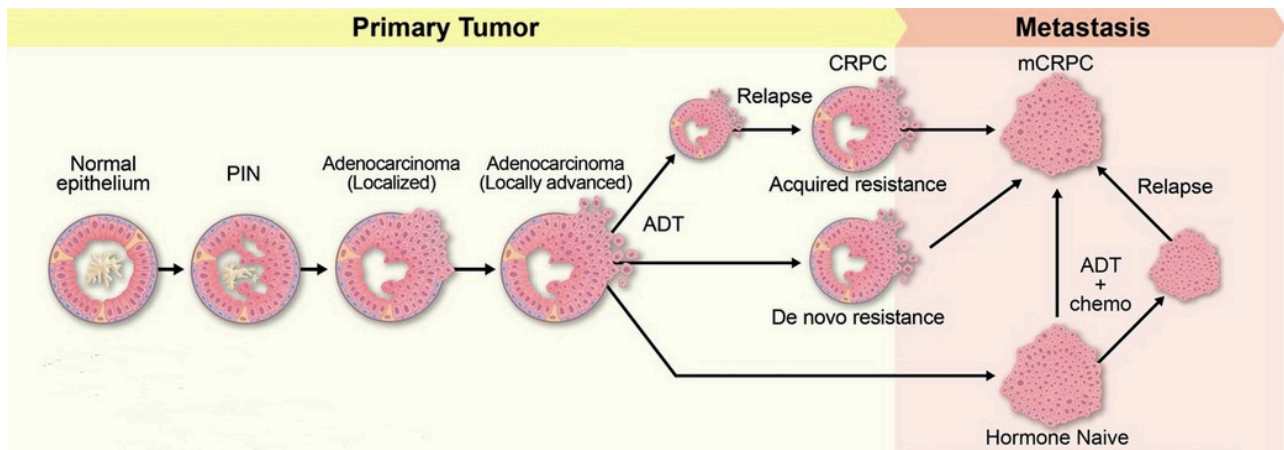


Figure 3. Schematic representation of the progression of prostate cancer from normal epithelium to metastatic castrate-resistant prostate cancer⁷.

Another equally important genetic alteration occurs to the oncogenic, metastasis-associated protein 1 (MTA1). An overexpression of MTA1 plays a significant role in tumor progression and metastasis, and is typically associated with more aggressive tumors¹². Together, MTA1 with AR, promote PCa and metastasis, leading to morbidity and death¹³. Therefore, an urgent need exists to develop therapeutic strategies that effectively suppress AR-reactivation and MTA1-associated tumor promoting signals in PCa.

Key Molecular Players of Prostate Cancer

(i) Metastasis-Associated Protein 1 (MTA1)

The primary objective of our laboratory over the years has been to identify key molecular drivers of PCa. In previous studies, MTA1 was found to be strongly associated with clinically aggressive PCa, including features, such as increased tumor grade, angiogenesis, and metastasis. Moreover, MTA1 protein expression is known to be higher in hormone refractory and metastatic PCa compared to localized tumors^{14,15}. Previous studies in prostate-specific phosphatase and tensin homolog (*Pten*) deletion models (in which *Pten* deletion promotes MTA1 overexpression) have demonstrated the tumor promoting ability of MTA1 and its associated survival pathways in PCa¹³. Furthermore, a loss of MTA1 in MTA1-knockdown models demonstrated reduced aggressiveness and metastatic potential of PCa^{16,17}.

Mechanistically, MTA1 has a dual function as master transcription co-regulator and as part of the nucleosome remodeling and deacetylation (NuRD) co-repressor complex^{12,18}. As a transcription regulator, MTA1 has the ability to promote tumor progression by directly overexpressing target oncogenes, such as *CTSB*, *ETS2*, and *IL-1 β* ; while downregulating target tumor suppressor genes^{15,16}. In the NuRD co-repressor complex, MTA1 is involved in histone deacetylation and chromatin remodeling, thereby playing an important role in gene silencing of tumor suppressors, such as *p53* and *PTEN*^{12,14,18} (Figure 4).

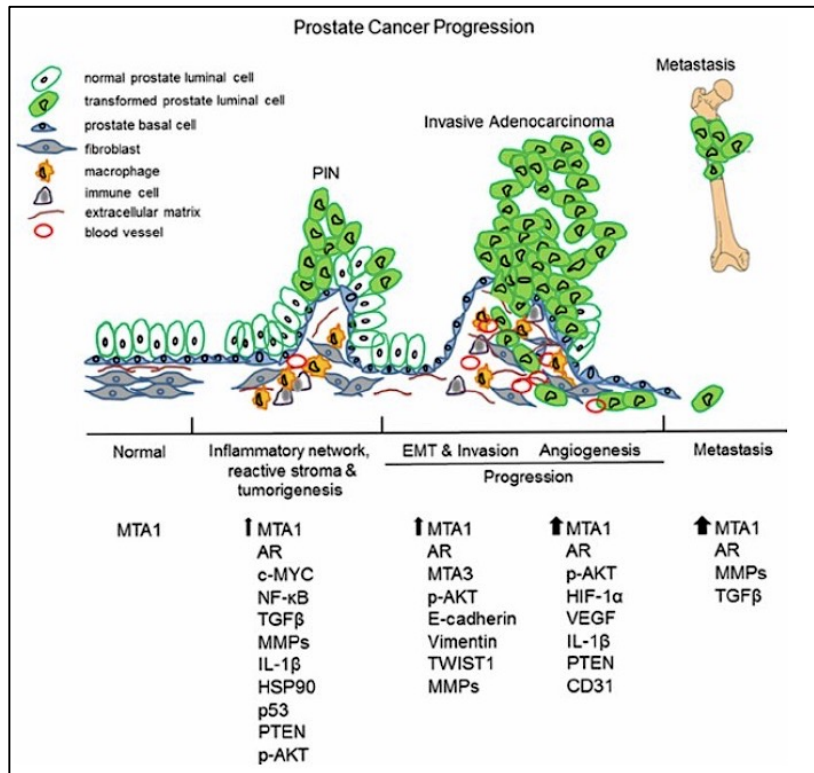


Figure 4. Schematic diagram showing the role of MTA1 and other markers in different stages of PCa. MTA1 overexpression in PCa is associated with inflammation, invasiveness, angiogenesis, recurrence, bone metastases, and overall poor prognosis¹².

As an important promoter of tumor progression and metastasis, MTA1 makes a prime pharmacological target in the treatment of PCa, and may also serve as a prognostic biomarker for progression or recurrence of the disease.

(ii) Androgen Receptor (AR)

The role of AR and its treatment-resistance is a topic of much interest in our laboratory. AR-mediated signaling is critical for the male sexual phenotype, but it also has a major role in PCa. AR is activated by binding to androgens in the cytoplasm. It then dimerizes and translocates to the nucleus where, like MTA1, it functions as a transcription factor that regulates the expression

of downstream target genes^{19,20} (Figure 5). Some AR-regulated genes include KLK4, MMP-2, Caspase-2, and p21, which have functions in cell proliferation, invasion, and metastasis^{21,22}. AR is not an MTA1-associated gene; nevertheless, overexpression of both genes often co-exists in aggressive tumors and are both responsible for the progression of PCa.

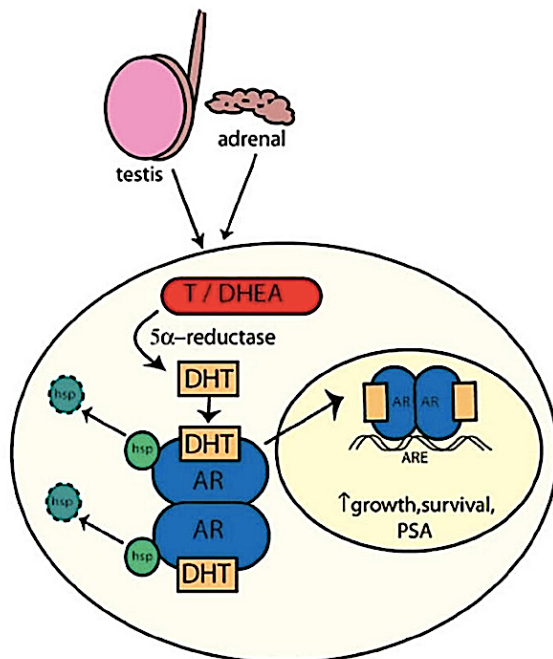


Figure 5. Schematic presentation of AR-signaling in PCa. National Cancer Institute²⁰.

Mutation of AR to the androgen-independent AR-V7 variant has significant consequences on treatment efficacy in CRPC due to resistance to ADT, such as LHRH agonists and GnRH antagonists. In such cases, AR-V7 could serve as a possible alternative pharmacological target. Enzalutamide, a 2nd generation anti-androgen, is indicated for the treatment metastatic CRPC^{23,24}. But, despite this, metastatic CRPC continues to have a poor prognosis, suggesting that a need exists for superior activity against AR-V7 in this aggressive stage of PCa.

Pharmacological Inhibition of Prostate Cancer

The treatment approach for PCa depends largely on the stage of the disease. For precancerous high-risk cases, active surveillance is all that is usually recommended. For early stage or small, localized tumors, surgery and radiotherapy are often indicated. As the cancer progresses, it is likely to require pharmacotherapy, such as ADT, which works to deprive the hormone-responsive tumor of androgens. As the cancer becomes increasingly androgen-independent and aggressive, it is likely to require antiandrogens, such as enzalutamide, whose efficacy is eventually reduced due to drug resistance. Chemotherapy may be considered for very late stage cases, but is believed to have limited benefit²⁵ (Figure 6).

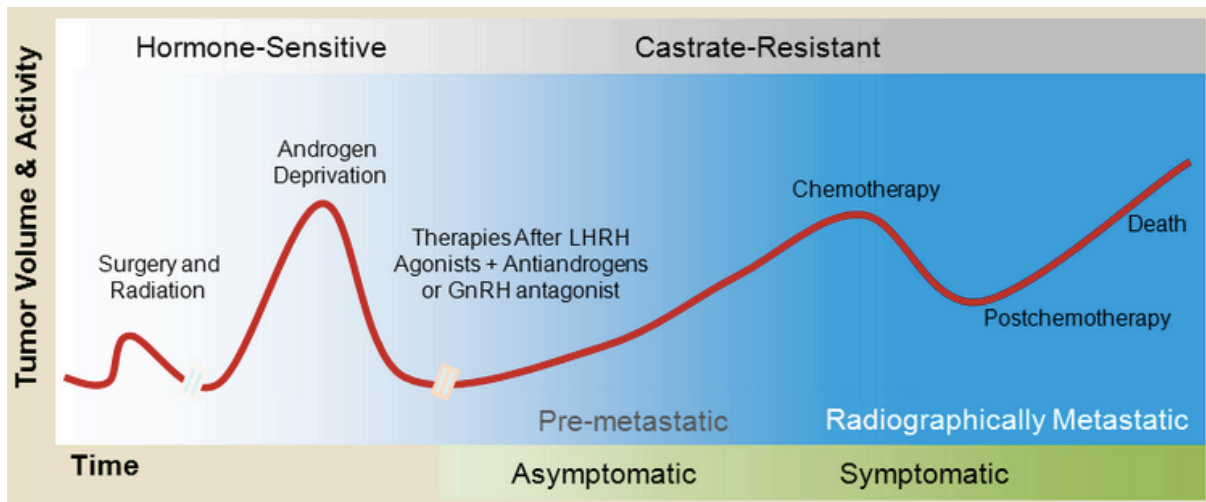


Figure 6. Schematic representation of prostate cancer over time, relating hormone dependency, aggressiveness, and treatment²⁶.

Current treatment options for advanced PCa offer some benefits, but remission is temporary, and mortality rates remain high. Therefore, a need exists not only for measures that actively treat PCa to reduce mortality, but that also delay or prevent the onset of the disease. Ideally, such therapeutic approaches should also be target-specific to improve efficacy and limit the incidence of adverse events.

Since MTA1, AR and AR-V7 drive the progression of PCa and CRPC, these would make ideal pharmacological targets for therapeutic strategies against the disease.

(i) Nutritional Polyphenols

Our laboratory has had a long relationship with natural stilbene compounds, such as resveratrol and pterostilbene (Figure 7). These compounds are derived from the skin of grapes and blueberries, and have been widely studied for their anticancer and anti-inflammatory properties, both in preventive and therapeutic strategies. In vitro and in vivo studies have shown that resveratrol and pterostilbene reduce cell viability, tumor progression and metastatic potential in PCa by inhibiting MTA1 and MTA1-mediated pathways^{18,26-28}.

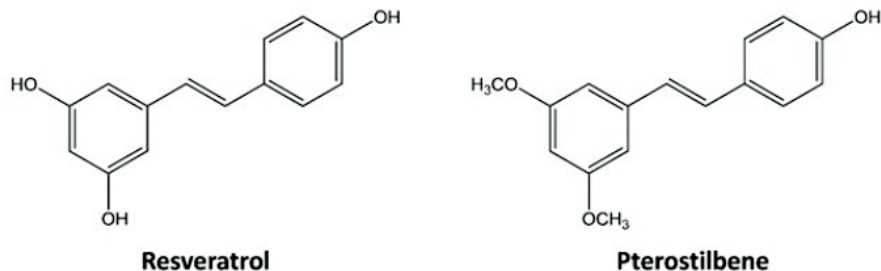


Figure 7. Polyphenolic chemical structure of resveratrol (left) and pterostilbene (right). Stilbenoids are hydroxylate analogs of stilbene, whose typical structure consists of two benzene rings linked by a two-carbon chain. In pterostilbene, methoxy groups replace hydroxyl groups in the meta-position.

In previous studies, we demonstrated that resveratrol and pterostilbene epigenetically restore PTEN expression by targeting oncomiRs of the miR-17 family in PCa²⁶. Resveratrol was also found to enhance p53 acetylation in PCa by inhibiting the MTA1/NuRD complex^{18,29}. We showed that resveratrol treatment reduced mitotic activity and angiogenesis in PCa xenografts, and caused a noticeable delay in tumor growth¹³. In addition, we demonstrated that the stilbene analogs, trimethoxy-resveratrol and piceatannol, when administered orally, suppress tumor formation and growth of PCa xenografts³⁰.

With encouraging results from the investigations of resveratrol and pterostilbene, we began to explore other natural stilbenes that could have superior efficacy and bioavailability. Our focus turned to Gnetin C, a novel resveratrol dimer, derived from the seeds of the Melinjo plant, a species that is native to southeast Asia (Figure 8).

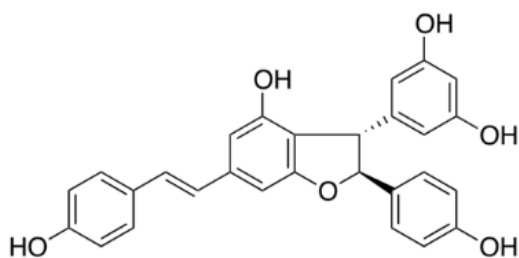


Figure 8. Chemical structure of Gnetin C, a dimer of trans-resveratrol.

We demonstrated that, compared to resveratrol and pterostilbene, Gnetin C has a greater potency in downregulating MTA1, AR, and AR-V7 in vitro¹⁶ (Figure 9). It has a lower IC₅₀ value as determined by cell viability assays, and a superior ability to mitigate metastatic potential¹⁶. Gnetin C was also found to substantially downregulate erythroblastosis E26 transformation-specific 2 (ETS2), via not only an MTA1-mediated pathway, but also some other pathway independent of MTA1, suggesting that Gnetin C has additional mechanisms of action yet to be explored¹⁶. We found that Gnetin C more potently inhibits MTA1 in xenograft studies, but we are yet to learn of its in vivo effects on AR and AR-V7³¹. We were also able to detect higher concentrations of Gnetin C in tumor xenograft tissue compared to resveratrol and pterostilbene, indicating that Gnetin C could have a better bioavailability³¹.

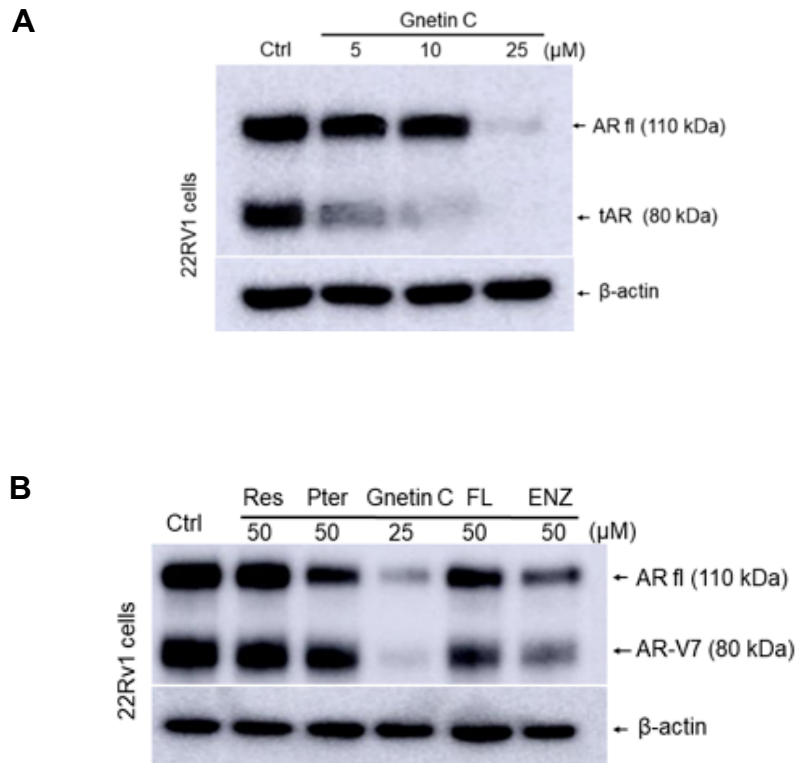


Figure 9. Representative western blot (A) showing dose-dependent reduction in full-length AR (AR fl) and truncated AR-V7 (tAR) in 22Rv1 treated with Gnetin C. Representative western blot (B) showing levels of AR and AR-V7 in 22Rv1 treated with resveratrol (Res), pterostilbene (Pter), Gnetin C, and the antiandrogens: Flutamide (FL), and enzalutamide (ENZ), with greatest potency seen after treatment with Gnetin C. Experiment conducted by Masters student, Ms. R Al Deabel.

(ii) Antiandrogens

ADT is indicated in the early stages of PCa where endogenous androgens play an important role in the growth and development of the tumor. It induces apoptosis of prostate epithelial cells and results in the regression of the tumor¹⁰. Although ADT has a high initial response rate, this remission is eventually curtailed by treatment-resistance; an event that is typically associated with the onset of aggressive CRPC and the emergence of AR-V7^{23,24}.

Previously, our laboratory investigated flutamide, an early generation anti-androgen, which is now understood to have limited efficacy in clinical CRPC³². More recently, however, we have been investigating enzalutamide, a 2nd generation anti-androgen approved for use in CRPC by the FDA^{23,25} (Figure 10). Mechanistically, enzalutamide targets several steps in the AR-signaling pathway. It blocks the AR binding pocket, preventing androgens from binding. It inhibits the AR-androgen complex from translocating to the nucleus, and it prevents this complex from binding to DNA, thus preventing it from regulating the expression of associated genes³³ (Figure 11).

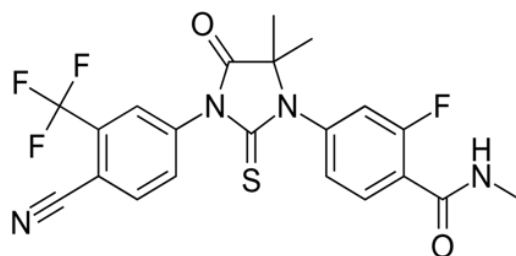


Figure 10. Chemical structure of enzalutamide

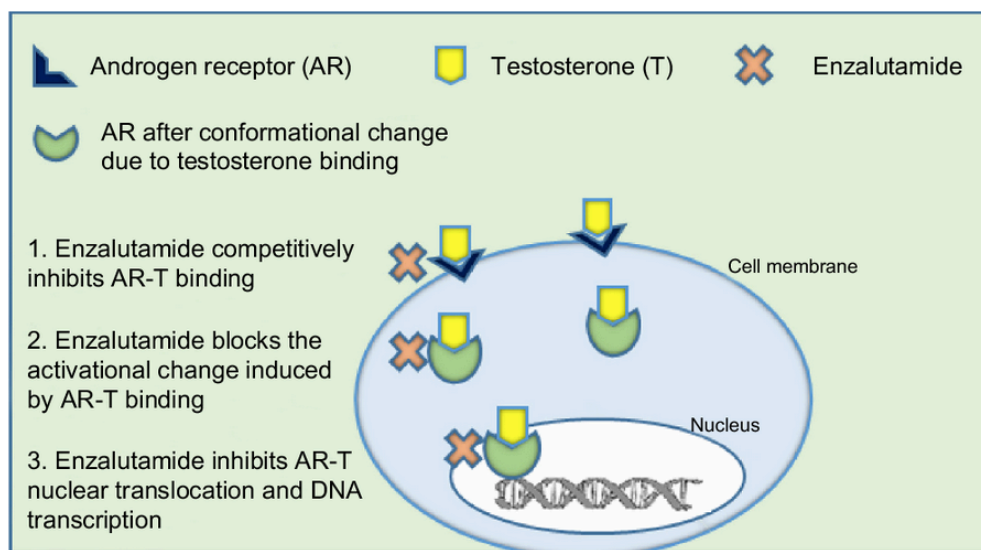
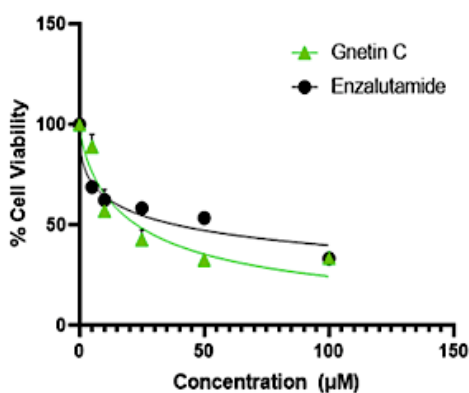


Figure 11. Mechanism of action of enzalutamide. Enzalutamide inhibits binding of testosterone to the AR, prevents translocation to the nucleus, and impairs AR-DNA binding³⁴.

Unfortunately, not all patients with CRPC are responsive to enzalutamide, and even among responders, benefits may be limited by the emergence of drug-resistance³⁴. Enzalutamide's activity at the AR-V7 receptor, if any, is not well-understood. The western blot in Figure 9 demonstrated that Gnetin C has greater potency in inhibiting AR and AR-V7 in 22Rv1 compared to enzalutamide. A cell viability assay also revealed that Gnetin C has greater cytotoxicity compared to enzalutamide (Figure 12). These are important findings considering that enzalutamide is currently regarded as standard care for clinical CRPC.



Compound	IC ₅₀ (µM)
Gnetin C	22.97
Enzalutamide	38.90

Figure 12. Cell viability assay shows that Gnetin C has a lower IC₅₀ value compared to enzalutamide. Experiment performed by Masters student, Mr. A Puaar.

(iii) Potential for Combination Therapy

Combination treatment is a favorable approach to cancer therapy. When a treatment blocks a particular signaling pathway, the tumor may develop resistance by activating an alternative pathway³⁵. This process may be exploited by drugs that target both pathways. Using a combination of drugs can present advantages. By targeting one or more important signaling

pathways, combination therapy can provide greater efficacy and reduce the risk of treatment resistance. Furthermore, additive or synergistic effects may permit the use of lower doses, thereby reducing the potential for toxicity: a common concern of anticancer therapy. Better tolerability leads to improved patient compliance, which in turn leads to better patient outcomes³⁶. However, it must be noted that not all combinations are favorable. At times, pathways and targets may be antagonistic³⁵.

Exploring different types of therapeutic combinations is one of our lab's priorities. It is known that although enzalutamide is indicated for CRPC in the clinic, it is not always an effective treatment among patients. The addition of Gnetin C to enzalutamide treatment may offer a beneficial action against AR, AR-V7 and MTA1. Our earlier in vitro findings demonstrated that the combination of Gnetin C and enzalutamide more potently inhibits both full-length AR and AR-V7 compared to either compound used as alone (Figure 13). When our cell viability data (IC₅₀ values) was analyzed by Compusyn software, we learned that certain concentrations could produce synergistic effects, while others could be antagonistic. The combination may also permit the use of a lower enzalutamide dose, thus reducing side-effects. In an epidemiological study, bone pain was reported in greater than 80 % of patients with CRPC²⁵. This was believed to be partly due to bone metastasis, but also due to osteoporosis caused by ADT and antiandrogens²⁵. Other serious complications of enzalutamide include seizures, encephalopathy, ischemic heart disease, falls and fractures. By using smaller doses of enzalutamide in combination therapy, we could reduce the incidence of these adverse events.

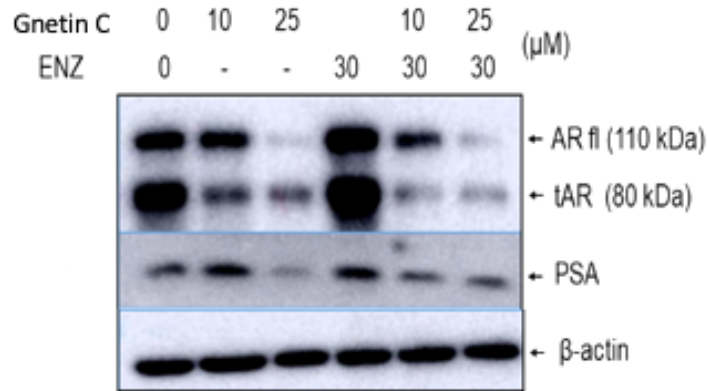


Figure 13. Representative western blot showing reduced levels of full-length AR (AR fl), AR-V7 (tAR), and PSA in 22Rv1 cells treated with Gnetin C monotherapy, enzalutamide (ENZ) monotherapy, and Gnetin C + enzalutamide combination. Experiment conducted by Masters student, Ms. R Al Deabel.

Prostate Cancer Cell Lines

In our laboratory, the pharmacodynamic effects of Gnetin C were studied in vitro in a range of diverse PCa cell lines. When studied in PC3M, a highly aggressive PCa cell line, and in DU145 cells, a moderately aggressive cell line, we found that Gnetin C downregulated MTA1 more potently than resveratrol and pterostilbene. Gnetin C also demonstrated significant MTA1-mediated inhibitory effects on cell viability, colony formation, and migration¹⁶. Our preliminary experiments in 22Rv1 cells, an aggressive PCa cell line which expresses both full-length AR and truncated AR-V7, also show that Gnetin C more potently downregulates MTA1, AR, and AR-V7, which is crucial for the treatment of CRPC and aggressive tumors. These promising results provide justification for studying Gnetin C in preclinical animal models in order to understand whether these benefits extend to the organism as a whole.

Preclinical Animal Models of Prostate Cancer

To understand the efficacy of Gnetin C *in vivo*, an appropriate animal model of PCa needs to be used to test the efficacy of the compound. The closer this model resembles the human condition, the more clinically relevant the findings will be. The type of model used depends on the overall goal of the investigation. No one animal model is best, but one may be more appropriate than another.

(i) Transgenic Mouse Models

Transgenic mice are murine models whose genotype has been manipulated in order to achieve a certain desired phenotype. This model is believed to closely resemble human pathology, where cancer usually develops from genetic alterations affecting oncogenes and tumor suppressor genes (TSG). The tumor develops within the organ of interest, which can later be excised and studied. This model is very informative because we can learn about the histological changes that take place as the cancer progresses and extrapolate this to the human condition. However, significant pitfalls of transgenic models include cost and the need for strategic breeding and genotyping. In addition, these studies are usually very time- and labor-intensive. And, although they are intended to simulate genetic alterations that occur pathologically, they cannot fully reproduce the genetic complexity of human tumors³⁷.

A technique that may be used to generate transgenic models is known as the Cre-LoxP recombinant system, which encompasses site-specific recombinase technology. The probasin promotor, specific to the prostate, is used to drive the expression of the Cre gene³⁸. This ensures that any genetic manipulations that take place using this technology remain localized to the prostate. The

Cre recombinase enzyme, encoded by the Cre gene, functions by recombining a pair of LoxP gene sequences. These LoxP sequences can be inserted at specific sites along the DNA molecule in order to either activate or repress genes³⁹. By flanking a tumor suppressor gene (TSG), such as *Pten*, with LoxP, the Cre recombinase enzyme can effectively delete this gene giving rise to a knock-out model³⁹. Alternatively, when a loxP-flanked STOP sequence is inserted between promoter and transgene, such as *MTA1*, Cre recombinase removes the STOP sequence and activates the expression of that transgene, creating a knock-in model³⁹.

Transgenic mice with the genotype, $R26^{MTA1/MTA1}; Pten^{+/f}; Pb-Cre^+$, are engineered using the Cre-LoxP system, whereby two additional MTA1 transgenes are knocked into the Rosa26 locus, the most genetically stable region of the mouse DNA⁴⁰, while one *Pten* allele is deleted. Pb-Cre positivity ensures that these genetic manipulations are specific to the prostate. This *Pten* heterozygous model represents an increased risk for developing PCa. Mice with this genotype typically exhibit precancerous PIN at 20 weeks of age⁴¹. It is a model that can be used to study the efficacy of Gnetin C as a chemopreventive agent against PCa.

Transgenic mice with the genotype, $R26^{MTA1/MTA1}; Pten^{ff}; Pb-Cre^+$, have two additional MTA1 transgenes knocked-in, while both *Pten* alleles are deleted. This genotype is very typical of aggressive adenocarcinoma in humans. Mice exhibiting this genotype tend to develop high-grade PIN with progression to invasive adenocarcinoma⁴². This model can be used to study the efficacy of Gnetin C as a therapeutic agent in PCa.

(ii) Xenograft Mouse Models

Xenograft mouse models involve implanting human PCa cells into athymic ('nude') mice. These mice are immunocompromised and are, therefore, less likely to reject the human tumor cells. Xenografts offer certain advantages over transgenic models. They are generally more affordable and do not require complex breeding strategies. These tumors can develop relatively quickly, and as such, these studies can be completed over a shorter time-period³⁷. Furthermore, we can select a specific human PCa cell line with a known genetic profile in order to more accurately reflect a particular stage or form of the disease as it occurs in humans. Disadvantages, however, include the need for sterile rodent housing due to the breed's poor immunity and lack of information concerning the urogenital system, prostate glandular morphology, and organization of tissues.

Xenografts may be implanted orthotopically where human tumor cells are injected directly into the corresponding organ of interest³⁷. Orthotopic xenografts are better models for studying organ-specific cancer, but the surgical technique may be extremely complex requiring the expertise of a veterinarian. It can also be very laborious and time-consuming depending on the number of mice used in the study. Alternatively, the cells may be implanted subcutaneously (s.c.).

Generating s.c. xenograft tumors from 22Rv1 PCa cells would make for an ideal CRPC model. 22Rv1 is a human PCa epithelial cell line derived from an androgen-dependent CWR22 xenograft propagated in mice having undergone castration-induced regression followed by relapse (AR reactivation)⁴³. This is a cell line which expresses both full-length AR and androgen-independent AR-V7, thus closely resembling the clinical presentation of CRPC in humans⁹. The implantation

of 22Rv1 cells tagged with the luciferase gene allows us to record bioluminescent images of the xenograft tumor in a noninvasive manner so that we may study the growth of tumor over real time.

Pharmacokinetic Profiling

Pharmacokinetics (PK) describes the fate of a compound in the body after it is administered. It is characterized by four main physiological processes: absorption, distribution, metabolism, and excretion (ADME). For a compound to be pharmacologically useful, it must be able to reach its site of action in clinically relevant concentrations. As a compound moves through the body, it faces many obstacles. After oral administration, it must first be released from its dosage-form and dissolve to form a molecular solution. In the stomach, it must be resistant to acidic degradation⁴⁴. And, when it reaches the small intestine, only ideal physicochemical properties will allow it to permeate the intestinal mucosa. As it migrates through the intestinal cell, it may be subjected to pre-systemic metabolism or pumped out by efflux transporters. If the compound is successful in overcoming these obstacles, it then reaches the hepatic portal circulation, where it is taken to the liver for biotransformation^{44,45}. The fraction that escapes first pass metabolism enters the systemic circulation for distribution. From here, it may reach its target site to exert a pharmacological effect, or it may distribute to other tissues producing no effect or unwanted effects. Eventually the compound is eliminated from the body by metabolism or renal excretion, or a combination of the two⁴⁶ (Figure 14).

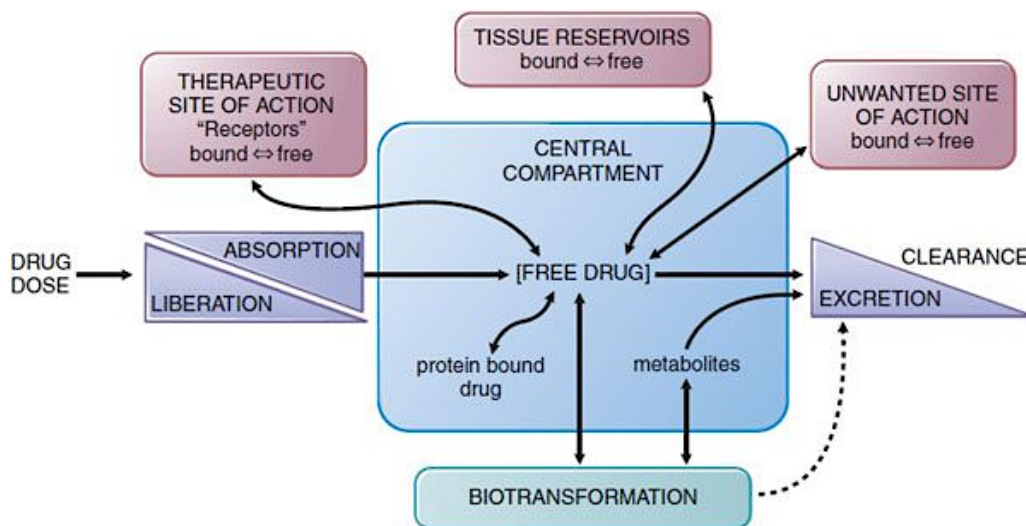


Figure 14. Schematic representation of the four main physiological processes of pharmacokinetics: absorption, distribution, metabolism, and excretion (ADME). Free drug and protein bound drug exist in equilibrium. Only free drug may move between compartments⁴⁶.

One of the limitations of natural polyphenols is their low bioavailability due to poor dissolution and high pre-systemic metabolism⁴⁴. Most natural compounds are lipophilic, which presents a problem for dissolution. But, this problem may be overcome by crafty formulation techniques, such as salt formation, micronization, micelle emulsions, and lipid-based delivery systems⁴⁷. Pre-systemic metabolism, however, presents a far greater challenge, and this is where natural compounds tend to fail. Extensive intestinal and hepatic metabolism contributes to a high clearance rate, short half-life, and a low overall systemic exposure^{48,49}. Recently, some compounds have been formulated in combination with enzyme inhibitors to enhance their systemic exposure, but this requires a thorough understanding of the specific metabolic pathways involved.

In a recent *in vivo* study, we found Gnetin C in tumor tissues at higher concentrations than either resveratrol or pterostilbene³¹, suggesting that Gnetin C may have a more favorable PK profile.

This is in keeping with a single-dose study in humans conducted by Tani et al. (2014) that measured a mean residency time (MRT) of ~36 hours for Gnetin C after oral administration of melinjo seed extract (MSE); while trans-resveratrol had an MRT of ~7 hours after it was administered at an equivalent dose⁴⁸. Nakagami et al. (2019) also reported an accumulation of Gnetin C in the serum of healthy human volunteers when orally administered each day for two weeks⁵⁰.

CHAPTER II. RESEARCH GOALS

The Knowledge Gap

From previous studies, we know that MTA1 and AR are key molecular drivers of PCa. In addition, we know that androgen-independent AR-V7, expressed in CRPC, also drives progression of the disease. Our in vitro findings have demonstrated that Gnetin C has superior potency in downregulating MTA1, AR, and AR-V7 compared to older stilbenes, such as resveratrol and pterostilbene.

With an appreciation of Gnetin C's pharmacodynamic superiority at the in vitro level, we are now motivated to further explore the efficacy of this compound in preclinical in vivo murine models of PCa. As a novel compound having undergone very limited research, particularly in PCa, it was important to understand its efficacy across various stages of the disease in a range of different treatment approaches and modes of administration. More specifically, we wanted to investigate Gnetin C's potential as chemoprevention in high-risk cases and as active treatment in advanced PCa and CRPC.

In addition to the lack of pharmacodynamic data available, there was also scant information about Gnetin C's PK properties. Earlier stilbenes have demonstrated a somewhat unsatisfactory bioavailability, which ultimately limits their clinical applicability. If Gnetin C demonstrates an improved bioavailability and overall PK profile, it will have greater clinical relevance.

Rationale and Justification

Advanced PCa and CRPC are difficult to manage and are associated with a high mortality rate. Only very limited success has been achieved through pharmacological intervention. A need, therefore, exists to identify novel molecular players that can serve as new pharmacological targets and to optimize treatment strategies in order to reduce the mortality. It is imperative that we find treatment approaches which are more effective, less toxic, and pharmacokinetically desirable. We need to consider options for not only monotherapy, but for combination therapy as well, as this could offer advantages such as synergism, reduced drug resistance, and improved tolerability.

Current National Comprehensive Cancer Network guidelines highlight that active surveillance alone is recommended for precancerous, high-risk patients⁵¹. We propose that, in addition to active surveillance, nutritional interception may provide the most adequate intervention for this population of patients. To this end, we intended to explore the potential of a Gnetin C-supplemented diet to prevent or delay the progression of PIN in high-risk subjects.

With Gnetin C having a dual activity against MTA1 and AR rivaling that of older stilbenes, and with its unique ability to inhibit AR-V7, Gnetin C could serve as a viable therapeutic option in aggressive and difficult to manage advanced PCa and CRPC. Earlier in vitro studies have demonstrated Gnetin C's superiority in inhibiting MTA1, AR, and AR-V7, leading to a reduction in cell viability, invasiveness, migration, and colony formation. The addition of Gnetin C to enzalutamide could offer benefits over enzalutamide monotherapy by increasing patient responsiveness to the treatment.

Progressing to in vivo studies is now justified and essential. In vitro studies offer us precursory information about the activity of a compound at the cellular and molecular levels. This gives us an indication as to whether the compound shows promise and warrants further investigation. But, successful in vitro results do not always extend to the organism as a whole. Ultimately, animal studies are necessary to ascertain whether the compound is clinically viable, both pharmacodynamically and pharmacokinetically.

Hypothesis

To answer questions we had about Gnetin C and its clinical applicability, the following study aims were proposed:

AIM 1

To investigate the efficacy of Gnetin C as a strategy for PCa prevention in a high-risk murine model.

- Does Gnetin C offer us an effective option for the prevention of PCa?

AIM 2

To investigate the efficacy of Gnetin C as an active treatment strategy in a high-grade PIN murine model.

- Does Gnetin C offer us an effective option for the treatment of PCa by reducing its severity and delaying progression?

AIM 3

To investigate the efficacy of Gnetin C as an active treatment strategy in a CRPC murine model.

- Does Gnetin C offer us an effective option for the treatment of CRPC?
- Does Gnetin C provide an additive benefit when combined with enzalutamide in the treatment of CRPC?

AIM 4

To estimate the pharmacokinetic parameters of Gnetin C.

- Does Gnetin C have a larger systemic exposure and longer half-life compared to other stilbenes?

We anticipate that the efficacy of Gnetin C will echo our in vitro results. We expect Gnetin C to outperform control, stilbenes, or other reference agents in Aims 1-3, showing a more potent inhibition of MTA1, AR and AR-V7, improved histopathology, and reduced systemic inflammation. We expect the combination of Gnetin C and enzalutamide to be more beneficial compared to either agent alone. Our PK studies are expected to reveal a greater half-life and systemic exposure for Gnetin C compared to resveratrol and pterostilbene.

We aspire to see these results provide justification for Gnetin C trials in human subjects with the hope that it improves morbidity and mortality associated with PCa.

Specific Research Aims

- To study the in vitro efficacy of Gnetin C in inhibiting cell viability.
- To compare IC₅₀ values of Gnetin C with earlier stilbenes and new, synthetically derived stilbenes, BT-546 (D1) and BT-547 (D2).
- To investigate the efficacy of Gnetin C mediated by the inhibition of MTA1, when used as a supplemented diet in transgenic mice with genotype: *R26^{MTA1/MTA1}; Pten^{+f}; Pb-Cre⁺* (high-risk PCa model).
- To investigate the efficacy of Gnetin C mediated by the inhibition of MTA1, when used as a treatment strategy in transgenic mice with genotype: *R26^{MTA1/MTA1}; Pten^{ff}; Pb-Cre⁺* (model for high-grade PIN).
- To investigate the efficacy of Gnetin C as inhibitor of MTA1, AR, and AR-V7 in a 22Rv1-generated xenograft model for CRPC.
- To study whether Gnetin C can provide additive effects when used in combination with enzalutamide in 22Rv1-generated xenograft model for CRPC.
- To estimate the PK parameters of Gnetin C by conducting a single-dose study.
- To compare Gnetin C's PK parameters with resveratrol and pterostilbene.

CHAPTER III. MATERIALS AND METHODS

Treatment Compounds

Gnetin C was a generous gift from Hosoda SHC Co., Ltd. (Fukui, Japan). Resveratrol, pterostilbene, and enzalutamide were purchased from Sigma-Aldrich (St. Louis, MO, USA). BT-546 (D1) and BT-547 (D2) were synthesized and donated by Dr. Bhaskar Das (Long Island University, Brooklyn). All compounds had $\geq 99\%$ purity. They were protected from light and stored at $-20\text{ }^{\circ}\text{C}$. Compounds were dissolved in pure dimethyl sulfoxide (DMSO) and then further diluted in either media or normal saline. Custom-prepared diets were formulated by Envigo Teklad Diets (Madison, WI). Five diets were prepared: Gnetin C 70mg/kg (high-concentration), Gnetin C 35mg/kg (low-concentration), pterostilbene 70 mg/kg, and standard diet (control). Diets were protected from light and stored at -4°C .

In Vitro Studies

(i) Cell Culture

PC3 (ATCC, USA) is a human PCa cell line derived from bone metastasis⁵². The PC3M cell line is a modified version of PC3, making it notably more aggressive with a high potential for metastasis. PC3M cells were a gift from Dr. R. Bergan (Northwestern University, Chicago, IL). PC3 and PC3M cells are often used to investigate molecular changes that occur in tumor progression of advanced prostate cancer. Unlike other less aggressive PCa cell lines, PC3 and PC3M cells do not express AR, AR-V7, prostate-specific antigen (PSA), or PTEN tumor

suppressor. 22Rv1 is derived from an androgen-dependent CWR22 xenograft propagated in mice after castration-induced regression and relapse. This cell line expresses both full-length AR and truncated, androgen-independent AR-V7 variant. It is weakly stimulated by dihydroxytestosterone⁴³. Cells were authenticated using short tandem repeat profiling at the Research Technology Support Facility, Michigan State University, and also found to be mycoplasma-free (Universal Mycoplasma Detection Kit, ATCC, Manassas, VA, USA).

PC3, PC3M, DU145 and 22Rv1 cell lines were maintained in RPMI-1640 (ThermoFisher Scientific, USA) containing 10% fetal bovine serum and kept in an incubator at 37 °C with 5% CO₂. Cell lines were used within 10–15 passages from thawing. For in vitro experiments involving treatment with resveratrol, pterostilbene, Gnetin C, and enzalutamide, cells were grown in conventional media, and then replaced with phenol red-free RPMI 1640 media containing 5% charcoal-stripped serum 4 hours prior to treatment. This media would provide a steroid-free background, thereby eliminating any potential for bias.

(ii) Generation of Stable 22Rv1 Cells with MTA1 Knockdown

22Rv1 cells were transduced with GIPZ MTA1 lentiviral shRNA (three clones), GIPZ GAPDH lentiviral shRNA, and GIPZ nonsilencing lentiviral shRNA. The GIPZ lentiviral shRNA system (GE Healthcare Dharmacon, Lafayette, CO, USA) contains a puromycin-resistant gene for selection of transduced cells and TurboGFP for monitoring the selection under the fluorescence microscope. For the preparation of the viral particles, we used the pCMV-ΔR8.91 packaging plasmid and the pMD.G envelope plasmid (Addgene, Cambridge, MA, USA). Cells were

transduced using RPMI 1640 medium, which contained 4 µg/mL polybrene (Sigma-Aldrich, St. Louis, MO, USA) with lentiviral particles at a multiplicity of infection = 8. On day 2 post-transduction, selection was initiated with 200 µg/mL puromycin (Sigma-Aldrich) and GFP-positive clones were selected and propagated.

(iii) Generation of Stable 22Rv1 Cells Tagged with Luciferase

To establish 22Rv1 cells expressing the luciferase gene (22Rv1-Luc), 22Rv1 cells were transduced with the lentiviral luciferase construct (prepared in-house using lentiviral plasmids from Addgene, Watertown USA). Stable clones were selected using the aminoglycoside, G418 (Geneticin) at a concentration of 1 mg/mL. Clonal populations of cells were expanded in vitro and tested for their luciferase activity. The purpose of tagging cells with the luciferase gene was to enable noninvasive bioluminescent imaging for in vivo studies.

To validate luciferase activity, 22Rv1-Luc cells were seeded by serial dilution in a 96-well plate and allowed to incubate at 37 °C and 5 % CO₂ overnight. The following day, each well was replenished with 100 µL of a freshly prepared solution of D-luciferin 150 µg/mL in media. The cells were then incubated at 37 °C and 5 % CO₂ for 10 minutes, after which, they were imaged using IVIS Lumina LT III (PerkinElmer, Waltham, MA, USA).

(iv) Cell Viability Assay

The MTT (3-(4,5-dimethylthiazol-2-yl)-2,5-diphenyltetrazolium bromide) assay was used to determine the viability of PC3, PC3M, and 22Rv1 cells after treatment with resveratrol, pterostilbene, Gnetin C, and enzalutamide. The assay allows us to draw conclusions about the anti-cancer efficacy of each compound.

Cells were seeded in a 96-well plate and maintained in conventional media in the incubator at 37 °C and 5 % CO₂ overnight (Table 1). The following morning, the media was replenished with phenol red-free RPMI-1640 with 5 % charcoal-stripped FBS. The cells were then incubated at 37 °C and 5 % CO₂ for a further 4 hours.

Table 1. Number of cells seeded per well for MTT assay

Cell Line	Number of cells seeded per well
PC3	2500
PC3M	1500
22Rv1	5000

Stock solutions of 5 mM, 10 mM, 25 mM, 50 mM, and 100mM were prepared for each compound, using DMSO as the diluent. Each stock solution was diluted 1000 times in media. After 4 hours of incubation, the existing media from each well was replenished with 100 µL of respective treatment. Each treatment was tested in triplicate. Treatment was replenished daily for a 72-hour

period. Treatment concentrations were selected based on previously conducted optimization studies.

At the end of the treatment, MTT (Sigma-Aldrich, Indianapolis, USA) solution was prepared at a concentration of 5 mg/mL in 1X PBS (phosphate-buffered saline). Twenty (20) μ L of MTT solution was added to each well, and allowed to incubate at 37 °C and 5 % CO₂ for a further 3-5 hours. The yellow MTT dye is reduced by NAD(P)H-dependent cellular oxidoreductase enzymes to crystalline purple-colored formazan in live (viable) cells⁵³. To dissolve the purple formazan crystals, an isopropanol solvent containing 4 mM HCl and 0.1 % Triton-X 100 was prepared.

After incubation with MTT, the media was aspirated and 100 μ L of solvent was added to dissolve the formazan. Absorbance of light at 590nm was read using a Biotek Synergy H1 microplate reader. Percentage viability was calculated by normalizing the optical density (OD) of the treatments against the vehicle-treated controls. Viability was plotted against treatment concentration to determine the IC₅₀ value by non-linear regression analysis using Prism v9 software (GraphPad Software, La Jolla, CA, USA).

(v) Treatments (for protein and RNA isolation)

Cells were seeded in culture-treated plates at an appropriate density that would achieve a confluency of 50-60 % by the following day, at which time, the media was replaced with phenol red-free RPMI-1640 containing 5 % charcoal-stripped FBS, and incubated at 37 °C and 5 % CO₂ for a period of 4 hours. Treatment stock solutions of resveratrol, pterostilbene, Gnetin C, and

enzalutamide (as described above) were diluted 1000 times in media to achieve final treatment concentrations of 5 μ M, 10 μ M, 25 μ M, 50 μ M, 100 μ M. These treatment concentrations were selected based on previously conducted optimization studies. The controls were vehicle-treated with DMSO diluted 1:1000 in media. The treatment concentrations selected were based on preceding experiments conducted in our laboratory. After 24 hours in treatment, cells were collected using a cell scraper and protein and RNA lysates were prepared for western blot analysis and qRT-PCR, respectively.

In Vivo Studies

(i) Generation of Transgenic Prostate-Specific MTA1 knock-in Mice

We generated a conditional mouse with the human MTA1 transgene knocked into the Rosa26 (R26) locus using the CAG-LoxP-Stop-LoxP(LSL)-2HA-MTA1-T2A-GFP-pA construct. In short, after the generation of a genetically modified founder mouse line Rosa26-3attP (R26P3) used for MTA1 sequence integration, resulting *MTA1* transgene embryos were injected into foster mice to produce MTA1 founders, designated as R26-LSL-MTA1 (Applied StemCell). We crossed *R26-LSL-MTA1* female mice with wild-type (WT), probasin promoter positive Pb-Cre4 (Cre^+) male mice (Jackson Laboratories) to generate transgenic lines that express MTA1 upon Cre-mediated removal of the LSL cassette, specifically in the prostate epithelium, $R26^{+/MTA1}; Cre^+$ ($R26^{+/MTA1}$). The male $R26^{+/MTA1}$ mouse was then backcrossed with a *R26-LSL-MTA1* female mouse to generate mice with biallelic overexpression of MTA1: $R26^{MTA1/MTA1}; Cre^+$ ($R26^{MTA1}$).

(ii) Generation of Transgenic Prostate-Specific Pten Knockdown Mice

A C57BL/6J female mouse homozygous for the “floxed” Pten allele was purchased from Jackson Laboratories and bred with our MTA1 transgenic mice ($R26^{MTA1}$) (Figure 15). In so doing, we were able to create two genotypes:

(a) $R26^{MTA1/MTA1}; Pten^{+/f}; Cre^+$, our model for high-risk PCa.

These male mice were fed diets supplemented with Gnetin C (high concentration), Gnetin C (low concentration), pterostilbene, and control for our chemoprevention studies.

(b) $R26^{MTA1/MTA1}; Pten^{f/f}; Cre^+$, our model for high-grade PIN.

These male mice received Gnetin C 7mg/kg body weight (bw) by i.p. injections for our therapeutic studies.

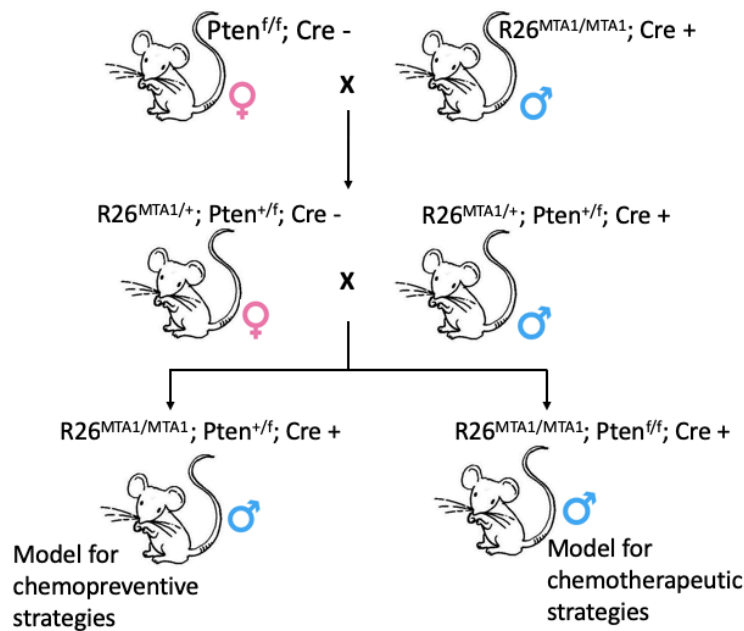


Figure 15. Breeding strategy to generate the required genotypes for studies involving transgenic mice.

(iii) Genotyping

Genotyping is a technique used to determine whether a certain DNA sequence (or ‘gene’) is either present or absent in the transgenic mouse genome. The breeding strategy described in Figure 15 can give rise to a number of possible genotypic combinations. We must ascertain which mice have the desired genotype before including them in the studies. This is best undertaken at the age of 3 weeks; the age mice would normally wean from their mother.

A small (2-3 mm) portion of tail-end was used to provide a sample of DNA from each mouse. This was performed under anesthesia (isoflurane) using the open-drop method. Each tail-end was submerged in 155 μ L of lysis buffer and Proteinase K (ThermoFisher Scientific), and allowed to incubate overnight in a water bath at 55 °C in order to lyse tissue and digest proteins. The samples were then heated to 85 °C for 45 minutes to inactivate proteinase K. After centrifugation, the supernatant, containing our DNA template, was collected and stored at 4 °C.

Next, the gene of interest was amplified in order to reach detectable concentrations. This was achieved by polymerase chain reaction (PCR) using an Eppendorf thermocycler. One cycle is composed of three main steps, each being temperature- and time-specific. First, the DNA molecule must be denatured so that it exists as single strands. Then, gene primers must anneal to the DNA molecule at their specific locations (Table 2). Followed lastly by extension, whereby DNA polymerase builds the new DNA strand using dNTP building blocks. The reaction was repeated for a total of 35 cycles.

Table 2. PCR primers used for genotyping

Gene of Interest	Forward Primer	Reverse Primer	Size of amplicon (bp)
PTEN	5'-CAA GCA CTC TGC GAA CTG AG-3'	5'-AAG TTT TTG AAG GCA AGA TGC-3'	156 (WT) 328 (Mutated)
MTA1	5'-AGC TAC GAG CAG CAC AAC GGG GT-3'	5'-CAC GCT TGG TTT CCG AGG AT-3'	715
Cre	5'-TCG CGA TTA TCT TCT ATA TCT TCA G-3'	5'-GCT CGA CCA GTT TAG TTA CCC-3'	393

The DNA samples were then resolved by gel electrophoresis. To do this, a 1 % agarose gel was prepared to which ethidium bromide (ThermoFisher Scientific) was added. Ethidium bromide is an intercalating agent which binds to DNA and fluoresces under UV light, enabling detection. When the gel solidified, it was placed in an electrophoresis chamber and submerged in 1X TAE (Tris-acetate-EDTA) buffer. The DNA samples were then loaded onto the gel, and electricity was run at 100 V, at room temperature for about 1 hour. Images of the gel were then taken using Amersham Imager 600 (GE Healthcare).

(iv) Experiment Design – Chemoprevention Study

After weaning (3-weeks old), male mice with genotype, $R26^{MTA1/MTA1}$; $Pten^{+/f}$; Cre^+ , were randomized to four groups receiving the following supplemented diets: Gnetin C 70mg/kg (high-concentration) diet, Gnetin C 35mg/kg (low-concentration) diet, pterostilbene 70 mg/kg diet, and control diet (Figure 16). These diets were fed *ad libitum* until sacrifice. Diet concentrations were selected based on previous experience. Human equivalent doses (HED) were based on formula:

HED (mg/kg) = Animal dose (mg/kg) x 0.081 (km ratio for mice)⁵⁴. For a 70 kg male, this equated to 26.6 mg/d (Gnetin C 35 mg/kg diet), 53.2 mg/d (Gnetin C 70 mg/kg diet), and 53.2 mg/d (Pterostilbene 70 mg/kg diet). These doses are well-tolerated and deemed safe humans^{50,55}.

Mice were monitored daily for general wellbeing and signs of toxicity. Their body weight and food intake was measured weekly. After 17 weeks, mice were sacrificed, at which time the urogenital system (UGS) was isolated and fixed in formalin for histology and immunohistochemistry (IHC). For protein and RNA studies, prostate tissues were dissected, snap frozen, and stored at -80°C . Blood was collected by cardiac puncture, and serum was isolated after coagulation (stored at -80°C). Serum was used for ELISA studies.

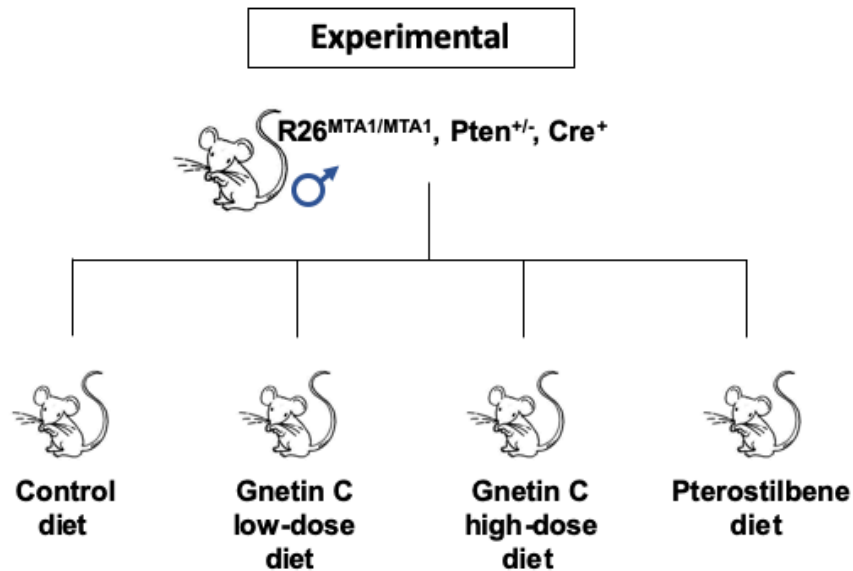


Figure 16. Schematic representation of experimental design where we investigated the efficacy of Gnetin C-supplemented diet as a chemopreventive strategy in high-risk model of PCa.

(v) Experiment Design – Chemotherapeutic Study

After weaning (3-weeks old), male mice with genotype, $R26^{MTA1/MTA1}; Pten^{ff}; Cre^+$, were randomly assigned to two study groups receiving one of the following treatments by daily i.p. injection: Gnetin C 7mg/kg bw or control (vehicle). The dose of Gnetin C was based on previous experience in a xenograft model (using 25 mg/kg and 50 mg/kg). Knowing that transgenic mice do not tolerate Gnetin C as well, a conservative dose was selected for this particular study. A third group comprised of male mice with normal prostates, having the Cre-negative genotype, $R26^{MTA1/MTA1}; Pten^{ff}; Cre^-$, served as a reference for our study (Figure 17).

Mice were monitored daily for general wellbeing and signs of toxicity. After 12 weeks, mice were sacrificed, at which time the UGS was isolated and fixed in formalin for histology and IHC. For protein and RNA isolation, prostate tissues were dissected, snap frozen, and stored at $-80\text{ }^{\circ}\text{C}$. Blood was collected via cardiac puncture and serum was isolated by centrifugation after coagulation (stored at $-80\text{ }^{\circ}\text{C}$). Serum was used for ELISA studies.

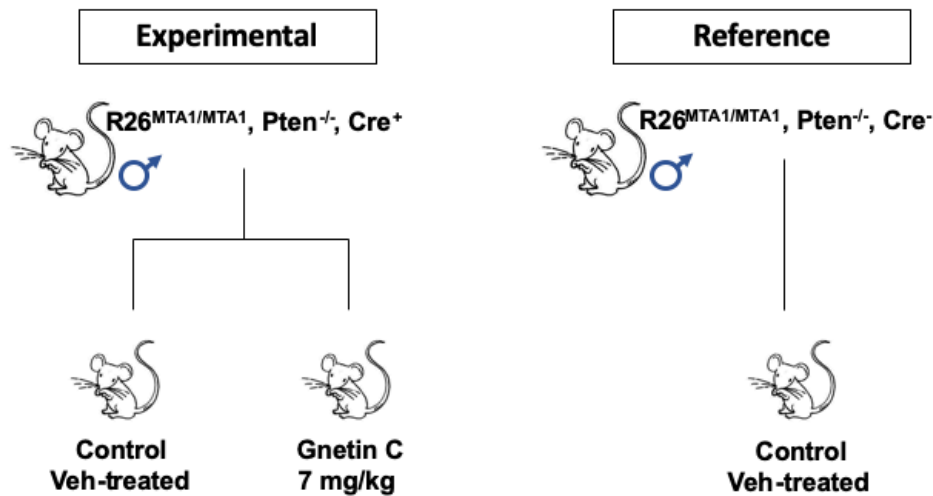


Figure 17. Schematic representation of experimental design investigating Gnetin C as active treatment in high-grade PIN model of PCa.

(vi) Generation of Subcutaneous Xenografts

22Rv1-luciferase tagged (22Rv1-Luc) cells were used to generate subcutaneous tumors in nude mice for the purpose of developing an in vivo CRPC model. The mice were housed in a sterile environment. Cages, bedding, and water were autoclaved, and food was irradiated and exposed to UV light. Mice were housed in individually ventilated cages, fed regular mouse chow, and exposed to 12-hour day/night cycles. Male *Foxn1^{nu/nu}* mice (4–5 weeks-old) were purchased from Envigo Rms, Inc (Indianapolis, IN, USA) and given time to acclimatize before being implanted with 2.5×10^6 22Rv1-Luc cells suspended in 200 μ L of 1:1 PBS/Matrigel (BD Biosciences, Bedford, MA, USA) by subcutaneous (s.c.) injection to the upper right thigh. Tumor growth was monitored by regular bioluminescent imaging and flux measurements. When flux measurements reached $\sim 1 \times 10^9$ photons/sec (p/s), a measurement equating a tumor volume of $\sim 150 \text{ mm}^3$ as determined by an earlier pilot study, treatment was commenced.

(vii) Experiment Design – CRPC Study

Mice were randomly assigned to five treatment groups: Control (vehicle), Gnetin C 40 mg/kg bw, Enzalutamide 7 mg/kg bw, Enzalutamide 10 mg/kg bw, and Gnetin C 40 mg/kg bw + Enzalutamide 7 mg/kg bw Combination. The dose selected for Gnetin C was based on previous experience with xenograft models where doses of 25 mg/kg and 50 mg/kg were used safely and effectively. Enzalutamide 10mg/kg was selected as a reference based on other publications of in vivo studies^{56,57}. A lower enzalutamide dose (7 mg/kg) was selected for the combination strategy.

Compounds were formulated in 10% DMSO in normal saline and administered by intraperitoneal (i.p.) injection daily. Although the initial goal had been to treat for 21 days, the experiment had to be terminated after 14 days of treatment due to excessively sized tumors in the control group (>700mm³). Mice were monitored daily for general wellbeing and signs of toxicity. Total body weight was measured twice weekly. Tumor dimensions were measured twice weekly using Vernier digital calipers and tumor volume was calculated according to formula, $V \text{ (mm}^3\text{)} = (\text{Length} \times \text{Width}^2)/2$. Bioluminescent images were also taken twice weekly.

For in vivo bioluminescent imaging, mice were anesthetized with inhalant, isoflurane 2%, using O₂ as the carrier gas via an XGI-8 gas anesthesia system (Caliper Life Sciences, Waltham, MA). Mice were then administered freshly prepared D-luciferin 150 mg /kg bw by i.p. injection and placed inside the IVIS Lumina LT III manifold (PerkinElmer, Waltham, MA, USA), where they received continuous anesthesia via a nose cone. Image analysis and flux measurement were performed using Living Image software (PerkinElmer, Hopkinton, MA, USA).

After sacrifice, tumors were excised, weighed, and divided into portions for further analysis. Tissues stored in 10% formalin were shipped to Reveal Biosciences (San Diego, CA) for sectioning, mounting to slides, and H&E staining. Unstained slides were later stained for proteins of interest by IHC. Tissues were also used for protein isolation and western blot analysis, and tissues stored in RNAlater (ThermoFisher Scientific) were used for RNA studies. Serum was collected by cardiac puncture.

Western Blot Analysis

Western blot analysis was used to semi-quantitate the protein of interest isolated from cells or tissue. Protein lysates were prepared from cells or homogenized tissue using Pierce RIPA and Extraction Buffer (ThermoFisher Scientific). Phosphatase and Protease inhibitors (ThermoFisher Scientific) were added to prevent degradation or enzymatic modification.

Protein quantification was performed using the Bradford Reagent Assay (ThermoFisher Scientific, USA) on a SmartSpec 3000 spectrophotometer (Bio-Rad Laboratories, Hercules, CA). Bovine Serum Albumen (ThermoFisher Scientific, USA) was used to prepare protein standards for the purpose of constructing standard curves of absorbance versus concentration.

Protein lysates were used to prepare samples containing an equal amount of total protein. 2X Laemmli sample buffer (Bio-Rad Laboratories, Hercules, CA) and β -mercaptoethanol (Bio-Rad Laboratories, Hercules, CA) were incorporated into the sample recipe to denature the proteins,

which is required for protein migration during polyacrylamide gel electrophoresis (PAGE). Samples were also boiled to aid in denaturation.

Samples containing 50 µg of protein were resolved on 10 % sodium dodecyl sulphate polyacrylamide gels. Precision Plus Protein Standard (Bio-Rad Laboratories, Hercules, CA) was used as a reference for molecular weight. Electricity was applied at 100 V for 2 hours at room temperature in a Mini-PROTEAN vertical electrophoresis cell (Bio-Rad Laboratories, Hercules, CA). This would cause negatively charged proteins to migrate towards the positively charged cathode, during which, proteins would separate according to their molecular weight, with smaller molecules traveling faster and furthest through the gel.

The proteins were then transferred onto a methanol-activated polyvinylidene difluoride (PVDF) membrane. A transfer 'sandwich' was assembled (Figure 18), and clamped tightly together to exclude air. The sandwich was submerged in transfer buffer (containing 25 mM Tris-HCl pH 8.3, 192 mM glycine, 20 % methanol) and electricity was applied at 200mA for 2 hours at room temperature (ice pack was included to prevent overheating). During transfer, negatively-charged proteins migrate towards the positively-charged electrode, but become immobilized when they encounter the PVDF membrane.

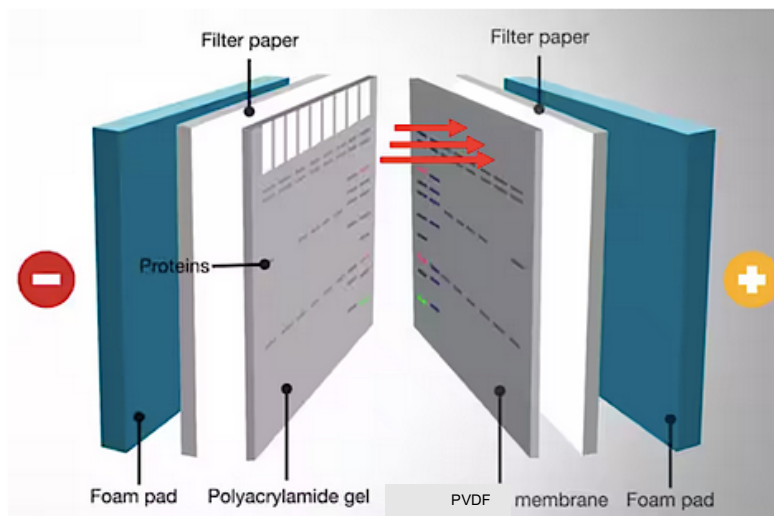


Figure 18. Gel-membrane transfer sandwich⁵⁷.

The membrane was blocked using 5 % non-fat dry milk in TBS-Tween 20 for an hour, and then probed for the protein of interest using primary antibodies overnight at 4 °C. This was followed by incubation with a secondary antibody (conjugated with horse-radish peroxidase (HRP)) for 1 hour at room temperature (Table 3). The secondary antibody binds to the primary antibody, which in turn is bound to the protein of interest.

Table 3. *Antibodies used for western blot and their dilution ratios.*

Protein of Interest	Primary Ab	Primary Ab Dilution ratio	Secondary Ab (IgG-HRP)	Secondary Ab Dilution ratio
MTA1	Cell Signaling Technology Danvers, USA (D40D1) Rabbit	1:1000	Goat Anti-Rabbit, Sigma- Aldrich St Louis, USA (A0545)	1:2500
AR	Santa Cruz Biotechnology Dallas, USA (sc-7305) Mouse	1:500	Goat Anti-Mouse Santa Cruz Biotechnology Dallas, USA (sc-2005)	1:2500
PTEN	Cell Signaling Technology Danvers, USA (D11E1) Rabbit	1:1000	Goat Anti-Rabbit, Sigma- Aldrich St Louis, USA (A0545)	1:2500
β -actin	Santa Cruz Biotechnology Dallas, USA (sc-47778), Mouse	1:2500	Goat Anti-Mouse Santa Cruz Biotechnology Dallas, USA (sc-2005)	1:2500

The blot was then developed using an enhanced luminol-based chemiluminescent (HRP-substrate) (ThermoScientific SupersignalWest Dura Extended Duration Substrate). The protein of interest, detectable as a band, was visible using the Amersham Imager 600 (GE Healthcare). The optical density of the band is directly proportional to the amount of the protein in the sample. Image J Software (NIH, Bethesda, MD) was used to measure the densitometry of the bands. Analysis was conducted by normalizing against a house-keeping protein: β -actin, GAPDH, or Hsp70. Such semi-quantitative analysis allows us to draw conclusions about the relative protein expression in cells or tissue after a treatment.

qRT-PCR

Total RNA was isolated from cell lines or tumor tissues using the miRNeasy Kit (Qiagen, USA). Seven hundred (700) μL of QIAzol (Qiagen, USA), a phenol/guanidine-based lysis reagent was used to lyse cells or tissue and denature proteins. The lysate was then transferred to the QIAshredder spin-column (Qiagen, USA) for additional lysing, followed by a 5-minute incubation period at room temperature to promote the dissociation of nucleoprotein complexes.

One hundred and forty (140) μL of chloroform (Qiagen, USA) was added to each lysate and mixed thoroughly. After centrifugation, the sample separated into 3 immiscible phases: a clear upper aqueous layer containing RNA, a white hazy interphase containing DNA, and a lower red, organic layer containing proteins and lipids. The upper aqueous phase was isolated and mixed thoroughly with absolute ethanol, resulting in the precipitation of RNA.

The sample was then transferred into a spin column (Qiagen, USA) and centrifuged. The follow-through was discarded, but the RNA remained bound to the silica membrane within the spin column. The RNA then underwent a series of washes using RWT buffer (Qiagen, USA) to remove biomolecules (carbohydrates, proteins, fatty acids etc.), and RPE buffer (Qiagen, USA) to remove traces of salts. The RNA on the membrane was then eluted in RNase-free H_2O , and a NanoDrop spectrophotometer (Shimadzu Scientific Instruments) was used to determine RNA concentration and purity.

This RNA was used as a template from which cDNA would be synthesized. PCR reactions were performed for each sample using SuperScriptIII First Strand Synthesis System (Invitrogen). Each

reaction consisted of 1 µg of RNA template, random hexamer primers, and deoxynucleotide triphosphate (dNTP). The mixture was heated to 65 °C for 5 minutes, during which time, the secondary structure of RNA denatures to form straight chains and the primer anneals to the RNA molecule. In a second reaction, reverse transcriptase (RT), RNase Out, dithiothreitol (DTT) 0.1 M, MgCl₂ 25 mM, and 10X RT buffer were combined. RNase Out is an RNase inhibitor and DTT is a reducing agent, both serving to prevent the degradation of RNA by inactivating enzymes with RNase activity. Equal volume of this mixture is added to the previous RNA mixture and subjected to one cycle of 25 °C for 10 min, followed by 50 °C for 50 min which is required for RT to synthesize one complementary strand of DNA hybridized to the original RNA strand. Finally, the temperature is raised to 85 °C for 5 min, which inactivates RT, ensuring only one strand of cDNA is produced. After cooling, RNase H (1 µL) is added to the mixture and incubated to 37 °C for 20 min. Its purpose is to digest the RNA from the hybrid strand.

The cDNA was diluted by a factor of 5 and mixed with gene-specific primer pairs which flank the target region (gene) intended for amplification (Table 4). SYBR Green master mix (ThermoFisher Scientific), a fluorescent dye, was added to the reaction mixture. SYBR Green selectively binds to double-stranded DNA as it forms during PCR, emitting a fluorescence as it intercalates between DNA bases. Each reaction was set up in a 96-well plate (25 µL per reaction), and carried out in triplicate. β-actin served as the reference house-keeping gene. The experiment was run on a LightCycler 480II (Roche, CA, USA), which detects the accumulation of the SYBR Green signal and reports the cycle threshold (Ct) value, which is the number of cycles required for signal detectability. Data was analyzed using the double-delta Ct method.

Table 4. Sequence of qPCR primer pairs used in this study.

Target	Sense strand	Anti-sense strand
MTA1	5'-AGC TAC GAG CAG CAC AAC GGG GT-3'	5'-CAC GCT TGG TTT CCG AGG AT- 3'
AR	5' GTGCTGGACACGACAACAAC 3'	5' ACTTGTGCATGCGGTACTCA 3'
PSA	5' AGTTCATGCTGTGTGCTGGA 3'	5' TCCAATTCCGGTAATGCACC 3'
β -actin	5'-CGT GGG CCG CCC TAG GCA CCA-3'	5'TTGGCTTAGGGTTCAGGGGGG 3'

Immunohistochemistry (IHC)

Tumors were dissected, fixed in 10 % formalin and shipped to Reveal Biosciences Inc. (San Diego, CA, USA) for tissue sectioning for hematoxylin and eosin (H&E) staining and IHC. The sections, which had been mounted onto glass slides, were then deparaffinized using heat and xylene, and rehydrated. Antigen retrieval was performed by boiling the slides in Antigen Unmasking Solution (Vector Labs, CA) for 30 min in a steamer. Slides were cooled and endogenous peroxidase activity was quenched using 3 % H₂O₂ for 5 min. Blocking was performed to prevent non-specific binding by using serum from the Vectastain ABC Elite Kit (Vector Laboratories, Burlingame, CA, USA) and incubating with the tissues for 30 minutes. This was followed by incubation with primary antibody targeting the protein of interest overnight at 4 °C (Table 5).

Table 5. Antibodies used for IHC and their dilution ratios

Protein of Interest	Primary Ab	Primary Ab Dilution ratio
Ki-67	Abcam Waltham, USA (ab16667) Rabbit	1:200
AR	Santa Cruz Biotechnology Dallas, USA (sc-816) Rabbit	1:500
MTA1	Cell Signaling Technology Danvers, USA (D48D1) Rabbit	1:50
PTEN	Cell Signaling Technology Danvers, USA (D11E1) Rabbit	1:150
CD31	Cell Signaling Technology Danvers, USA (D8V9E) Rabbit	1:500
Cleaved caspase 3	Cell Signaling Technology Danvers, USA (5A1E) Rabbit	1:100

The following day, sections were washed and incubated with the appropriate biotinylated secondary antibodies from the Vectastain ABC kit for 30 minutes at room temperature. To enhance the signal, the sections were incubated with ABC staining reagent (included in the VectaStain kit) for 30 minutes. The ABC staining reagent consists of HRP bound to avidin, a tetrameric biotin-binding protein, which binds to the secondary antibody resulting in a greater concentration of HRP enzyme at the antigenic site. The staining was developed using chromagen (ImmPACT DAB kit from Vector Labs, CA), which is the substrate for HRP. Slides were also counterstained with hematoxylin. The sections were then dehydrated and cleared using xylene. They were finally mounted with a cover slip.

Images were taken using the EVOS XL Core microscope (Life Technologies). Five randomly selected fields per slide were used for quantitation using ImageJ 1.50i software (NIH, Bethesda, MD, USA). Cells positively stained for Ki-67 were counted and expressed as a percentage of total cells, and cells stained for CD31 were expressed in terms of area. Cells stained for AR and MTA1 were given a staining intensity grade. A grade of one (1) was assigned to cells of lowest stain intensity through to four (4) for highest intensity. The grade was multiplied by the cell frequency to give a grade score. The grade scores were then added to give a total stain score. Glands displaying characteristics of PIN were counted and expressed as a percentage of total glands.

ELISA (Enzyme-Linked immunosorbent Assay)

Serum IL-2 and IL-6 levels were analyzed using commercially available Mouse IL-2 and IL-6 ELISA kits (Abcam, Boston, MA, USA). Pure standards were prepared using standard powder included in each kit. Concentrations ranging 0 - 1000 pg/mL were achieved by serial dilution. For IL-2 analysis, undiluted samples or standards of 50 μ L were added to the pre-coated 96-well strip tubes covered with an anti-tag antibody. The antibody cocktail (50 μ L) was then added and the mixture was allowed to incubate for 1 hour at room temperature on a shaker at 300 rpm. After three washings, 100 μ L of Streptavidin-HRP solution was added to each well and incubated for 1 hour at room temperature with gentle shaking. This was followed by three washings, after which, 100 μ L of 3, 3',5,5'-tetramethylbenzidine (TMB) developing solution was added to each well and allowed to incubate for 10 minutes with aggressive shaking. Immediately afterwards, 100 μ L of STOP solution was added and allowed to incubate for 1 minute. The OD values were then

measured at 450 nm using a Tecan Sunrise Absorbance microplate reader (Tecan, Mannedorf, Switzerland). The concentrations of IL-2 and IL-6 were estimated based on the standard curve.

Pharmacokinetic Studies

(i) Experiment Design – Single-Dose Study

Cre-negative, wild-type male transgenic mice were randomly selected for the PK study. The mice were 8-12 weeks old, weighed an average of 20 g, and had not received other treatment or been involved in any other study. They were fed regular mouse chow *ad libitum* and subjected to 12-hour day/night cycles.

On the morning of the study (at $t = 0$ min), all mice were administered Gnetin C (25 mg/kg) by i.p. injection. Then, blood was drawn from a single mouse at the following time points: $t = 15$ min, 30 min, 1 h, 2 h, 4 h, 6 h, and 12 h. Blood was collected by cardiac puncture after sacrifice by CO₂ asphyxiation.

(ii) Sample Preparation

After collection, whole blood was allowed to coagulate by leaving it undisturbed for 30-45 minutes at room temperature. Serum was isolated by centrifuging at 13,000 rpm for 10 minutes and collecting the resultant supernatant. It was stored at -80 °C until analyzed. Additional serum samples obtained from untreated mice were later used for the preparation of calibration standards.

To each serum sample, 200 μ L of diluent (0.1 % formic acid and acetonitrile at a ratio of 7:3 respectively) and 1 mL of diethyl ether (VWR Chemicals BDH; Radnor, PA, USA) were added. The samples were then centrifuged (Eppendorf 5810R; Hamburg, Germany) at 13,000 rpm, 4 $^{\circ}$ C for 5 min, and the supernatant was transferred to a clean microcentrifuge tube, where the diluent/solvent was evaporated off. The dried residue was reconstituted with 200 μ L of diluent and transferred to a glass insert for UPLC analysis.

Calibration standards were prepared by spiking blank serum with 200 μ L of standard solutions having Gnetin C concentrations of 0, 10, 50, 100, 500, and 1000 ng/mL . These were then subjected to the same extraction procedure described above for samples.

(iii) Instrumental Analysis: Determination of Gnetin C Concentrations by UPLC

Samples were analyzed by Ultra Performance Liquid Chromatography (UPLC) coupled with UV detection (Waters Acquity UPLC system, Milford, MA, USA). Separation was performed at room temperature using a reversed-phase column (Acquity UPLC BEH phenyl, 2.1 \times 50 mm, 1.7 μ m). 10 μ L samples were injected with an autosampler maintained at 10 $^{\circ}$ C. The mobile phase, consisting of 0.1% formic acid and acetonitrile, was pumped at a flow rate of 0.4 mL/min. The gradient system was used as follows: 20% acetonitrile (0-1 min), 20-50% acetonitrile (1-5 min), 50% acetonitrile (5-6 min), 50-20% acetonitrile (6-6.5 min), and linear gradient, 20% acetonitrile (6.5-8 min) for re-equilibration. The retention time for Gnetin C was 5.2 mins, and it was detected at a wavelength of 321 nm. Data acquisition was processed with Empower 3 software.

(iv) Data Analysis

The serum concentrations were plotted vs. time and analyzed using the Noncompartment Analysis (NCA) approach. C_{max} and T_{max} were estimated from the plot. The elimination rate constant (k) was estimated from the terminal slope of the log-transformed data. Area under the curve (AUC) was estimated using the trapezoidal rule:

$$AUC_{0-12h} = \frac{1}{2}(C_1 + C_2)(t_2 - t_1)$$

$$AUC_{0-\infty} = AUC_{0-12h} + \frac{C_{last}}{k}$$

Half-life ($t_{1/2}$) was estimated according to the formula:

$$t_{1/2} = \frac{0.693}{k}$$

Clearance (CL) was estimated according to the following formula:

$$CL/F = \frac{Dose}{AUC_{0-\infty}}$$

where F = fraction absorbed (bioavailability).

Clearance must be defined as CL/F because an absorption phase is required with the intraperitoneal route of administration. Therefore, F is not necessarily equal to 1.

Volume of distribution (Vd) was estimated according to the following formula:

$$Vd/F = \frac{Dose}{AUC_{0-\infty}} \left(\frac{1}{k} \right) = \frac{CL}{F} \left(\frac{1}{k} \right)$$

Statistical Analysis

Values are expressed as the mean \pm SEM of three independent experiments. Experiments with two experimental groups were analyzed using Student's two-tailed t-test; whereas experiments with more than two experimental groups were analyzed using one-way ANOVA. Two-way ANOVA was used when the dependent variable was analyzed on more than one occasion throughout the experiment (rather than at the end only). All graphs were plotted and analyzed using GraphPad Prism 9.0.2 (GraphPad Software, San Diego, CA, USA). The differences were considered significant when $p < 0.05$.

CHAPTER IV. RESULTS

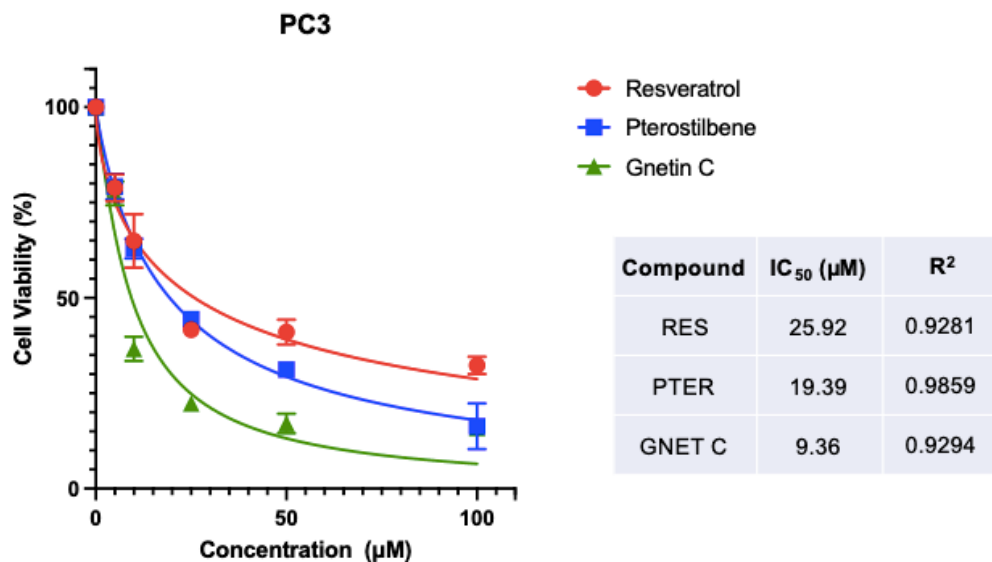
Preliminary In Vitro Investigations

(i) Gnetin C demonstrates greater cytotoxicity in PC3 and 22Rv1 cells compared to resveratrol and pterostilbene

MTT cell viability assays were conducted to compare the cytotoxicity of resveratrol, pterostilbene and Gnetin C in aggressive PC3 and 22Rv1 PCa cell lines. Both cell lines overexpress MTA1. PC3 has lost the expression of PTEN, PSA, and AR; whereas 22Rv1 expresses both full-length AR and androgen-independent AR-V7. The cells were treated with resveratrol, pterostilbene, and Gnetin C for 72 hours in concentrations ranging 5-100 μ M. Treatments were replenished every 24 hours.

The results demonstrated that Gnetin C has the lowest IC₅₀ value, suggesting that it is more potent in inhibiting PC3 and 22Rv1 cells compared to resveratrol and pterostilbene (Figure 19). This greater potency of Gnetin C may be, at least partially, due to more efficient targeting of MTA1, AR, and AR-V7. As expected, pterostilbene showed greater potency compared to resveratrol.

A



B

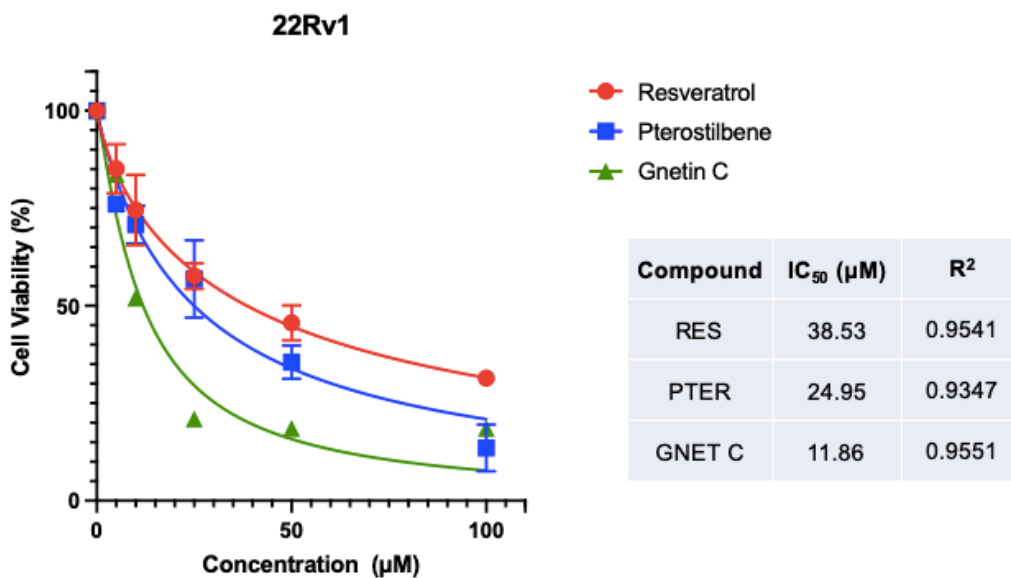


Figure 19. Representative MTT assays in PC3 (A) and 22Rv1 (B) cells after treating with resveratrol (RES), pterostilbene (PTER) and Gnetin C (GNET C). Corresponding IC₅₀ values are tabulated (right). Data represent mean \pm SEM of three independent experiments performed in triplicate. Data determined to be statistically non-significant by one-way ANOVA.

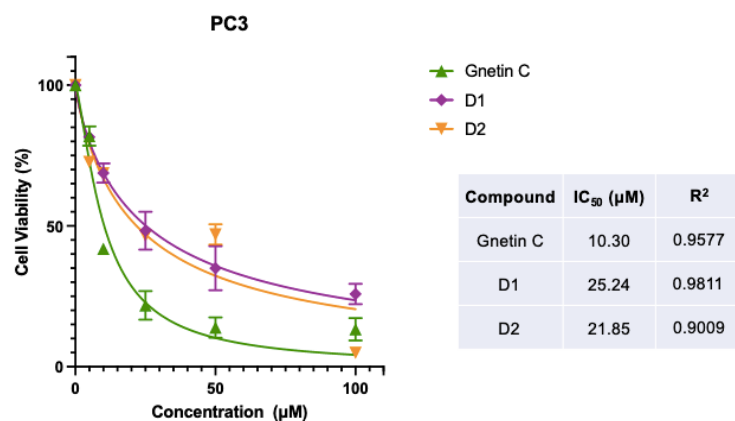
(ii) Gnetin C demonstrates greater cytotoxicity compared to synthetic stilbene analogs

MTT cell viability assays were conducted to compare BT-546 (D1), BT-547 (D2), and Gnetin C in their ability to inhibit PC3, PC3M, and 22Rv1 cells. PC3M is a highly malignant variant of the PC3 cell line. Like PC3, PC3M overexpresses MTA1, while also having lost PTEN, PSA and AR expression.

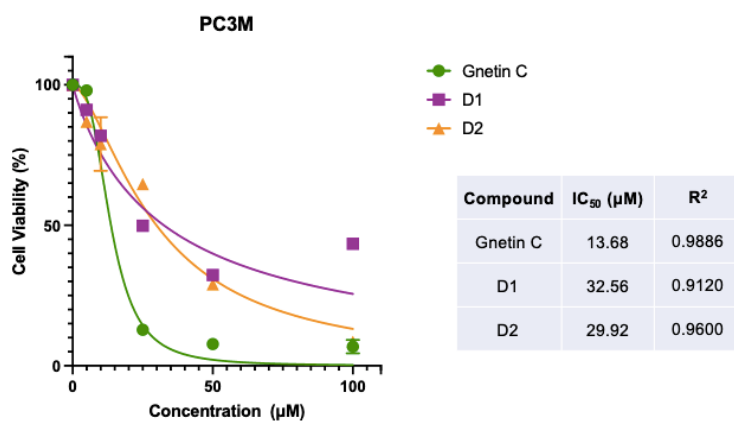
D1 and D2 were gifts donated by Dr. Bhaskar Das (Long Island University, Brooklyn), and had been freshly synthesized in-house. These new compounds, which have never been studied in PCa, are synthetic stilbene boron-containing derivatives of resveratrol. They are assumed to share a similar pharmacological activity to their parent compound. Their chemical structure cannot be revealed for proprietary reasons. The presence of boron within their structure is believed to improve their MTA1-binding capacity. For the MTT assay, the cells were treated with D1, D2, and Gnetin C for 72 hours in concentrations ranging 5-100 μ M. Treatments were replenished every 24 hours.

The results indicated that Gnetin C had the lowest IC_{50} value for each cell line, suggesting that it has greater cytotoxicity compared to D1 and D2 (Figure 20).

A



B



C

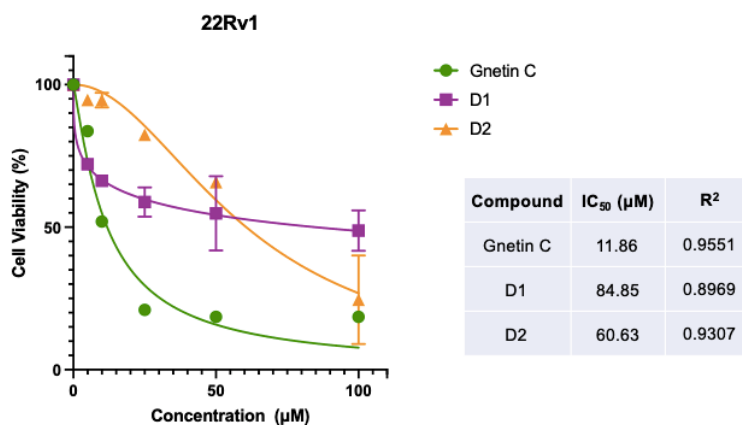


Figure 20. Representative MTT assays in PC3 (A) PC3M (B), and 22Rv1 (C) cells after treating with Gnetin C, D1 and D2. Corresponding IC₅₀ values are tabulated (right). Data represent mean ± SEM of three independent experiments performed in triplicate. Data determined to be statistically non-significant by one-way ANOVA.

Aim 1: Gnetin C as a Chemopreventive Agent in High-Risk PCa Model

Aim 1 involves the use of transgenic mice with the genotype: $R26^{MTA1/MTA1}; Pten^{+/-}; Cre^{+}$ (*MTA1* overexpression and *Pten* heterozygosity). This genotype typically represents a high-risk PCa model characterized histologically by high-grade PIN by 20 weeks of age⁴¹. It is an ideal model in which to study Gnetin C as a dietary chemopreventive agent for PCa.

(i) Experimental design - revisited

When male mice with the desired genotype were weaned from their mother (3-4 weeks of age), they were randomly assigned to one of four study groups (n = 6 per group) receiving the following supplemented diets:

- i. Control diet
- ii. Gnetin C 35mg/kg – low concentration (Gnetin C₃₅ diet)
- iii. Gnetin C 70mg/kg – high concentration (Gnetin C₇₀ diet)
- iv. Pterostilbene 70mg/kg (Pter₇₀ diet)

Mice were fed *ad libitum* for the duration of the study (17 weeks). Body weight and food intake measurements were made weekly. At the study's conclusion, the mice were sacrificed, and blood and UGS were collected and used for histological and molecular evaluation (Figure 21).

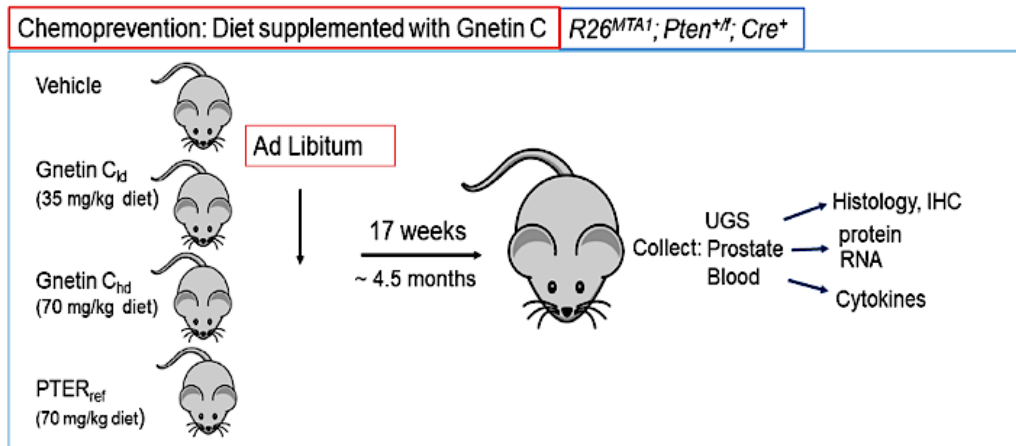


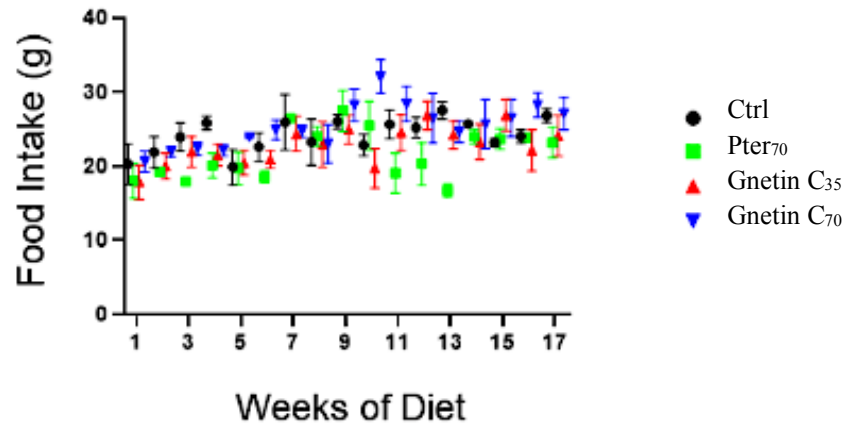
Figure 21. Flow chart depicts experimental design for study investigating the efficacy of Gnetin C as a chemopreventive strategy in a high-risk transgenic model for PCa.

(ii) Effect of Gnetin C-supplemented diet on food intake and body weight

Consumption of diet was measured by weight on a weekly basis in order to establish consistency and eliminate the potential for bias between the study groups. Body weight was also recorded weekly, and was used as a measure for possible toxicity associated with the diets.

The results showed that diet supplementation with either pterostilbene or Gnetin C did not have any significant effect on either body weight or food intake compared to control (Figure 22). There does appear to be an overall weight gain over time, but this applies to the control group as well, and is most likely attributed to other factors, such as age.

A



B

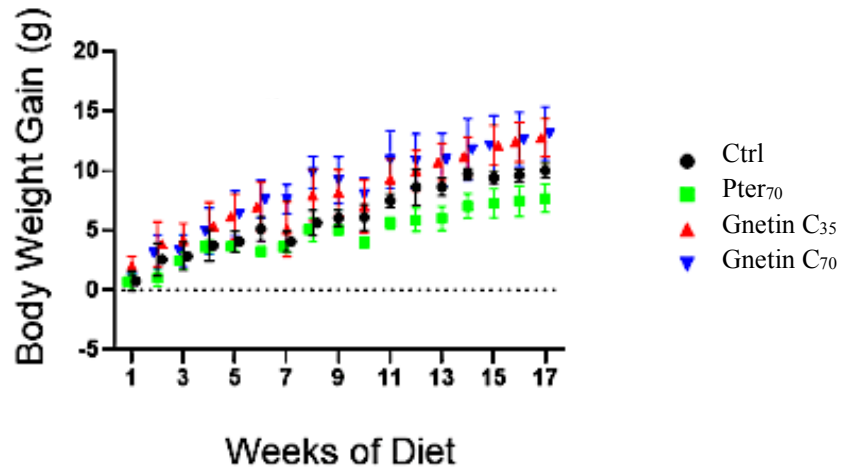


Figure 22. Effects of diets on food intake (A) and average body weight (B) in mice. Data represent mean \pm SEM, $n=6$ per group. Data determined to be statistically non-significant by two-way ANOVA.

(iii) Effect of Gnetin C-supplemented diet on prostate anatomy

At the end of the study, the UGS was removed and digitally recorded before being sent away for sectioning (for H&E and IHC). Mouse prostate is composed of four distinct lobes (anterior, dorsal, lateral, and ventral); whereas human prostate is a single lobe having peripheral, transition, and central zones⁵⁸. Most human PCa is found in the peripheral zone. Although some believe that the dorsolateral lobes are similar to the human peripheral zone, the general consensus is that no direct histological or pathological relationship exists between any mouse lobe and human prostate zone⁵⁹.

Figure 23 presents ex vivo UGS images of a representative mouse from each study group. The anterior lobes of the prostate can be seen outlined in black, positioned inferior to the seminal vesicles. Our results demonstrated that mice fed Gnetin C-supplemented diets (high and low concentrations) had smaller anterior prostates compared to those fed Control diet. This suggests that Gnetin C is associated with less proliferation and hyperplasia.

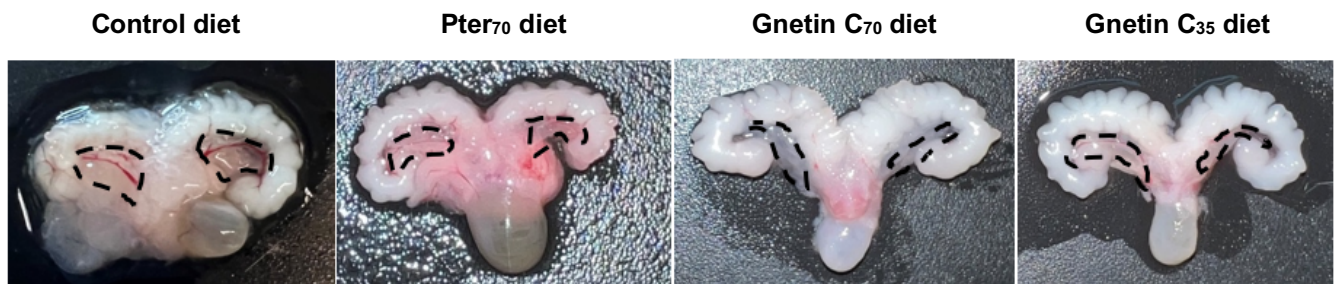


Figure 23. Representative images of UGS of mice from each study group. The anterior prostates (marked) in mice fed Gnetin C-supplemented diets were smaller compared to the Control.

(iv) Gnetin C₇₀ diet diminishes PIN progression in R26^{MTA1/MTA1}, Pten^{+/-}, Cre⁺ mice

The H&E staining of UGS tissues expectedly showed that prostates from mice fed Control diet exhibited the greatest number and severity of PIN foci. These prostates were characterized by disorganized hypercellularity, cribriform, major tufting and papillary infolding. Basement membranes were visibly intact suggesting no microinvasion had occurred, and thereby clearly exhibiting PIN by definition. Mice fed Pter₇₀, Gnetin C₇₀, and Gnetin C₃₅ diets displayed significantly less proliferation and infolding, restored ductal structures, and an overall favorable histology compared to mice fed Control diet (Figure 24). Quantitative analysis showed that mice fed Gnetin C₇₀ diet had the least number of PIN foci compared to Pter₇₀ (having the same dose) and Gnetin C₃₅ (Figure. 25).

IHC staining demonstrated that prostates of mice fed Gnetin C₇₀ diet had the lowest expression of Ki67 and CD31, suggesting this diet inhibited proliferation and angiogenesis with the greatest efficacy (Figures 24 and 25). It also inhibited MTA1 more potently than other diets. Notably, Gnetin C at half the concentration (Gnetin C₃₅) showed either the same or greater potency in inhibiting Ki67, MTA1, and CD31 compared to Pter₇₀. Although quantitative analysis was not possible for PTEN (due to cytoplasmic staining), visually we can appreciate that the staining is more intense in mice fed Gnetin C₇₀ diet compared to Control and Pter₇₀, indicating that an upregulation of PTEN is associated with this compound (Figures 24 and 25).

Taken together, these results demonstrate that chemoprevention using Gnetin C₇₀ diet had the greatest efficacy in preventing or reducing the progression of PIN. We believe that these effects are most likely mediated through MTA1 inhibition.

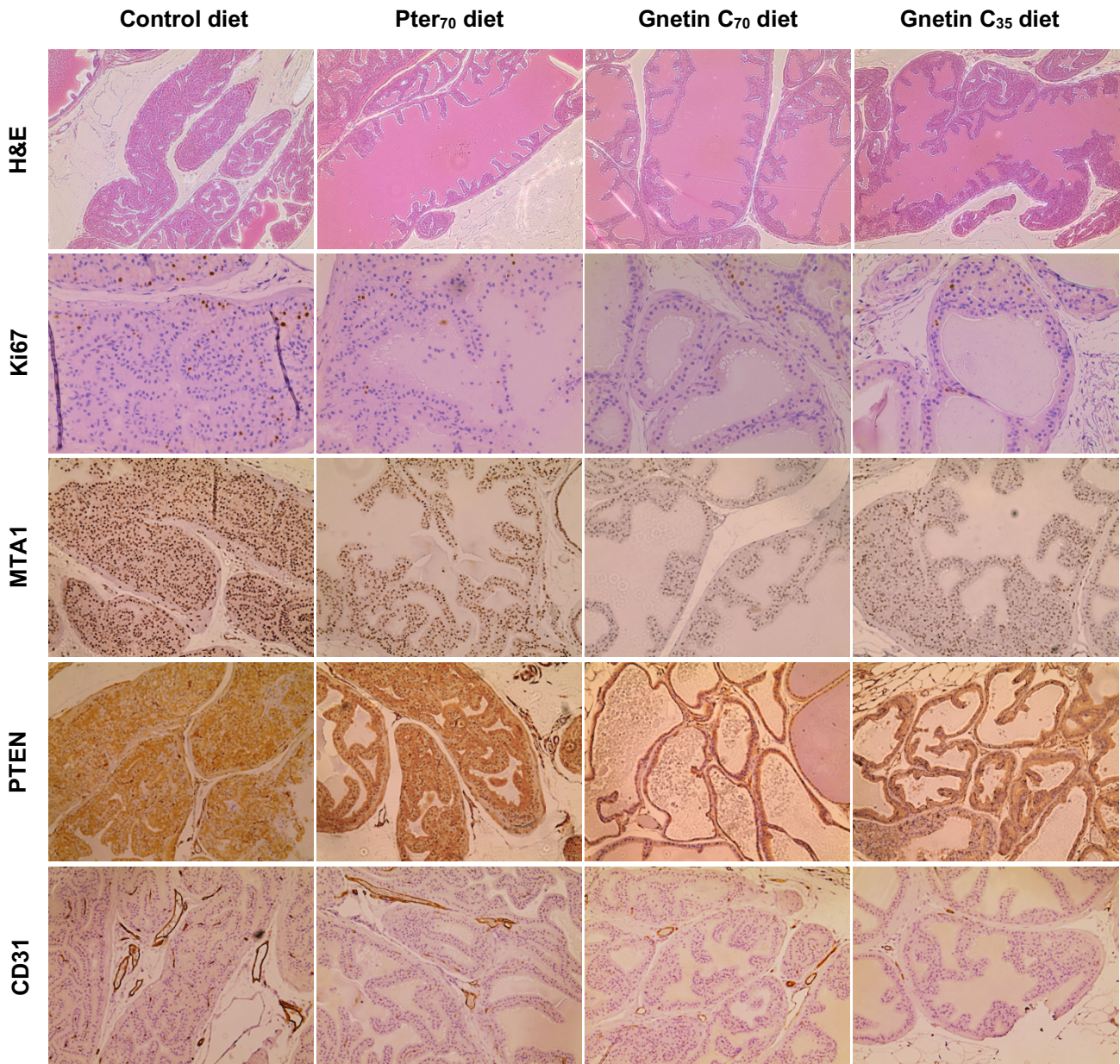


Figure 24. Representative H&E and IHC staining for Ki67, MTA1, PTEN, and CD31 in R26 MTA1/MTA1, Pten^{+/-}, Cre + mice receiving Control diet, Pter₇₀ diet, Gnetin C₇₀ diet, and Gnetin C₃₅ diet for chemoprevention of high-grade PIN. H&E images were taken at 10x. MTA1, PTEN, CD31 images were taken at 20x magnification. Ki67 images were taken at 40x magnification.

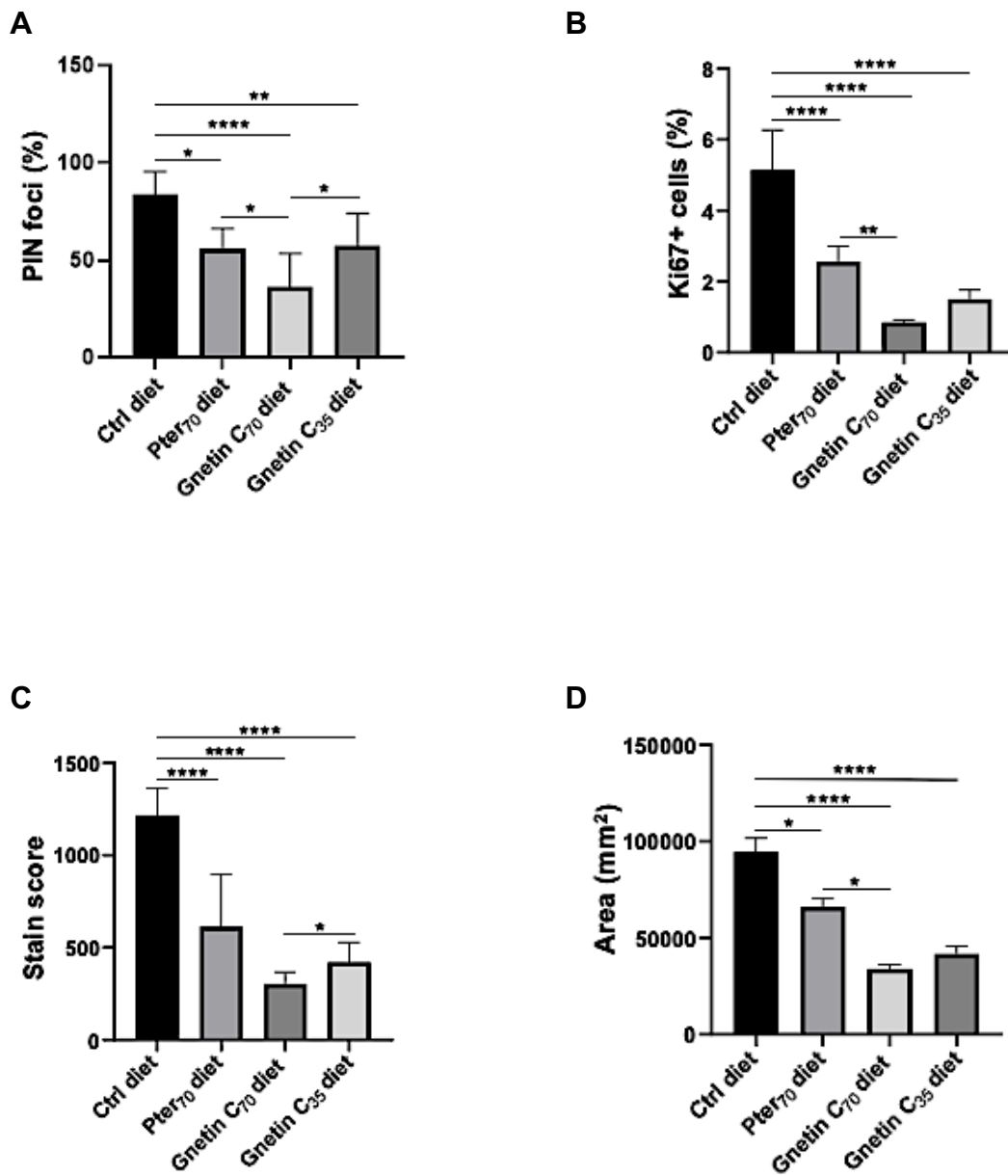


Figure 25. Quantitation for PIN foci (A) by counting the number of PIN-positive glands; expressed as a percentage. Quantitation for Ki67 (B) by counting number of stained cells; expressed as percentage. Quantitation of MTA1 (C) by assigning each cell a stain intensity value of 1-4 and multiplying this by cell frequency to determine overall stain score. Quantitation of CD31 (D) by determining area of stained cells (mm²). Data represent mean \pm SEM of glands/cells counted in five randomly selected fields per sample, n=3 per group. **p* < 0.05; ***p* < 0.01; *****p* < 0.0001 (one-way ANOVA).

(v) Effect of Gnetin C-supplemented diet on MTA1 and PTEN protein expression

Western blot was used to measure MTA1 and PTEN protein expression in prostate tissue lysates. MTA1 levels from mice fed Gnetin C- and pterostilbene-supplemented diets were significantly reduced compared to Control. Although no statistical significance was noted between the stilbene-supplemented diets themselves, the overall trend indicated that Gnetin C had greater potency in reducing MTA1 (Figure 26).

In blot A (Figure 26, A), MTA1 was not detected for a mouse fed Gnetin C₃₅ diet. This was most likely due to heterogeneity among subjects. Blot B (Figure 26, B) was performed to determine the MTA1 and PTEN protein expression among three mice fed Gnetin C₃₅ diet and to illustrate how heterogeneity between subjects may influence results.

In contrast to the inhibitory effects on MTA1, diets supplemented with pterostilbene and Gnetin C restored PTEN levels in prostate tissues, thus reaffirming the inverse relationship that exists between MTA1 and PTEN. Although the Pter₇₀ diet was the most effective compared to Control, Gnetin C-supplemented diets were still able to offer some benefit in restoring PTEN levels. It is believed that Gnetin C diet restores PTEN levels through MTA1-mediated signaling.

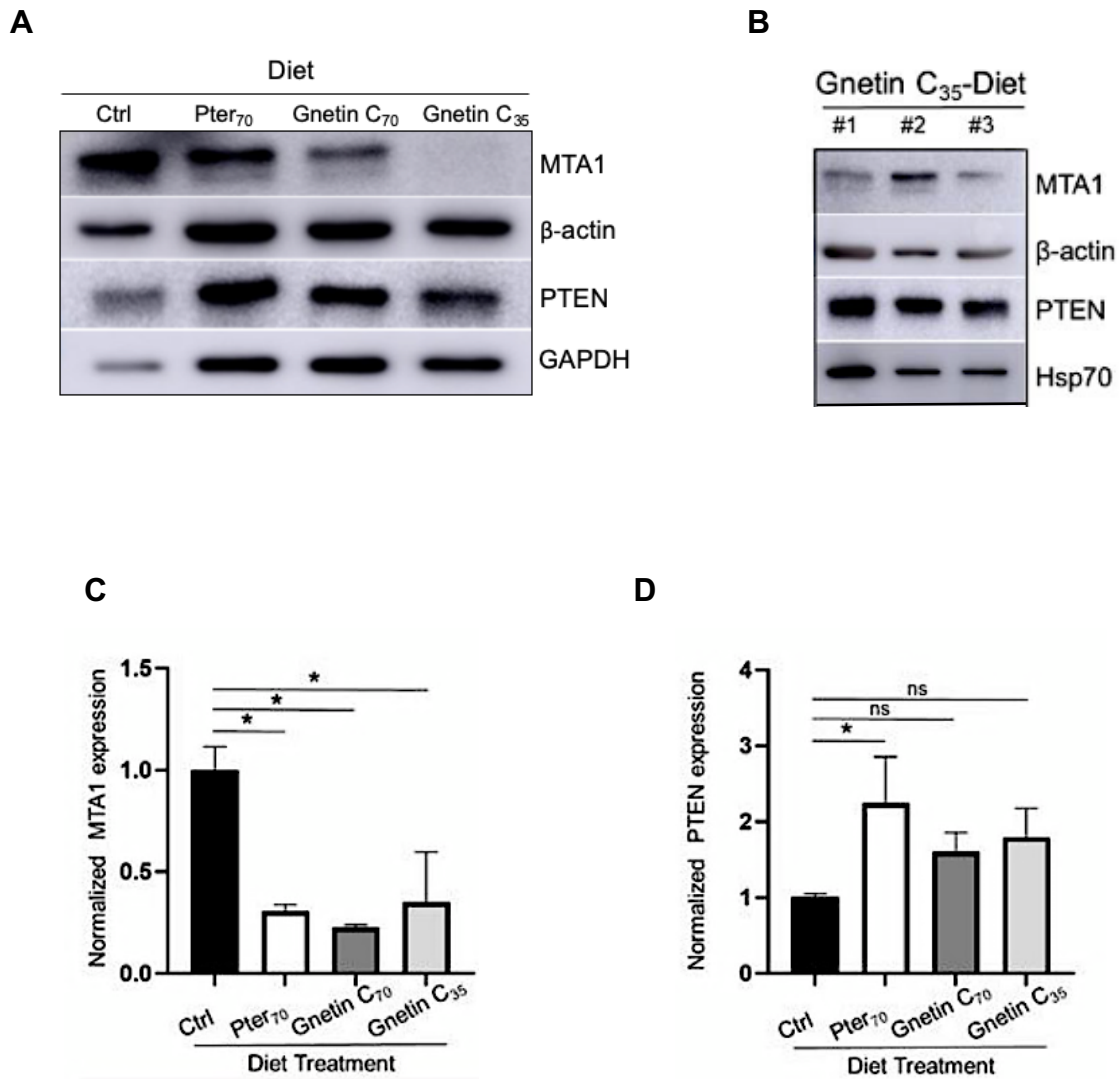


Figure 26. Representative western blot of MTA1 and PTEN protein levels in prostate tissues from mice in different study groups (A). β -actin and GAPDH were used as loading controls. Representative western blot images of MTA1 and PTEN protein levels in prostate tissues from three mice fed Gnetin C₃₅ (B). β -actin and Hsp70 were used as loading controls. Quantitation of relative expression of MTA1 and PTEN in prostate tissues from mice in different study groups (C and D). Bands were quantified by densitometry and normalized against either β -actin, GAPDH, or HSP70 using Image J software. Data represent mean \pm SEM from three independent experiments, $n=3$ per group. $*p < 0.05$ (one-way ANOVA).

I would like to give credit to Mr. P Parupathi and Ms. L Devarakonda for their assistance in conducting these western blots.

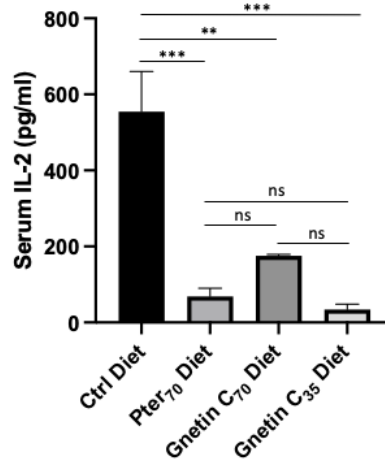
(vi) Effect of Gnetin C-supplemented diet on cytokine levels

To evaluate the effect of Gnetin C-supplemented diets on systemic inflammation, ELISA was used to determine pro-inflammatory IL-2 and IL-6 levels in mouse serum. The results showed significantly reduced levels of serum IL-2 levels in mice fed stilbene-supplemented diets compared to Control (Figure 27, A). No statistically significant difference was found between the Gnetin C- and pterostilbene-supplemented diets. Interestingly, Gnetin C supplementation at the lower concentration of 35 mg/kg (Gnetin C₃₅) reduced IL-2 levels more potently than Gnetin C₇₀ and Pter₇₀ diets.

Although not found to be statistically significant, Gnetin C₃₅ and Pter₇₀ diets reduced pro-inflammatory IL-6 serum levels compared to Control. A seemingly paradoxical increase in IL-6 levels was seen in mice fed high-concentration Gnetin C₇₀ diet (Figure 27, B). Although the result was unexpected, it is in keeping with similar reports suggesting that certain polyphenols may be more potent as anti-inflammatory and anticancer agents at lower doses⁶⁰⁻⁶².

Overall, this data suggests that low-concentration Gnetin C-supplemented diet (Gnetin C₃₅) is beneficial in reducing systemic inflammation.

A



B

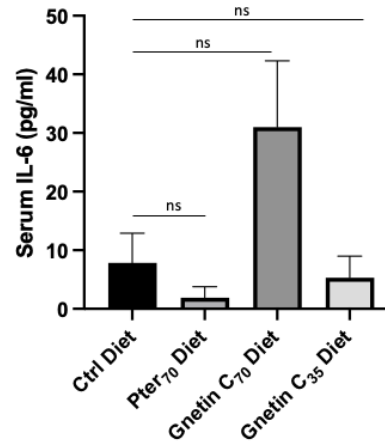


Figure 27. Effects of diets on the levels of circulating IL-2 (A) and IL-6 (B) inflammatory cytokines detected in murine serum by ELISA. Data represent mean \pm SEM of two independent experiments performed in duplicate, $n=3$ per group. ** $p < 0.01$; *** $p < 0.001$ (one-way ANOVA).

Aim 2: Gnetin C as a Therapeutic Agent in Advanced PCa Model

This study involved the use of transgenic mice with the genotype: $R26^{MTAI/MTAI}$, $Pten^{ff}$, $Pb-Cre^+$ (*MTAI* overexpression and *Pten* knockout). This genotype gives rise to a high-grade PIN PCa model. This model was used to study the efficacy of Gnetin C as a therapeutic agent in advanced PCa.

(i) Experimental design – revisited

Male mice with the desired genotype were weaned at 3-4 weeks of age, and randomly assigned to one of three study groups receiving the following treatments administered by daily i.p. injection (Figure 28):

- i. Control (vehicle), n = 3
- ii. Gnetin C 7mg/kg bw, n = 5
- iii. Reference (Cre-negative mice), n = 2

Cre-negative (wild-type) mice having normal prostate were used as a reference. The mice received their respective treatment for the duration of the study (10-12 weeks). At the end of the study, the mice were sacrificed, and blood and UGS were collected for histological and molecular evaluation.

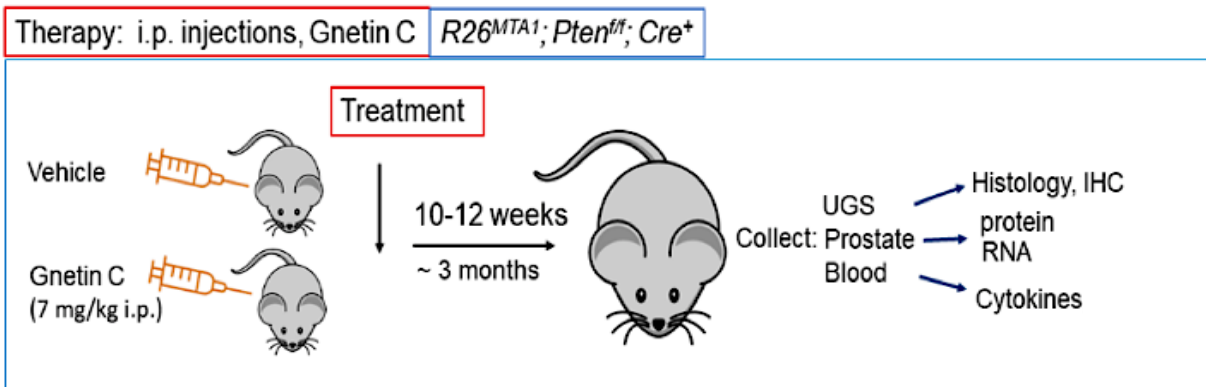


Figure 28. Experimental design for investigating the efficacy of Gnetin C as a therapeutic strategy in a transgenic model for high-grade PIN.

(ii) Gnetin C treatment improves histopathology of high-grade PIN

H&E staining of tissues from $R26^{MTA1/MTA1}; Pten^{ff}; Cre^{-}$ (wild-type) mice demonstrated the appearance of normal prostate tissue, which is typically characterized by nicely defined glands and luminal space, intact basal layer, normal continuous lining of epithelial cells, and minor infolding (Figure 29). Prostates with our experimental genotype, $R26^{MTA1/MTA1}; Pten^{ff}; Cre^{+}$, treated with vehicle (control), developed high-grade PIN with disorganized, highly proliferative, fused glandular structures, obvious cribriform, and major papillary infolding and tufting.

Prostates which had been treated with Gnetin C i.p. injection demonstrated favorable histopathology with restored ductal structures and significantly fewer PIN foci compared to vehicle-treated prostates (Figures 29 and 30). Gnetin C-treated prostates had more clearly defined epithelial lining and discernable lumen with only minor infolding.

Stained slides showed that, compared to Control, Gnetin C-treated prostates had significantly fewer Ki67-positive cells, indicating less proliferation. It also showed significantly less staining for oncogenic MTA1, as determined by the reduced intensity stain score (Figures 29 and 30). Treated tissues had significantly less staining for CD31, suggesting less angiogenesis compared to Control. Prostate tissues treated with Gnetin C also displayed significantly more cells expressing cleaved caspase-3 compared to Control and normal prostate tissue, indicating that Gnetin C is associated with an increase in apoptosis (Figures 29 and 30).

In all, these results demonstrated that, compared to Control, Gnetin C has greater efficacy in restoring prostate architecture and preventing tumor progression.

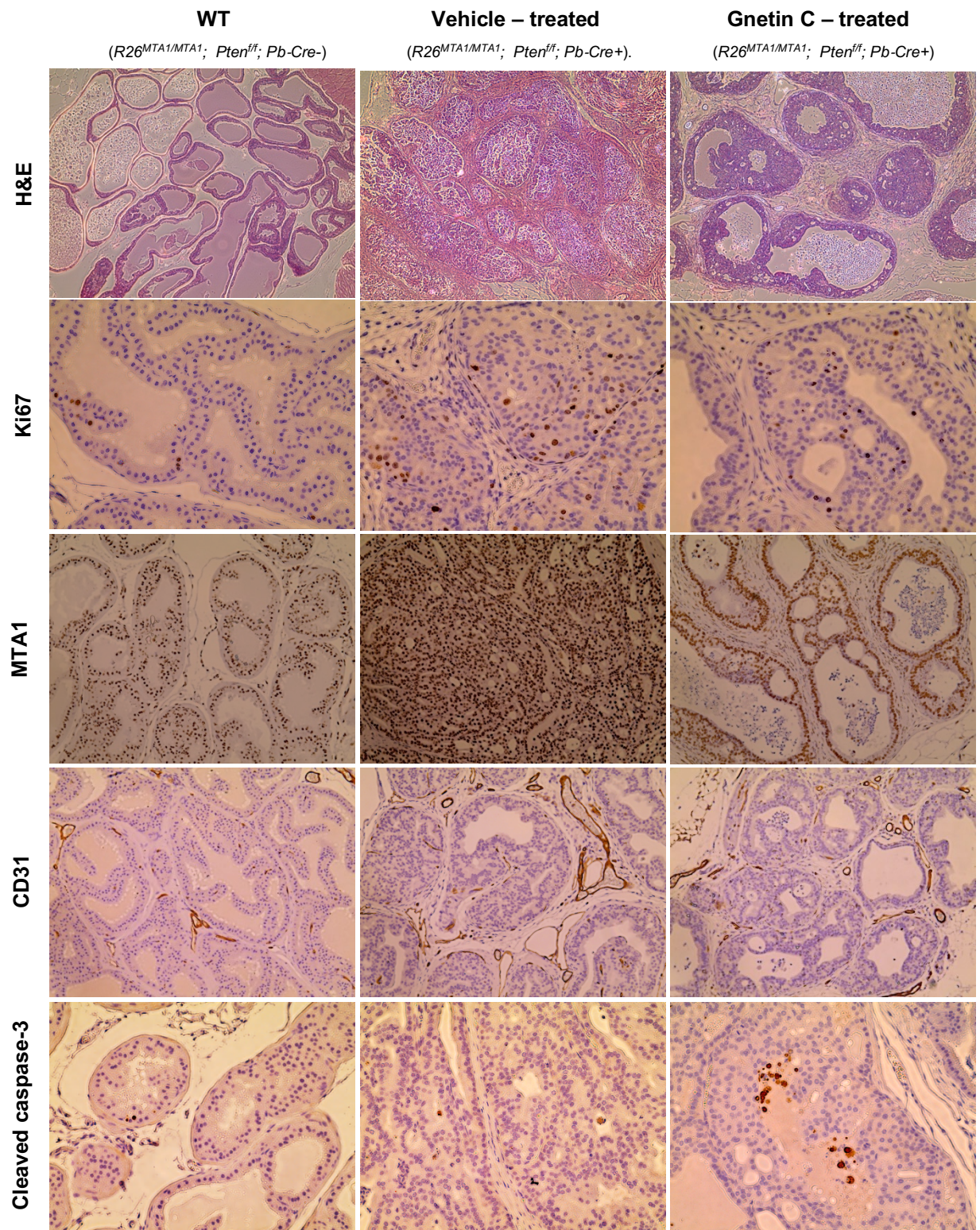


Figure 29. Representative H&E (top) and IHC staining for Ki67, MTA1, and CD31 in Cre-negative (Reference) and R26^{MTA1/MTA1};Pten^{fl/fl};Cre+ mice receiving vehicle (control) and Gnetin C i.p. 7 mg/kg. H&E images were taken at 10x; MTA1 and CD31 images were taken at 20x; Ki67 and Cl.Cas-3 images were taken at 40x magnification.

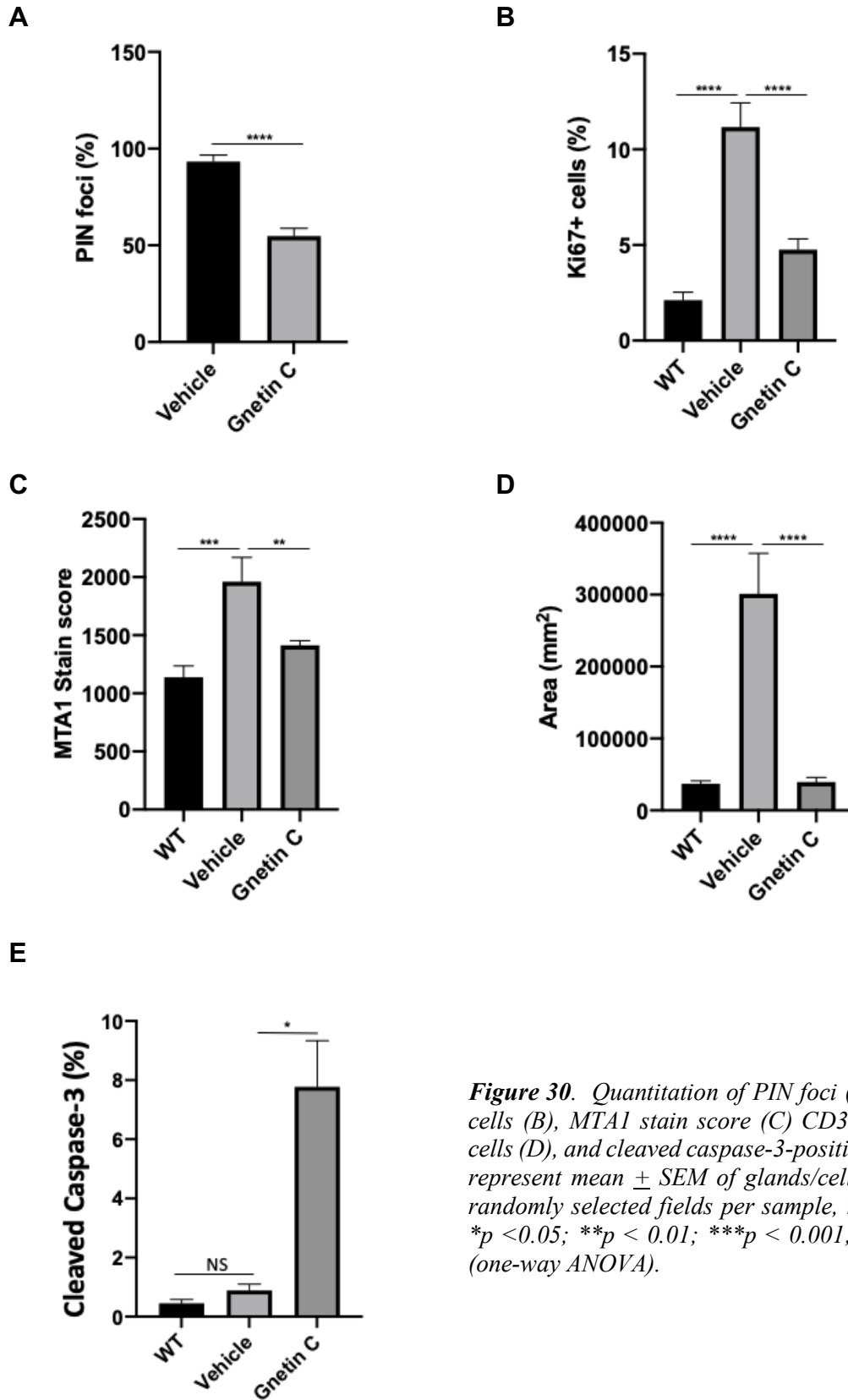


Figure 30. Quantitation of PIN foci (A), Ki67-positive cells (B), MTA1 stain score (C) CD31 area of stained cells (D), and cleaved caspase-3-positive cells (E). Data represent mean \pm SEM of glands/cells counted in five randomly selected fields per sample, n=2-5 per group. * $p < 0.05$; ** $p < 0.01$; *** $p < 0.001$; **** $p < 0.0001$ (one-way ANOVA).

(iii) Gnetin C reduces MTA1 protein expression in high-grade PIN

Prostate tissue collected at the end of the study was analyzed by western blot to evaluate MTA1 protein expression. The results demonstrated that Gnetin C significantly reduced the expression of MTA1 compared to Control (Figure 31). The variation in band density between mice within the same group is due to interindividual heterogeneity. It is believed that Gnetin C, at least partially, exerts its anticancer activity via the MTA1 pathway.

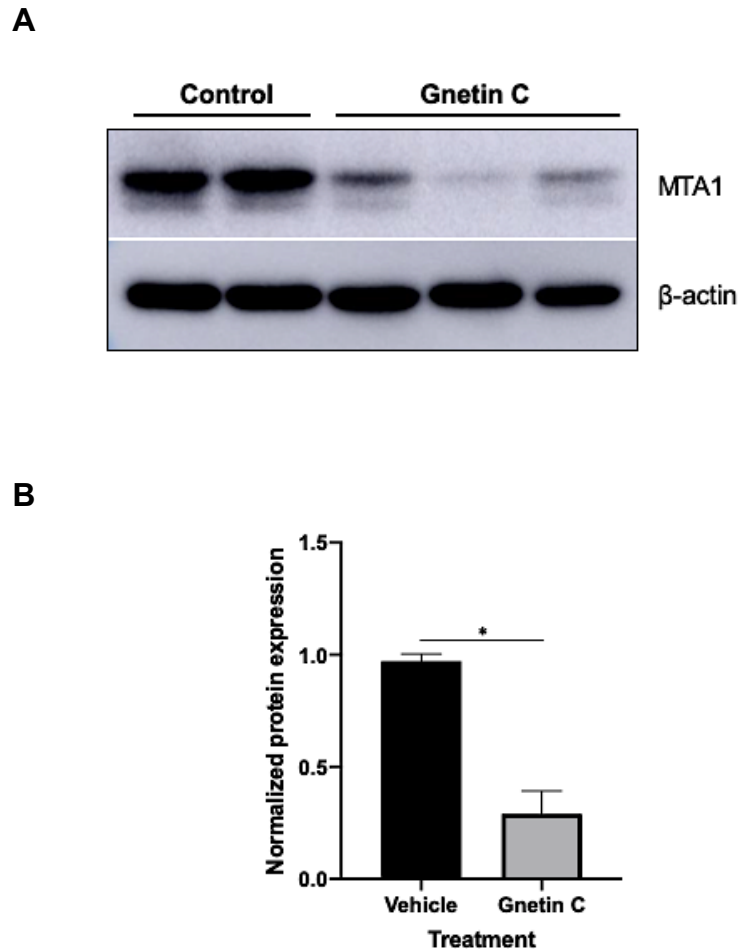


Figure 31. Representative western blot (A) and quantitation (B) showing a significant decrease in MTA1 expression in prostate tissues treated with Gnetin C. Bands were quantified by densitometry and normalized against β -actin using Image J software. Data represent mean \pm SEM, $n = 3-5$ mice per group * $p < 0.05$ (Unpaired t -test).

(iv) Effect of Gnetin C on inflammatory cytokines

To evaluate the effect of Gnetin C treatment on systemic inflammation, ELISA was used to determine pro-inflammatory IL-2 levels in mouse serum. The results showed reduced levels of circulating IL-2 in the serum of mice treated with Gnetin C compared to Control (Figure 32). Although these results were not found to be statistically significant, they demonstrate a trend towards the ability of Gnetin C to reduce inflammation associated with PCa.

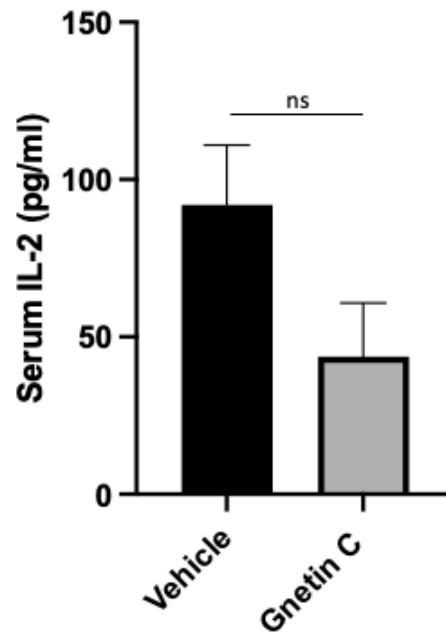


Figure 32. Effect of Gnetin C on the levels of circulating IL-2 in murine serum by ELISA. Data represent mean \pm SEM of two independent experiments performed in duplicate, $n=3$ per group. Data determined to be statistically non-significant by unpaired t -test.

Aim 3: Gnetin C as a Therapeutic Agent in a CRPC Model

The goal of Aim 3 was to better understand the role of MTA1 and AR in CRPC, and to evaluate the efficacy of Gnetin C in targeting these signaling pathways. We also wanted to learn whether Gnetin C might be able to chemosensitize cancer cells to enzalutamide and offer added benefits through use of combined therapy.

Subcutaneous xenograft generated by 22Rv1 cells was used as the CRPC model. 22Rv1 cells were selected because they express full-length AR, AR-V7, and MTA1. These are known to be important molecular drivers of CRPC.

(i) Generation of 22Rv1 MTA1-knockdown cells

To better understand the role of MTA1 and its signaling in CRPC, a 22Rv1 MTA1-knockdown model was generated. Should the expression or tumor-promoting effect of an oncogene diminish in an MTA1-knockdown model (and conversely, increase in an overexpression model), we can surmise that a positively correlated relationship exists between MTA1 and that marker.

Using the GIPZ lentiviral shRNA system, five 22Rv1 knockdowns were established:

- i. shNS (non-silencing negative control)
- ii. shGAPDH (specificity control)
- iii. shMTA1 #1 (clone 1)
- iv. shMTA1 #2 (clone 2)
- v. shMTA1 #3 (clone 3)

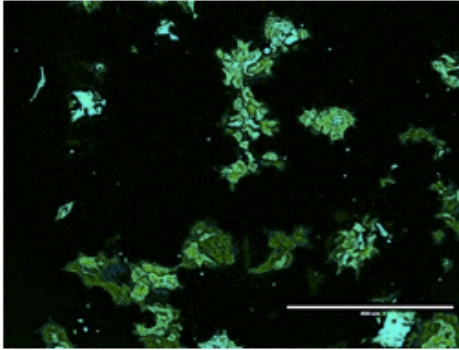
N.B. These knockdown cells are intended for mechanistic studies that are beyond the scope of this particular dissertation.

The GIPZ lentiviral shRNA system also contains a TurboGFP reporter gene. Accordingly, fluorescence microscopy was used to confirm that cells were successfully transduced (Figure 33). GFP transfection efficiency was not quantitated. These results are based on visual detectability only.

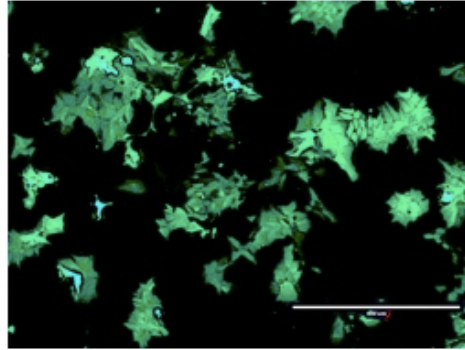
Protein and RNA lysates from knockdown cells were analyzed by western blot and qRT-PCR, respectively, in order to validate transduction and to compare the MTA1-knockdown efficiency across the three clones (#1, #2, #3). Whichever clone demonstrates the greatest degree of MTA1 knockdown will be selected for future mechanistic studies. Western blot results demonstrated that, compared to shNS control cells, all three shMTA1 clones were capable of significantly reducing the protein expression of MTA1, having no statistically significant difference with respect to each other. The trend, however, points to clone #3 as being the most efficient in knocking down MTA1 (Figure 34, A).

qRT-PCR results corresponded favorably with the western blot data (Figure 34, B). These showed a statistically significant reduction in MTA1 mRNA levels for all three shMTA1 clones compared to shNS control, with clone #3 showing the most efficient knock down at the transcription level. 22Rv1 shMTA1 #3 will most likely be selected for experiments that follow.

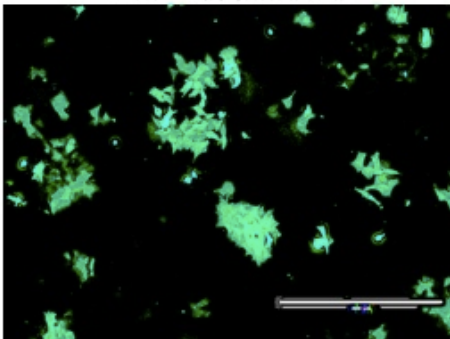
22Rv1 shNS



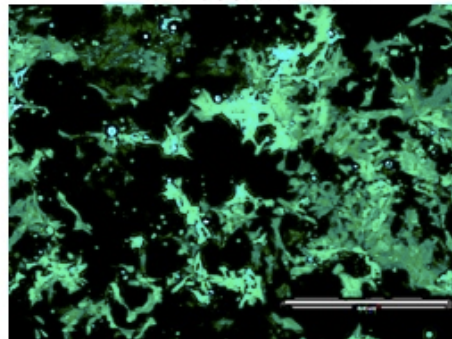
22Rv1 shGAPDH



22Rv1 shMTA1 #1



22Rv1 shMTA1 #2



22Rv1 shMTA1 #3

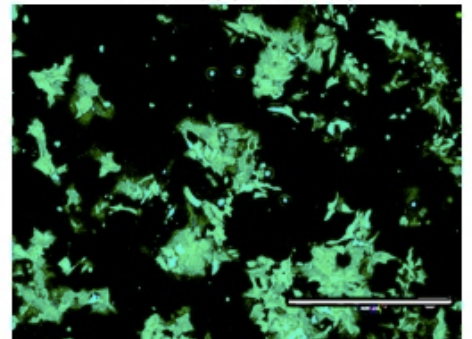


Figure 33. GFP expression was detected for all knockdowns by fluorescence microscopy (10x). GFP expression was not quantitated for this experiment.

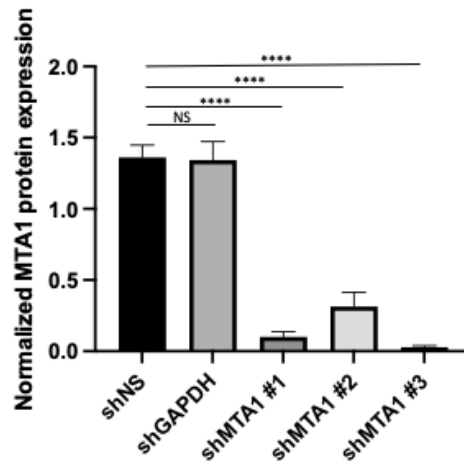
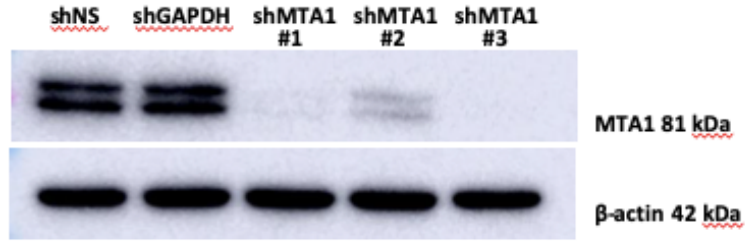
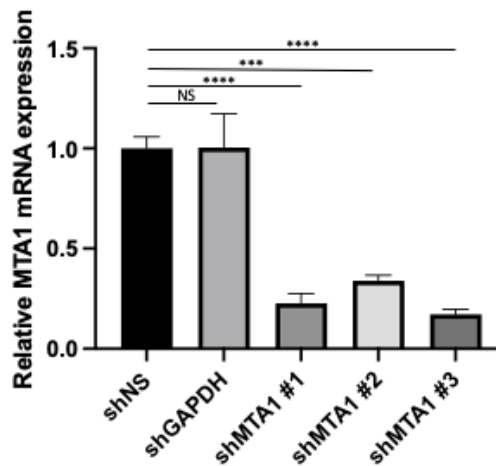
A**B**

Figure 34. Representative western blot and densitometric analysis (A) demonstrate that shMTA1 #3 clone has the greatest efficiency in reducing MTA1 protein expression. β -actin was used as a loading control. qRT-PCR of MTA1 mRNA expression (B) also confirms that shMTA1 #3 clone has the greatest knockdown of MTA1. Levels were normalized relative to shNS control. Changes in mRNA expression were calculated by the $2^{-\Delta\Delta C_t}$ method. Data represent mean \pm SEM of three independent experiments; ** p = <0.01; *** p = <0.001; **** p = <0.0001 (One-way ANOVA).

(ii) Generation of 22Rv1 luciferase expressing cells (22Rv1-Luc)

The luciferase gene is not mammalian in nature, and therefore, needs to be introduced into the 22Rv1 cells by transduction. The purpose for tagging our cells with the luciferase gene was to enable bioluminescent imaging of our xenografts after they are implanted. Luciferase catalyzes the oxidation of luciferin (administered to the mouse by i.p. injection), producing light as a byproduct (Figure 35). This light can be captured as an image and quantified. The amount of light emitted (or 'flux') is directly proportional to the number of cells expressing luciferase, which in turn, is directly related to tumor size. The advantage of this technology is that the tumor can be studied in vivo in a noninvasive manner allowing us to monitor its growth over real time.

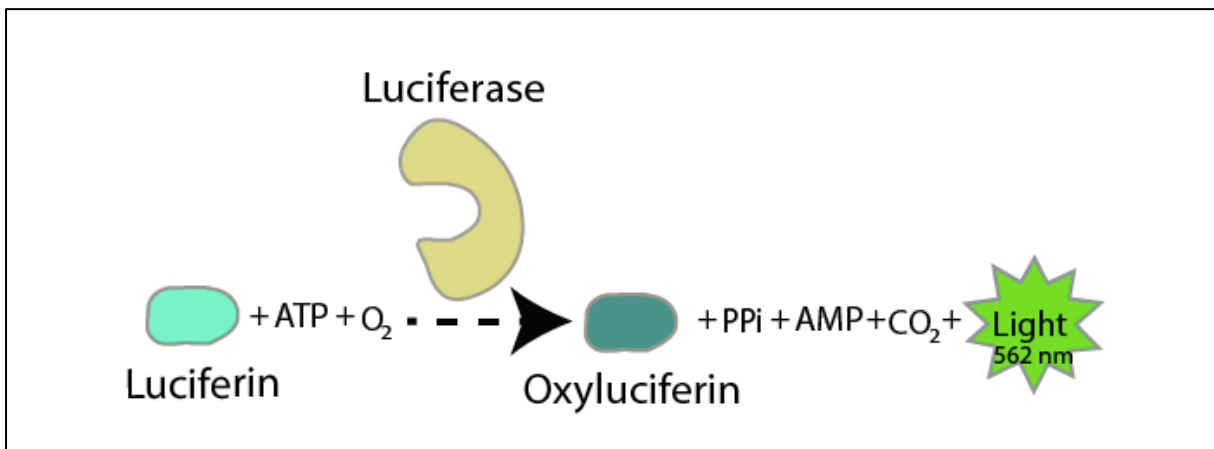


Figure 35. Schematic representation of the light produced from the oxidation of luciferin to oxyluciferin: a reaction catalyzed by the luciferase enzyme.

The lentiviral genome carrying the luciferase gene was also tagged with a G418-resistant gene. Treating the media with G418 at a concentration of 1 mg/mL would enable selection of cells stably transduced with luciferase. These cells are henceforth referred to as 22Rv1-Luc cells (Figure 36, A).

Prior to implantation, these cells were validated for luciferase activity. This bioluminescent assay involved seeding 22Rv1-Luc cells in a 96-well plate by serial dilution and then treating with D-luciferin. After a brief incubation period, the plate was imaged using the IVIS Lumina LT III instrument. The results from the assay showed that the 22Rv1-Luc cells were indeed bioluminescent, and that the degree of radiance positively correlated with cell number (Figure 36, B). Repeat experiments (from one row to the next) also produced a similar degree of bioluminescence demonstrating consistency and reproducibility. This ensures that when radiance is used as a measure for tumor size, it will be reliable and unbiased.

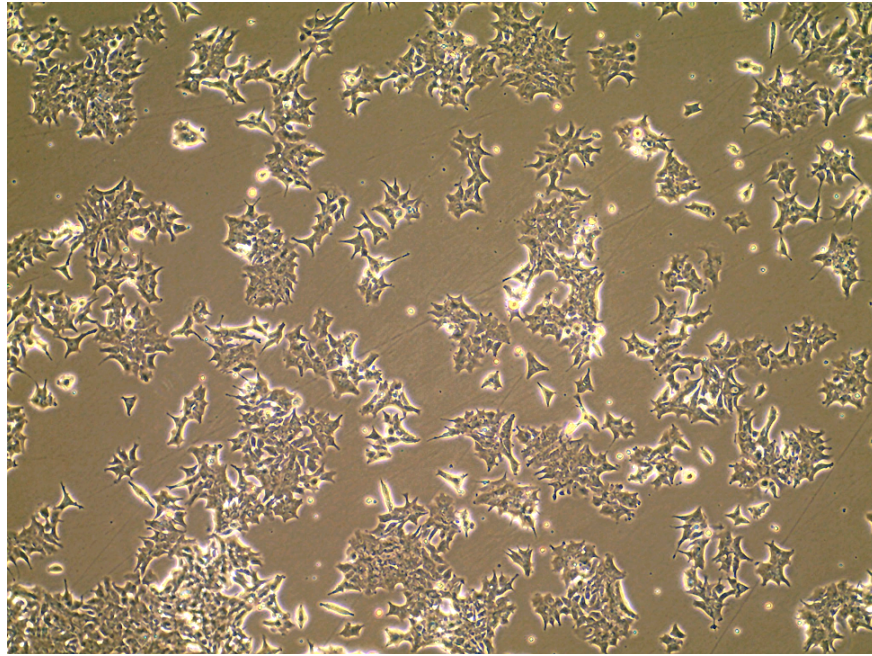
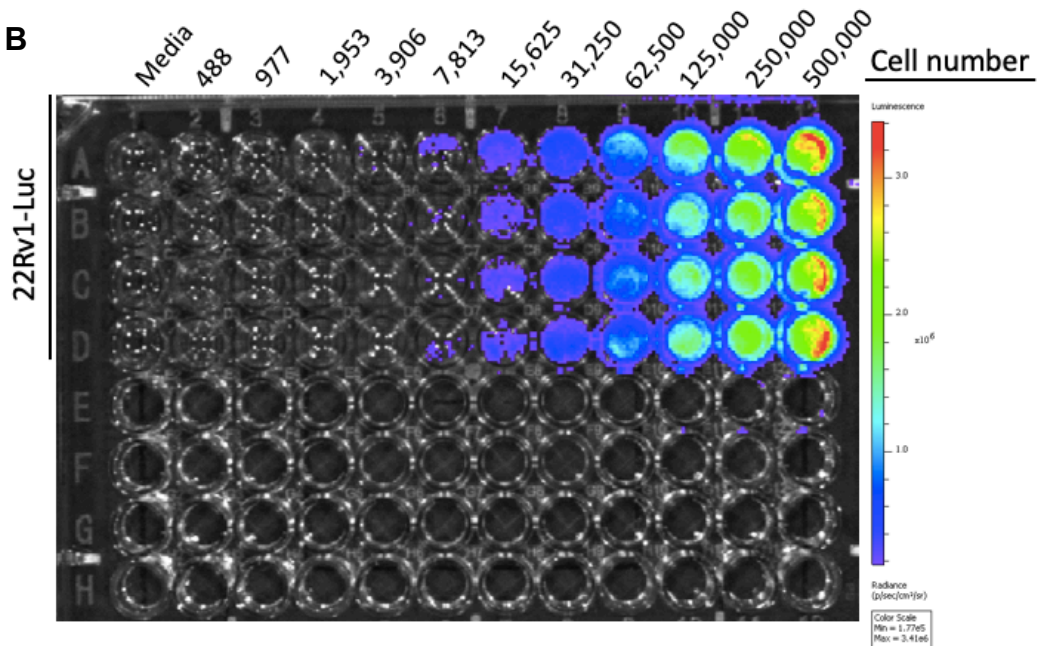
A**B**

Figure 36. Representative image of 22Rv1-Luc cells (A) taken by light microscopy at 10x magnification. Bioluminescent assay (B) validates *in vitro* luciferase activity in 22Rv1-Luc cells.

In a similar fashion, the 22Rv1 knockdown cells generated earlier were also tagged with luciferase by transduction. Luciferase activity in these cells was also confirmed by performing bioluminescent assays (Figure 37). Results demonstrated that bioluminescence across all five knockdowns was roughly equal, particularly for shMTA1 #3 and shNS, which are the two most likely knockdowns to be used in future mechanistic studies. This is important so that the effects seen in knockdown variants in future studies can be directly comparable.

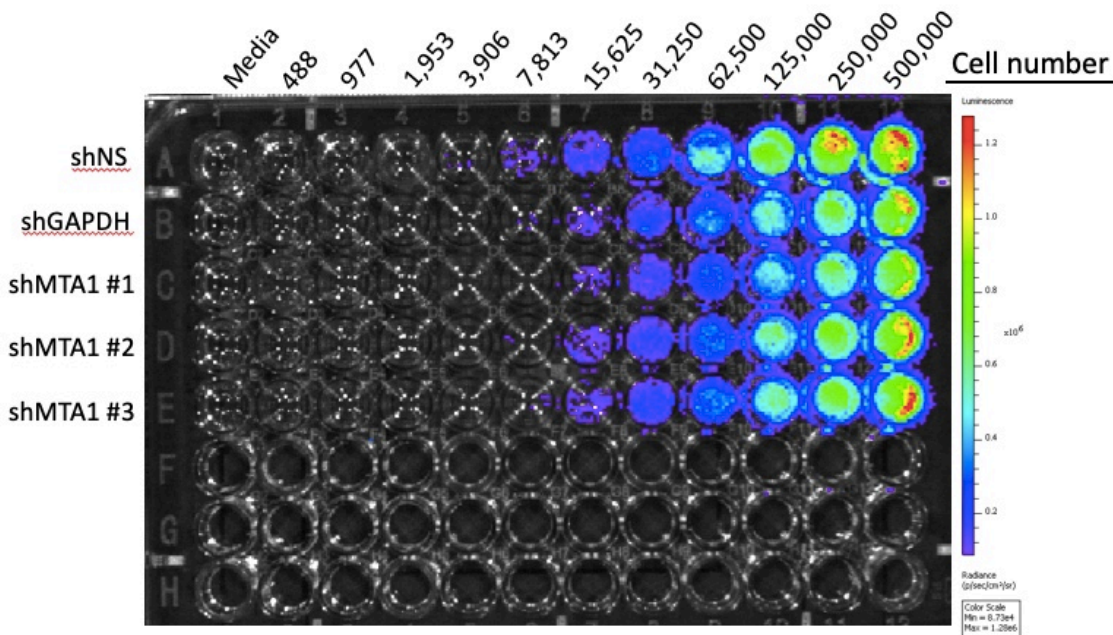


Figure 37. Bioluminescent assay confirms equal *in vitro* luciferase activity in 22Rv1-Luc MTA1 knockdown cells.

(iii) Experimental design - revisited

22Rv1-Luc cells were used to generate subcutaneous xenograft tumors in nude mice, thus giving rise to our *in vivo* model for CRPC. After implantation, bioluminescent images and flux measurements were made every second day. When tumors reached a total flux value of 1×10^9 p/s, mice were randomly assigned to one of the five treatment groups and treatment was initiated:

- i. Control (Vehicle)
- ii. Gnetin C 40 mg/kg (Gnetin C₄₀)
- iii. Enzalutamide 7 mg/kg (Enz₇)
- iv. Enzalutamide 10 mg/kg (Enz₁₀)
- v. Gnetin C 40 mg/kg + Enzalutamide 7 mg/kg (Gnetin C₄₀ + Enz₇)

Treatments were administered by *i.p.* injection daily for 2 weeks, after which, the mice were sacrificed and tissues and blood collected for histological and molecular evaluation (Figure 38). Mice were monitored daily for general wellbeing. Body weight and tumor volume were measured twice weekly. Bioluminescent images and flux measurements were also taken twice weekly.

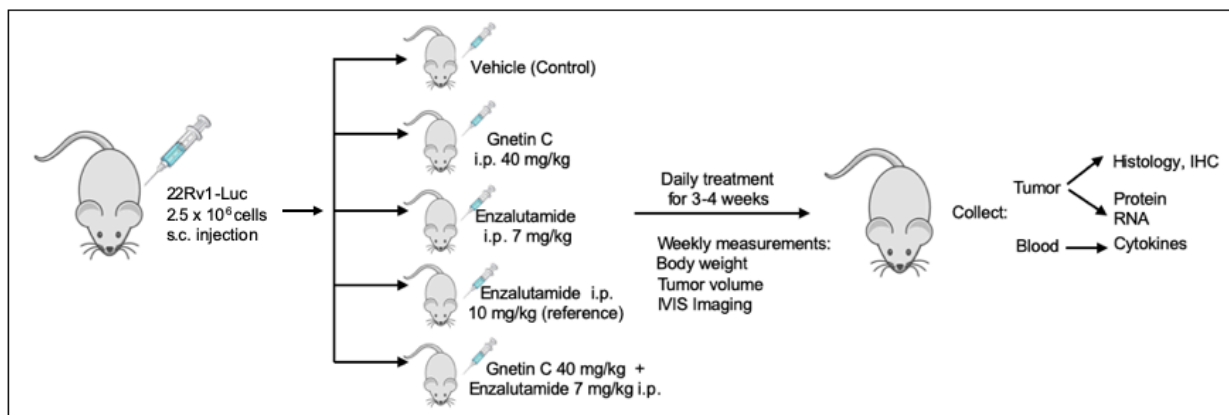


Figure 38. Flow chart depicts experimental design for study investigating the efficacy of Gnetin C as monotherapy and in combination with enzalutamide in a *s.c.* xenograft model for CRPC; *n*=6-7 per group.

(iv) Effect of treatments on body weight

Body weight measurements were made twice weekly not only as a means for establishing consistency and eliminating bias between the treatment groups, but also as a possible determinant of toxicity associated with the treatments. The results showed that the treatments did not have any significant effect on body weight compared to the control (Figure 39).

(v) Effect of treatments on tumor volume

The volume of the tumor was calculated twice weekly. To do this, the length and width of the tumor were measured using Vernier digital calipers. As a rule, the longest diameter of the tumor was measured as its length, and the diameter perpendicular to the length was measured as the width. Measurements were taken without compressing the tumor. The tumor volume was then calculated using the formula: $V (\text{mm}^3) = (\text{Length} \times \text{Width}^2)/2$.

The results demonstrated that tumors treated with Gnetin C₄₀, Enz₇, and Enz₁₀ were significantly smaller than Control, yet not significantly different from each other. Interestingly, however, tumors treated with Combination therapy were visibly larger. Their volumes were comparable to the volumes of Control tumors and were significantly larger than tumors of other treatments (Figure 40). This was an unexpected result. A possible explanation could be that this combination, or specifically the doses used, may have produced antagonist effects. Further investigation was required.

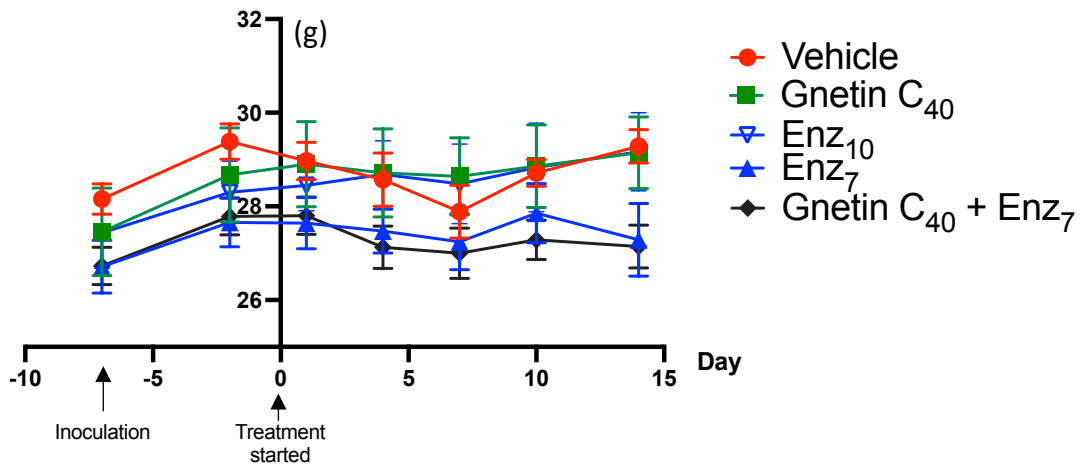


Figure 39. Effects of treatment on average body weight in mice. Data represents mean \pm SEM; n=6-7 per group. Data determined to be statistically non-significant by two-way ANOVA.

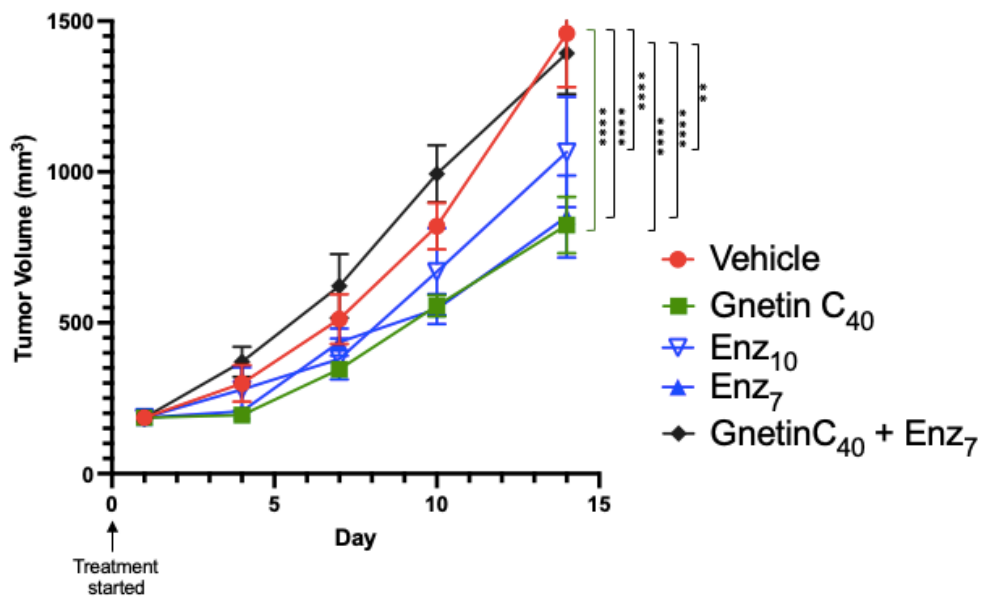


Figure 40. Tumor volumes were measured twice weekly starting from day one after treatment was commenced. Data represent mean \pm SEM, n=6-7 per group; ** $p < 0.01$; *** $p < 0.0001$ (One-way ANOVA).

(vi) Effect of treatment on tumor weight

At the end of treatment, tumors were removed, photographed, and weighed. Photographic images of tumors correlate somewhat with tumor volume. Tumors treated with Gnetin C₄₀, Enz₇, and Enz₁₀ were smaller in size compared to Control and Combination-treated tumors (Figure 41). The images also confirm a certain similarity in size between Control and Combination-treated tumors. A striking feature is the high degree of vascularization of Control and Combination-treated tumors.

Tumor weights showed a similar trend whereby tumors treated with Gnetin C₄₀, Enz₇, and Enz₁₀ monotherapies had lower weights compared to either Control or Combination therapy (Figure 42).

Overall, evaluation of gross anatomy suggests that monotherapy may be more effective than the Combination treatment. However, it should be noted that differences in tumor density and composition may influence tumor size, volume, and weight. Cell packing, infiltration of host (mouse) cells, degree of vascularization, presence of inflammation or edema, or fibrosis may increase tumor size and lead to erroneous conclusions. Bioluminescent assays may help reveal more about the tumors.

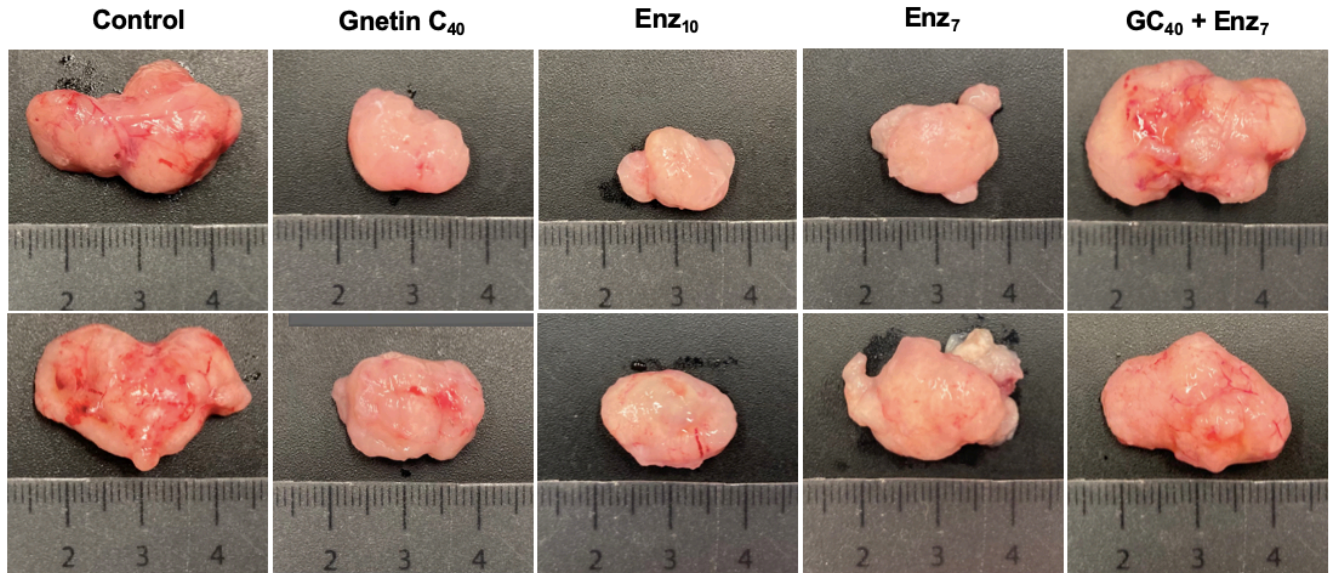


Figure 41. Representative images of tumors from each study group.

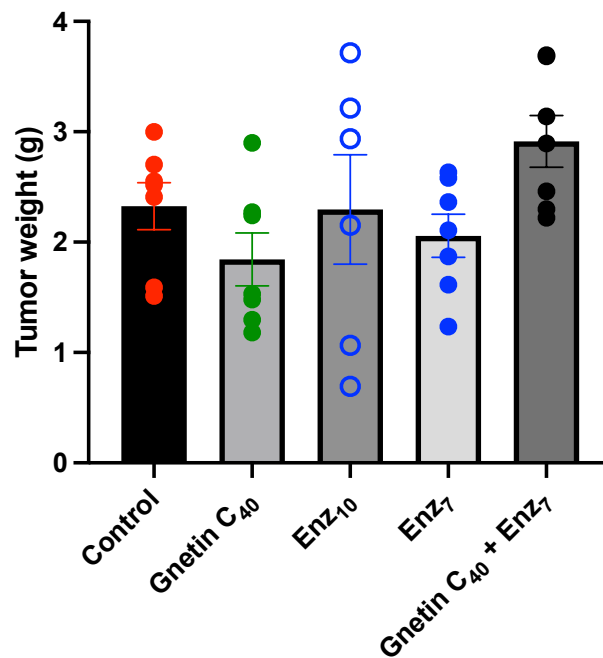


Figure 42. Tumor weights measured at the end of treatment. Data represents mean \pm SEM; $n=6-7$ per group. Data determined to be statistically non-significant by one-way ANOVA. This was most likely due to considerable variation in tumor weights within each treatment group.

(vi) Noninvasive bioluminescent assay of castrate-resistant tumors

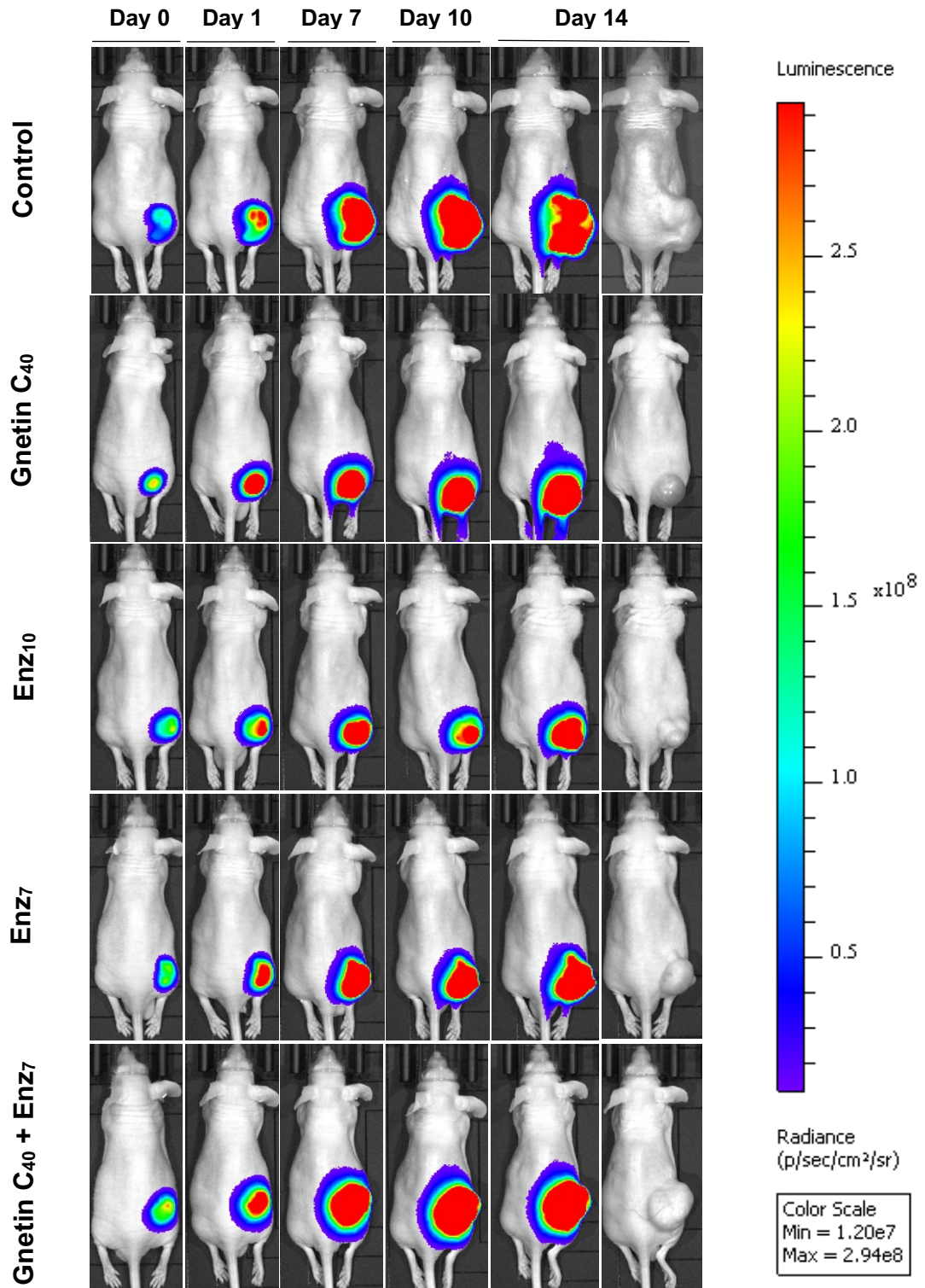
Bioluminescent imaging (BLI) provides an opportunity for noninvasive, real-time monitoring of tumor growth. Because only live 22Rv1-luciferase tagged cells are capable of generating light, this makes BLI a highly specific technique for evaluating tumor development. The total light, or flux, emitted is directly proportional to the size of the tumor.

Tumor growth was monitored by twice weekly BLI until Day 14 of treatment. In keeping with tumor volume and weight data, BLI showed a reduced bioluminescent signal from tumors treated with Gnetin C₄₀, Enz₇, and Enz₁₀ compared to Control. The bioluminescent signal from Combination-treated tumors was slightly less than Control (Figure 43, A).

Quantitation of normalized total flux confirmed that tumors treated with Gnetin C₄₀, Enz₇, and Enz₁₀ had significantly less flux than Control (Figure 43, B). Although not statistically significant, Combination-treated tumors also displayed a lower total flux compared to Control.

These findings correlate somewhat with gross anatomy suggesting that castrate-resistant tumors responded more favorably to Gnetin C₄₀, Enz₇, and Enz₁₀ monotherapies, compared to Combination therapy. It is important to consider, however, the limitations associated with BLI. Features of the tumor microenvironment, such as necrosis, hypoxia, or edema can reduce light signal, leading to an inaccurate interpretation of data⁶³. By Day 14, many of the tumors (including almost all of the Control tumors) displayed a notable reduction in flux despite having a progressive increase in tumor volume. In order to eliminate the likelihood of bias or error from our data, we have treated flux values for Day 14 as outliers (Figure 43).

A



B

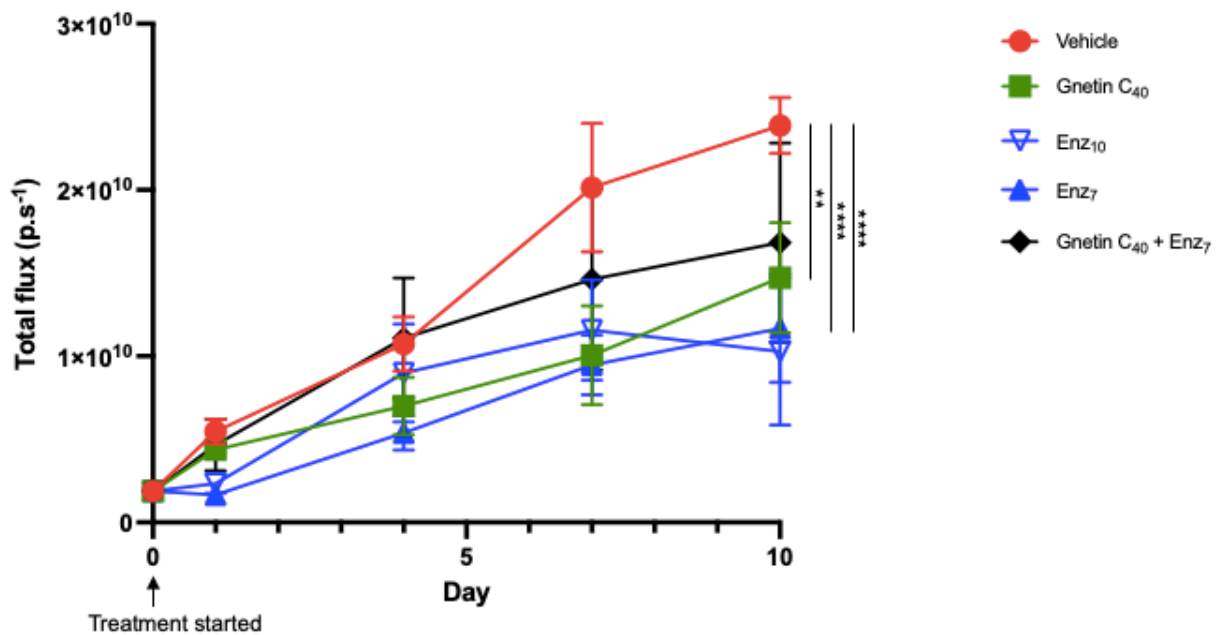


Figure 43. Representative bioluminescent images (dorsal view) for each study group taken at days 0, 1, 7, 10, and 14. Grayscale images were taken on day 14 (A). Quantitation of normalized total flux (B). Data represent mean \pm SEM, $n=6-7$ per group; ** $p < 0.01$; **** $p < 0.0001$ (Two-way ANOVA).

(vii) Effect of treatment on histopathology of CRPC

The histological nature of xenograft tumor tissue is such that it lacks the typical structure of the prostate gland or UGS. Xenograft tumor is composed of epithelial 22Rv1-Luc cells having multiplied from the time of implantation. Host cells are also likely to have infiltrated the growing tumor, such as endothelial cells for angiogenesis, fibroblasts and collagen forming fibrotic tissue, cytokines and immune cells with possible inflammation, edema and swelling. Although this tissue lacks the structure of the prostate or UGS, its microenvironment is not unlike that of human PCa.

H&E slides of Control tumors revealed a densely packed, highly proliferated histology when compared to treated xenograft tumors (Figure 44). Treated tumors also had significantly fewer Ki67-positive cells, indicating less proliferation compared to Control. In stark contrast from our gross anatomy data, Combination-treated tumors were associated with significantly less proliferation compared to Enz₇ or even high dose Enz₁₀, performing similarly to Gnetin C₄₀ (Figures 44 and 45).

All treatments showed significantly less staining for AR compared to Control. Interestingly, Combination-treated tumors expressed significantly less AR compared to Enz₇ and Gnetin C₄₀. Similarly, all treated tumors showed significantly less staining for MTA1 compared to Control, with Combination-treated tumors expressing the least .

All treatments showed significantly less staining for CD31 compared to Control, suggesting less angiogenesis. Combination-treated tumors showed comparable expression of CD31 with Gnetin C₄₀ and Enz₁₀, but significantly less than Enz₇. Treated tumors also displayed a significantly

greater number of cleaved caspase-3-positive cells compared to Control, indicating that all treatments were associated with an increase in apoptosis. However, Combination-treated tumors had significantly greater cleaved caspase-3 staining compared to Enz₇ and Gnetin C₄₀.

These findings are quite interesting because while tumor volume, weight, and BLI data indicated that tumors were not responding to Combination therapy, histological data suggests that Combination therapy is more efficacious in improving histopathology compared to Gnetin C₄₀, Enz₇, and even Enz₁₀ monotherapies.

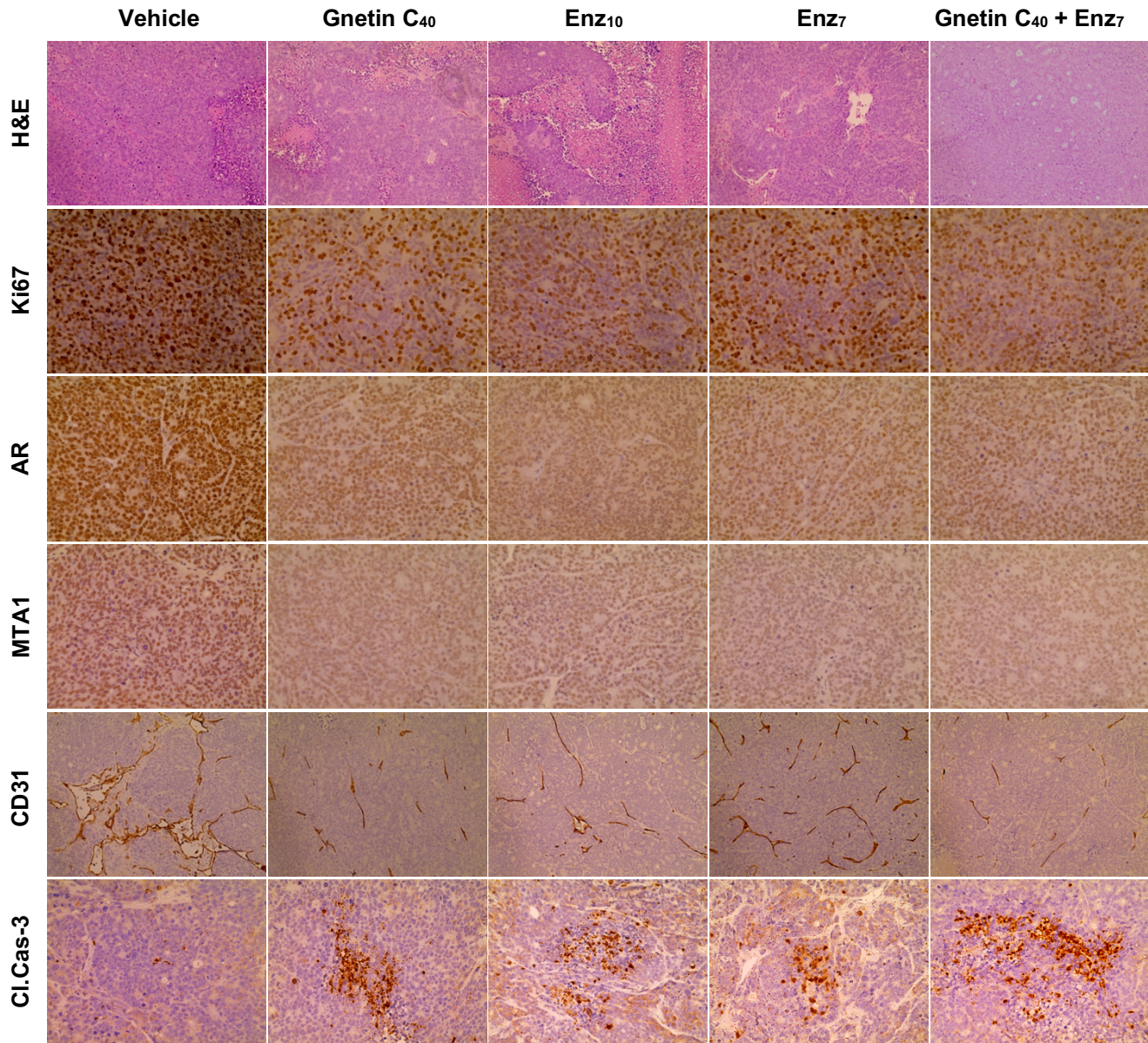


Figure 44. Representative H&E (top) and IHC staining for Ki67, AR, MTA1, CD31 and cleaved caspase-3 in 22Rv1-Luc xenograft tumor tissue treated with Vehicle (Control) Gnetin C40, Enz10, Enz7, and Gnetin C40 + Enz7 by i.p. injection. H&E images were taken at 20x; Ki67, AR, MTA1, and Cl.Cas-3 images were taken at 40x; CD31 images were taken at 20x magnification.

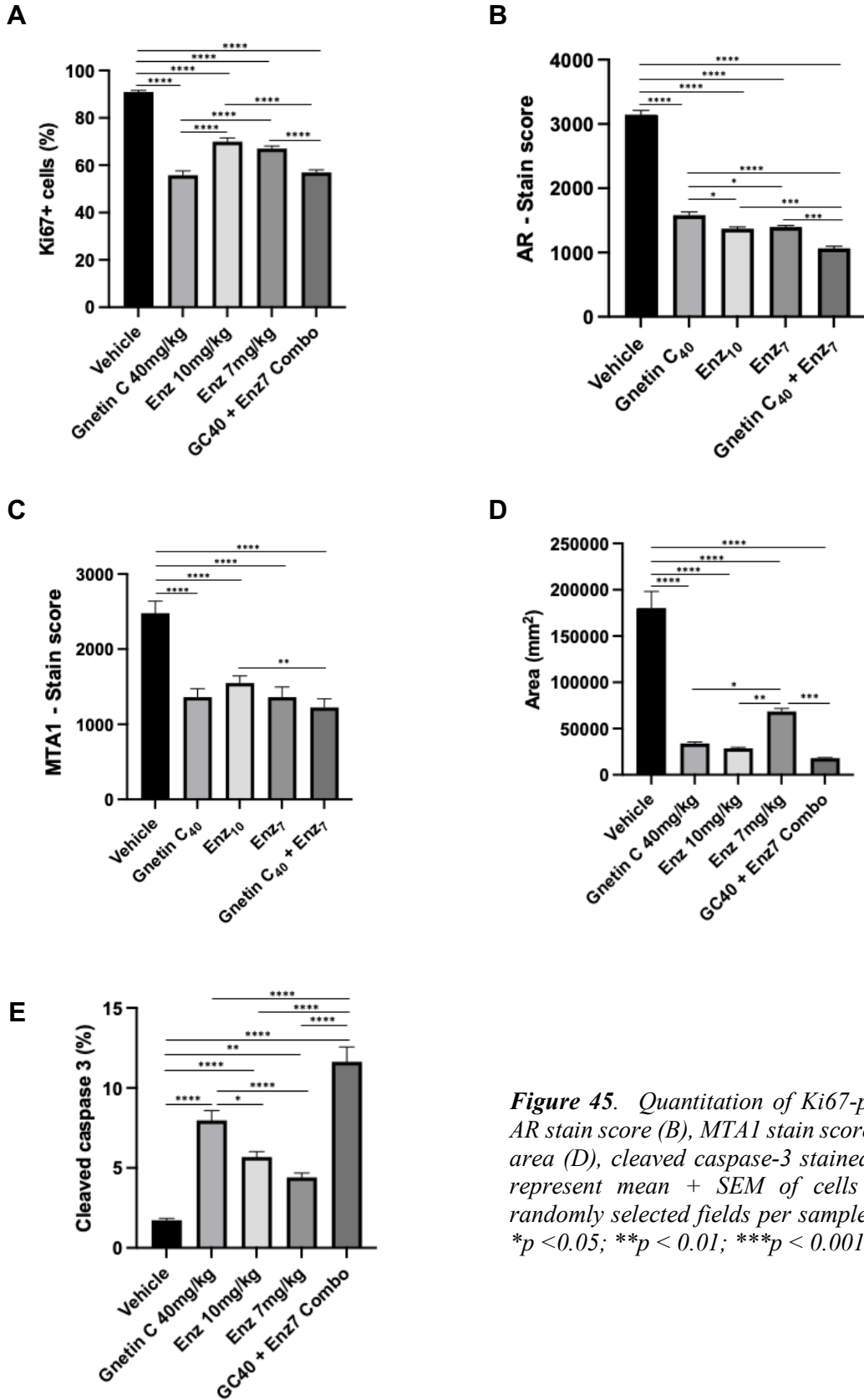


Figure 45. Quantitation of Ki67-positive cells (A), AR stain score (B), MTA1 stain score (C), CD31 stain area (D), cleaved caspase-3 stained cells (E). Data represent mean + SEM of cells counted in five randomly selected fields per sample, n=4 per group. * $p < 0.05$; ** $p < 0.01$; *** $p < 0.001$; **** $p < 0.0001$

(viii) Effect of treatment on MTA1, AR, and AR-V7 expression in model for CRPC

Western blot was performed to measure MTA1, full-length AR, and truncated AR-V7 protein expression in the 22Rv1-Luc tumor lysates (Figure 46).

All treatments were capable of reducing MTA1 expression in xenograft tumor tissue compared to Control, with Combination therapy showing the greatest inhibition. Tumors treated with Combination therapy expressed less MTA1 compared to Gnetin C₄₀, Enz₇, and even Enz₁₀ monotherapies.

All treatments significantly reduced full-length AR compared to Control, and of all the treatments, Combination therapy was the most potent in inhibiting AR. Although not found to be statistically significant, Combination therapy was able to reduce AR protein expression more effectively than either agent used alone and high dose Enz₁₀.

All treatments reduced AR-V7 expression in xenograft tumor tissue compared to Control. Gnetin C₄₀ monotherapy was able to reduce AR-V7 more potently than either Enz₇ or Enz₁₀, which is in keeping with our earlier in vitro data. Moreover, the Combination treatment showed the greatest potency in inhibiting AR-V7 in the xenograft tumors.

Overall, the western blot results seemed to echo IHC and histology findings. In all cases, it would appear that Gnetin C₄₀ + Enz₇ Combination treatment displayed greater efficacy than either compound used alone. Although gross anatomy findings were somewhat contradictory, our molecular data suggests that the combination could be beneficial.

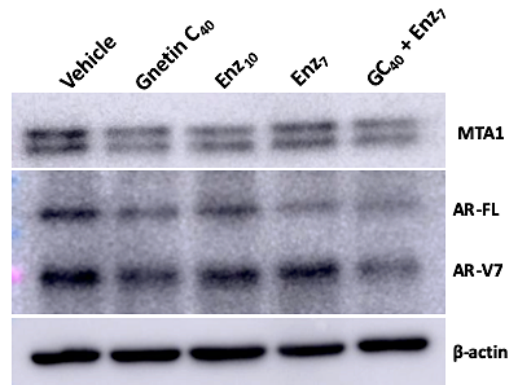
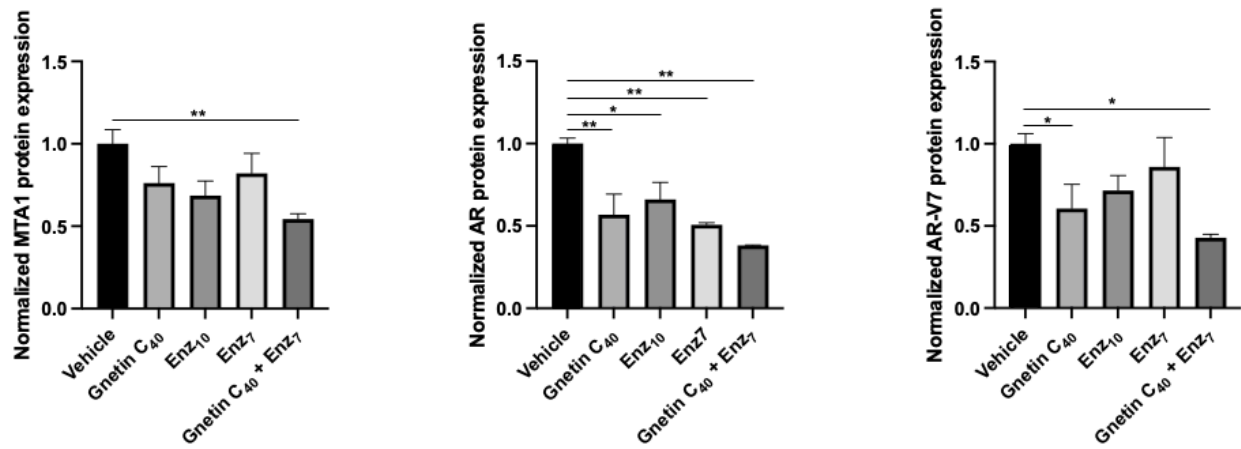
A**B**

Figure 46. Representative immunoblot (A) and densitometric analysis (B) demonstrate that Combination treatment is associated with the greatest efficacy in reducing MTA1, AR, and AR-V7 protein expression. β -actin was used as a loading control. Data represent mean \pm SEM, $n = 4$ per group; * $p < 0.05$; ** $p < 0.01$; (One-way ANOVA).

Aim 4: Gnetin C – Pharmacokinetic Single-Dose Study

The objective of this study was to characterize the PK profile of Gnetin C, a relatively new and unknown compound. Previously, we discussed the importance of conducting PK studies parallel to in vitro pharmacodynamic studies. The drug must be able to reach the site of action in clinically relevant concentrations. If a compound cannot do this, it will not be effective, no matter how efficacious it had proven to be in in vitro pharmacodynamic studies. In other words, in order for a compound to be of clinical relevance, it must be suitable both pharmacodynamically and pharmacokinetically.

In our previous study, Gadkari et al. 2020, we were able to detect and quantify Gnetin C in tumor xenograft tissue, suggesting that it had been able to reach its target site after i.p. administration³¹. On the contrary, concentrations of resveratrol and pterostilbene were not quantifiable. This might also suggest that, comparatively, Gnetin C could have an overall higher systemic exposure (AUC), and therefore, more likely to reach the site of action in therapeutically relevant concentrations.

This study was conducted to understand how this promising result relates specifically to the four main physiological processes of pharmacokinetics: absorption, distribution, metabolism, and excretion (ADME). By conducting an in vivo plasma concentration vs. time study, I was able to estimate Gnetin C's basic pharmacokinetic parameters: systemic exposure (or AUC), clearance (Cl/F), half-life ($t_{1/2}$), and volume of distribution (Vd/F). So far, Gnetin C has demonstrated pharmacodynamic superiority over other stilbenes. It is anticipated that it will demonstrate desirable PK properties as well.

(i) Experimental design - revisited

Wild-type transgenic mice (Cre-negative) were randomly selected for this study. These mice were 8-12 weeks of age, weighing an average of 20 g, and had not received any prior treatment. On the morning of the study, all mice were administered Gnetin C by i.p. injection at a dose of 25 mg/kg. Although, ideally, for PK studies the intravenous route would have been preferred, no member of the laboratory possessed this technical skill at the time of the study.

Blood was drawn by cardiac puncture from a single mouse at the following time points (with respect to dosing): pre-treatment, 15 min, 30 min, 1 h, 2 h, 4 h, 6 h, and 12 h (Figure 47). These blood samples were then analyzed to determine the concentration of Gnetin C, from which PK parameters could be estimated.

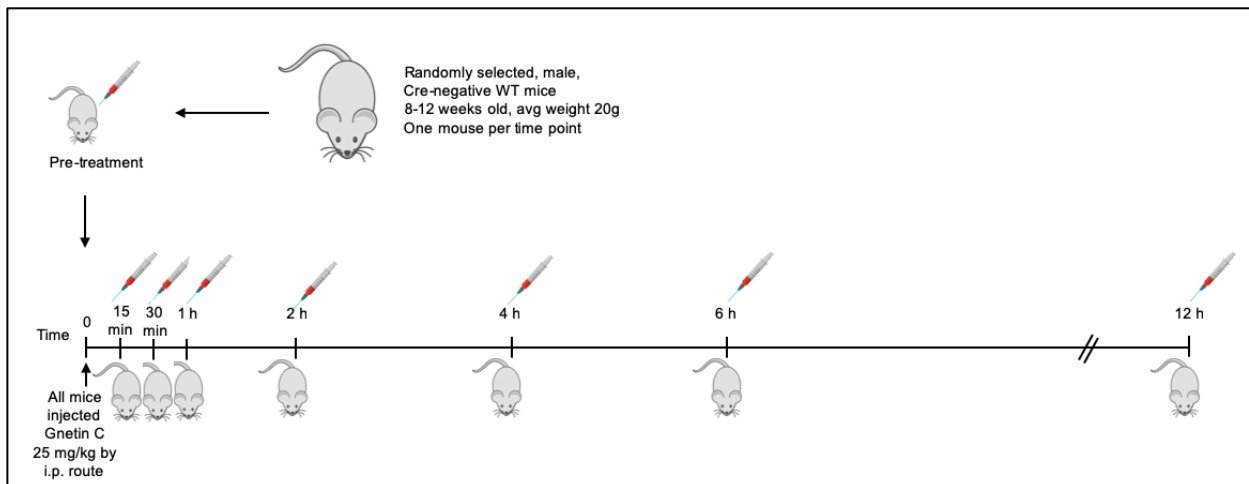


Figure 47. Timeline depicting dosing and blood collection, $n = 1$ mouse per time-point.

(ii) Determination of Gnetin C concentrations by UPLC

After blood was collected, it was allowed to clot before serum was isolated. These serum samples and standards were then analyzed by UPLC. Detection of Gnetin C in the serum samples was made by comparing the sample chromatogram against the standard chromatogram, where the standard Gnetin C peak was used as a reference (retention time = 5.2 minutes) (Figure 48).

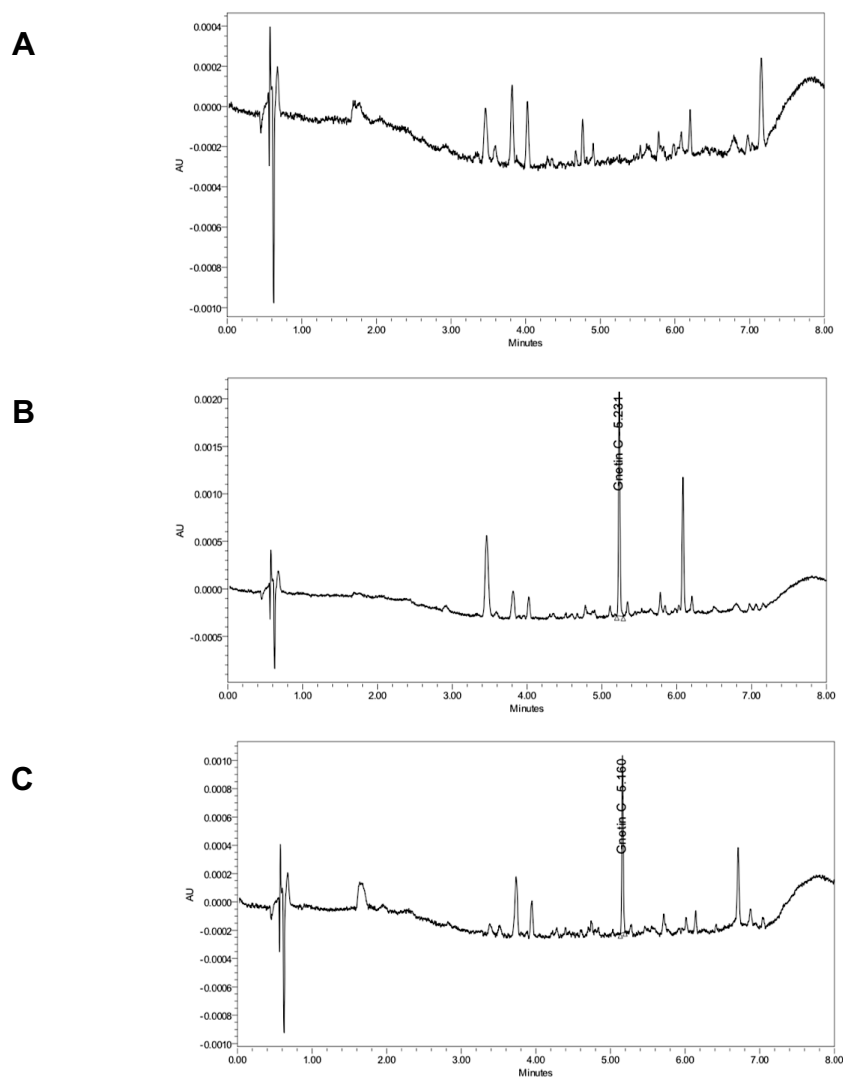


Figure 48. Representative chromatograms for the pre-treatment sample (A), where Gnetin C peak is absent. Representative chromatogram for standard 100ng/mL (B) shows a resolved peak at Rt 5.2 min. Representative chromatogram for serum sample $t = 6$ h (C) showing a corresponding peak at 5.2 minutes.

The Gnetin C concentration for each time point was determined using a standard curve based on UV absorbance. The Gnetin C standards used to construct the calibration curve had known concentrations of 10, 50, 100, 500, and 1000 ng/mL. The calibration curve for Gnetin C was confirmed to be linear within the range of 10-1000 ng/mL ($r^2=0.9992$). It was plotted as area under the peak (reflecting UV absorption) vs. concentration (Figure 49).

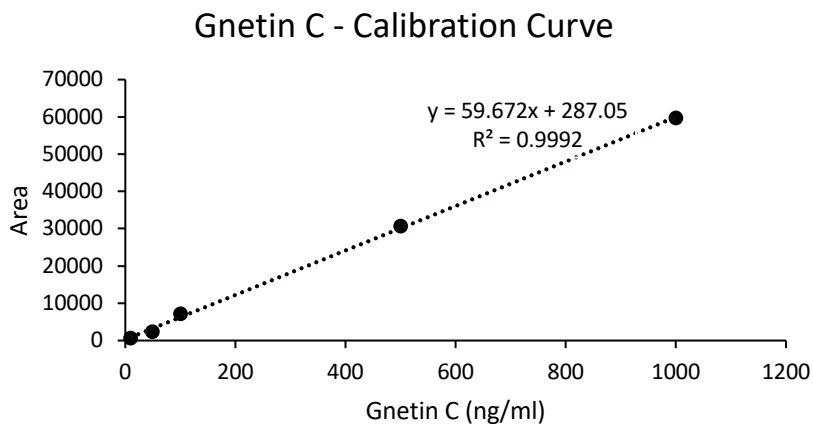
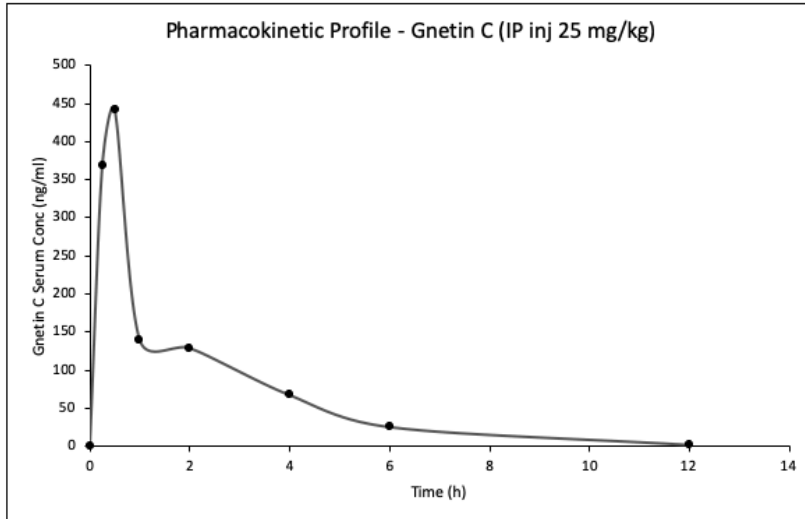


Figure 49. Calibration curve for Gnetin C quantitation by UPLC.

(iii) Data analysis

After Gnetin C concentrations for each time point were determined, a serum concentration vs. time graph was plotted (Figure 50). The graph commences from the point of origin (0,0). This is because at $t = 0$, the time at which Gnetin C was injected, a concentration of 0 ng/mL is expected in the central compartment (blood) since the i.p. route of administration requires an absorption phase. Following this, the serum concentration rises until it reaches a peak, known as C_{max} , at about 30 minutes (T_{max}). In this case, C_{max} has been found to be 441.74 ng/mL. At the peak, the rate-in of Gnetin C equals the rate-out. Then, as most of the absorption has taken place, the

rate-out becomes larger than the rate-in, and a decline in serum concentration is observed. The serum concentration declines in a biphasic fashion as indicated from the semi-log plot (Figure 51).



Time (h)	Conc (ng/ml)
0	0
0.25 (15min)	367.87
0.5 (30min)	441.74
1	140.35
2	129.26
4	67.86
6	25.90
12	2.41

Figure 50. Plot for Gnetin C serum concentration vs. time. Sample concentrations of Gnetin C are tabulated to the right.

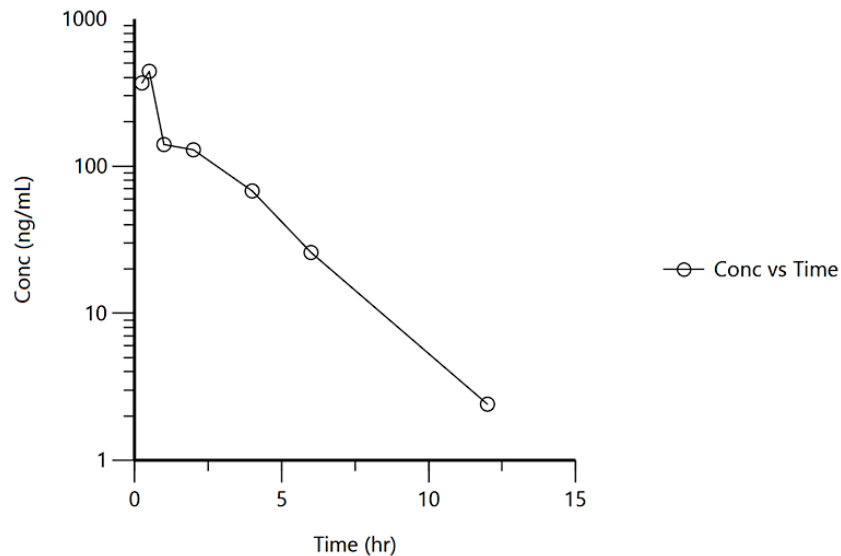


Figure 51. Semi-log plot of serum concentration of serum Gnetin C vs. time. Linearized data demonstrates how serum concentration declines in a biphasic fashion. Note an equilibrium distribution plateau exists between 1 and 2 hours. I would like to give credit to Dr. G Stagni for her assistance in analyzing this data using WinNonlin.

The systemic exposure, or AUC, was estimated using the trapezoidal rule. The elimination rate constant (k) was determined from the terminal slope of the log-transformed data (Figure 52). And, the half-life ($t_{1/2}$), clearance (CL/F), and volume of distribution (Vd/F) were calculated from the relevant PK equations as outlined in the Methodology. These pharmacokinetic parameters are listed below in Table 6.

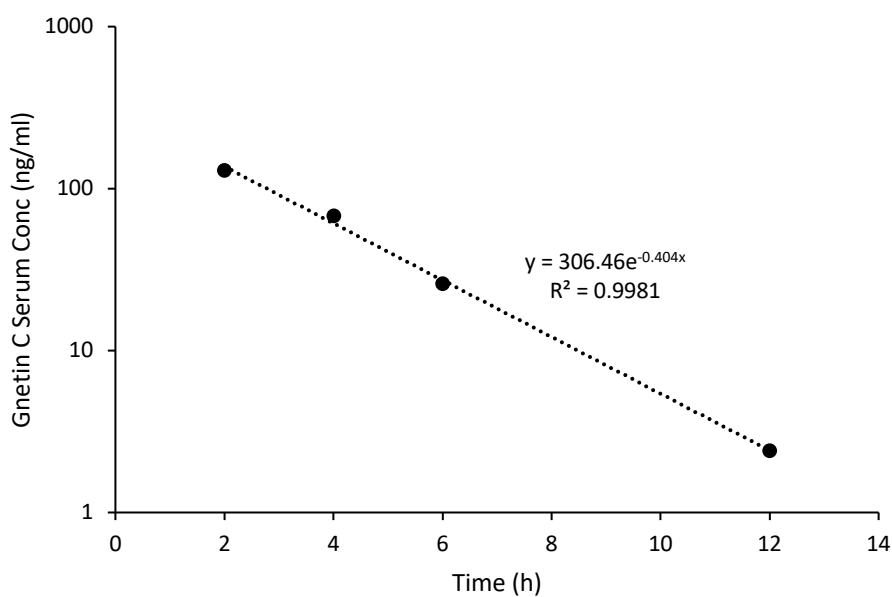


Figure 52. Terminal phase data, where k (elimination constant) = 0.404 h⁻¹

Table 6. Gnetin C pharmacokinetic parameters

Parameter	Value	Units
k	0.404	h ⁻¹
AUC ₍₀₋₁₂₎	803.3	µg.h/L
AUC _(0-inf)	809.3	µg.h/L
CL/F	30.9	L/h/kg
T _{1/2}	1.7	h
Vd/F	76.5	L/kg

CHAPTER V. DISCUSSION AND CONCLUSIONS

Dissertation Findings

Stilbenes have been studied extensively in our laboratory at LIU. These agents are known to act on multiple target and signaling pathways. Through their action on MTA1, resveratrol and pterostilbene have shown to increase apoptosis and inhibit tumor cell survival, angiogenesis, inflammation, and metastatic potential in in vitro and in vivo models of PCa. Gnetin C, a resveratrol dimer, is a relatively new stilbene. Throughout our research, we have reported that Gnetin C shows greater potency in inhibiting MTA1 and MTA1-associated signaling pathways compared to resveratrol and pterostilbene¹⁶. In in vitro studies, Gnetin C more potently reduced cell viability, colony formation, and migration, and in an in vivo PC3M xenograft study, it was more efficacious in slowing tumor progression than either resveratrol or pterostilbene^{16,31}. We have also found greater concentrations of Gnetin C in tumor tissue, suggesting that it could have greater bioavailability and an overall better clinical relevance.

The overarching goal for this dissertation was to investigate the efficacy of Gnetin C in in vivo murine models reflecting different stages of human PCa. For Aim 1, we investigated Gnetin C-supplemented diet (in high and low concentrations) in a transgenic murine model for high-risk PCa in an effort to understand whether Gnetin C could be beneficial as chemoprevention. Results demonstrated that compared to Control and Pter₇₀ diets, both Gnetin C diets (Gnetin C₇₀ in particular) more potently inhibited PIN foci, proliferation and angiogenesis. Impressively, Gnetin

C even at half concentration (Gnetin C₃₅) showed greater efficacy in inhibiting Ki67, MTA1 and, CD31 compared to Pter₇₀.

Gnetin C diets more potently inhibited MTA1 as seen in IHC and protein lysates. Although Pter₇₀ diet upregulated PTEN more potently, Gnetin C diets were still able to restore PTEN more efficaciously than Control. Gnetin C₃₅ reduced serum pro-inflammatory cytokine, IL-2, compared to Control and Pter₇₀. Gnetin C₃₅ was also able to reduce serum IL-6 compared to Control, although not as potently as Pter₇₀. Interestingly, Gnetin C₇₀ diet caused a paradoxical increase in IL-6 levels. This is, however, in keeping with reports claiming that polyphenols exert greater anti-inflammatory and anticancer activity at lower doses, and may even be antagonistic at higher doses^{64,61,62}.

In clinical practice, patients deemed at high-risk of PCa are monitored, but are not offered any interventional therapy. Our data suggests that in addition to active surveillance, a Gnetin C-supplemented diet may prove to be most beneficial in reducing the onset or progression to PCa in moderate- and high-risk patients.

For Aim 2, we investigated the efficacy of Gnetin C as a treatment in a transgenic high-grade PIN model of PCa. Gnetin C-treated prostates displayed a favorable histopathology when compared to Control, having restored ductal structures, reduced proliferation and angiogenesis, and increased apoptosis. Prostate tissues also showed a downregulation in MTA1 protein. Reduced levels of serum IL-2 suggests that Gnetin C treatment is able to reduce systemic inflammation associated with PCa. Altogether, the results indicated that Gnetin C treatment was effective in reducing

overall tumorigenicity and progression of PCa. The efficacy of Gnetin C, at least in part, is most likely due to its activity against MTA1 and MTA1-associated pathways.

Earlier in vitro studies had revealed that Gnetin C more potently inhibits MTA1, full-length AR, and truncated AR-V7 in 22Rv1 cells compared to resveratrol and pterostilbene. Gnetin C was also found to have greater potency against AR and AR-V7 compared to enzalutamide, suggesting that Gnetin C may be beneficial in the treatment of CRPC, which is known for expressing AR-V7. This was an interesting finding given that enzalutamide is currently an FDA-approved treatment for CRPC, a stage of PCa that is notoriously difficult to treat. By targeting both MTA1 and AR, which are unassociated signaling pathways, Gnetin C is said to exert a dual action against PCa, and possess a unique role in the treatment of CRPC.

Aim 3 of this dissertation investigated the efficacy of Gnetin C in an in vivo xenograft model for CRPC generated from 22Rv1 cells. From our earlier in vitro studies, we learned that the combined use of Gnetin C and enzalutamide could be beneficial. So, from our in vivo xenograft model, we hoped to derive information about Gnetin C when administered as monotherapy and combination therapy with enzalutamide.

The results from Aim 3 seemed conflicting initially. Tumors treated with Gnetin C monotherapy responded well. The efficacy of Gnetin C is believed to be, at least in part, due to more efficient targeting of MTA1, AR, and AR-V7. Bioluminescent data along with tumor volume and tumor weight data suggested that the Combination strategy may have been antagonistic in nature. However, histology and molecular investigations suggest otherwise. Tumors treated with Gnetin

C₄₀ + Enz₇ Combination showed less proliferation and angiogenesis, with an increase in apoptosis compared to Gnetin C and enzalutamide monotherapy. IHC also demonstrated that the Combination treatment was associated with a greater reduction in MTA1 and AR expression compared to Gnetin C or enzalutamide alone. Furthermore, western blot showed that the Combination therapy more potently inhibited MTA1, AR, and AR-V7 in xenograft tissue compared to either agent used alone.

This discrepancy between gross anatomy and molecular findings requires further investigation. Differences in tumor density, infiltration of host cells, vascularization, inflammation, edema, fibrosis, and other tumor-related processes may influence gross anatomy and lead to erroneous conclusions about the efficacy of treatments. Professional examination of the histological composition of the xenograft tissue may help shed light on this issue. Bioluminescent imaging also has its limitations. The presence of edema and hypoxia are known to attenuate the luminescent signal, which may have affected the Control tumors or tumors from other treatments.

Based on our molecular findings, the Gnetin C₄₀ + Enz₇ Combination treatment showed greater efficacy compared to either compound used alone, and could provide a beneficial option in the treatment of CRPC in humans. Although the improvement in efficacy is largely additive, rather than synergistic, it is important to consider other advantages of combination therapy that make it a preferred treatment option. For example, smaller doses are often more effective in combination treatments. In our studies, it was found that enzalutamide 7 mg/kg when used in combination with Gnetin C was often more effective than enzalutamide 10 mg/kg monotherapy. In turn, the use of smaller doses may reduce the incidence of toxicity or adverse events, which are legitimate

concerns associated with chemotherapy³⁶. Moreover, the use of multiple agents targeting different signaling pathways may also reduce the risk of treatment resistance, which is yet another common dilemma concerning cancer treatment³⁵.

The objective of Aim 4 was to define the PK parameters of Gnetin C, and make comparisons between the PK profiles of Gnetin C, resveratrol and pterostilbene. The original intention for Aim 4 was to perform the same PK study for all three compounds, using the same species, breed, gender, age, route of administration and dose; thus, enabling the profiles to be unbiased and directly comparable. Due to unforeseeable circumstances, however, the PK study was only possible for Gnetin C. This has been cited as a limitation of my dissertation (below).

In a study conducted by Mutlu et al. (2020), mice administered a single IV dose of resveratrol were found to have a half-life comparable to that of Gnetin C as estimated by our studies (~2 hours)⁶⁵. But, the inconsistencies in experimental design are vast, and so this raises questions about the comparability of our data. Our earlier findings where Gnetin C was discovered in higher concentration within tumor tissue is an indication that Gnetin C has an overall greater systemic exposure compared to resveratrol or even pterostilbene³¹. This could be due to greater absorption at the site of delivery, reduced clearance by either metabolism or excretion, or even better tissue partitioning and distribution. Despite a species difference, these results are in keeping with studies conducted in human volunteers showing a higher mean residency time associated with Gnetin C compared to resveratrol after a single oral dose⁴⁸, and a further study showing accumulation of Gnetin C in serum over time⁵⁰. It is possible that Gnetin C's superior pharmacodynamic properties may be partially due to its favorable PK profile.

Limitations

A severe limitation of this study was the lack of accessibility to the UPLC instrument, which was required for quantitating Gnetin C, resveratrol, and pterostilbene for our pharmacokinetic studies. We had been collaborating with organic chemist, Dr. Qing Cai, who had developed an analytical method and operated the UPLC instrument, which was the property of the Lachman laboratory. Gaining approval to use the equipment and scheduling times for analysis presented challenges. Moreover, when Dr. Cai resigned from her position at LIU, no one was left with the expertise to operate the instrument. So, the study was cut short, having only had time to analyze serum samples for Gnetin C.

Future Direction

(i) Short-term

Currently, arrangements are in place for pathologist, Dr. Ching Yang, LIU (Post) to examine our 22Rv1 xenograft tissue slides (Aim 3). We hope to learn more about the histological nature of these tissues and to better understand the disparity that exists between our gross anatomy and molecular findings.

To appreciate the role of MTA1 and its signaling in 22Rv1 cells, we will conduct mechanistic studies using in vitro MTA1 overexpression and knockdown models. 22Rv1 shMTA1 clones were prepared earlier (Aim 3). These cells may also be used to generate xenografts to study MTA1-mediated signaling in an in vivo model for CRPC. Similarly, to learn more about the role of AR

and its signaling in 22Rv1 cells, mechanistic studies may be conducted using AR overexpression and knockdown models.

Pharmacokinetic studies are needed to investigate the oral bioavailability of Gnetin C. This is essential because the oral route may ultimately be the preferred mode of administration for this compound, coupled with the understanding that natural polyphenols are often associated with poor bioavailability due to high pre-systemic metabolism^{48,49}. Such studies can be undertaken using in vitro models replicating human intestinal epithelium; followed by in vivo plasma concentration vs. time studies. To estimate absolute oral bioavailability (F), Gnetin C studies need to be performed for both oral and intravenous administration.

(ii) Long-term

Our laboratory has an interest in learning more about the role that Gnetin C and other stilbenes can play in PCa that has gained a neuroendocrinal (NE) phenotype. Neuroendocrine prostate cancer (NePC) usually develops from adenocarcinoma in response to drug-induced AR signaling inhibition and is often associated with CRPC (CRPC-NE). NePC and CRPC-NE are highly aggressive variants of PCa and are associated with a very poor survival rate.

22Rv1 cells would make an adequate preclinical model in which to study neuroendocrinal transformation in CRPC (CRPC-NE) and the role that Gnetin C can play in reducing its severity⁶⁶. Developing an in vitro model for NePC is somewhat more challenging. In a suitable cell line, certain microenvironments or signaling molecules may be used to induce a NE phenotype, such as hypoxia or androgen deprivation⁶⁶. Yuan et al. (2007) explain that androgen-sensitive LNCaP

cells are capable of being transdifferentiated into a NE-like phenotype by being cultured in an androgen-reduced media⁶⁷. Such transdifferentiated LNCaP cells express increased levels of classical NE markers, such as neuron-specific enolase (NSE), chromogranin A (CgA), and neurotensin.⁶⁷ Puca et al. (2019) explain that transfection with Snail (transcriptional repressor of E-cadherin) can cause cells to undergo NE transdifferentiation, and subsequent knockdown of Snail can revert the phenotype⁶⁶.

For these studies, Gnetin C may be administered as monotherapy or in combination with an agent such as alisertib, an investigational aurora kinase A (AURKA) inhibitor. The overexpression of AURKA, a member of the serine/threonine kinase family involved in mitosis, is believed to play an oncogenic role in CRPC-NE³⁴. Gnetin C combined with Alisertib may offer benefits in the treatment of CRPC-NE or NePC. Synthetic analogs of Gnetin C with higher potency may also be considered for the treatment of CRPC or NePC.

Closing Statement

In conclusion, these results show that Gnetin C has superior pharmacodynamic and pharmacokinetic properties compared to other stilbene compounds. By demonstrating that Gnetin C more potently reduces the progression of PCa in a variety of preclinical applications, this dissertation advocates for the trial of Gnetin C in human studies as chemopreventive and treatment strategies for PCa.

This research has answered questions and filled many gaps in our knowledge, but there is more work yet to be done. Current management of PCa exhibiting a neuroendocrinal phenotype is unsatisfactory. An investigation of the efficacy of Gnetin C and its synthetic analogs in CRPC-NE and NePC, while challenging, could provide a much-needed therapeutic solution to this otherwise refractory and life-threatening form of PCa.

CHAPTER VII. REFERENCES

1. National Cancer Institute. Understanding Prostate Changes: A health guide for men. <https://www.cancer.gov/types/prostate/understanding-prostate-changes> (2014).
2. Liu, A. Y. & True, L. D. Characterization of Prostate Cell Types by CD Cell Surface Molecules. *Am. J. Pathol.* **160**, 37–43 (2002).
3. Park, J. W. *et al.* Prostate epithelial cell of origin determines cancer differentiation state in an organoid transformation assay. *Proc. Natl. Acad. Sci. U. S. A.* **113**, 4482–4487 (2016).
4. The University of Utah. Normal Histology. *The Internet Pathology Laboratory for Medical Education* <https://webpath.med.utah.edu/HISTHTML/NORMAL/NORM079.html>.
5. The University of Utah. Prostate Pathology. *The Internet Pathology Laboratory for Medical Education* <https://webpath.med.utah.edu/TUTORIAL/PROSTATE/PROSTATE.html#1>.
6. American Cancer Society. Key Statistics for Prostate Cancer | Prostate Cancer Facts. <https://www.cancer.org/cancer/prostate-cancer/about/key-statistics.html>.
7. Wang, G., Zhao, D., Spring, D. J. & DePinho, R. A. Genetics and biology of prostate cancer. <http://genesdev.cshlp.org> doi:10.1101/gad.315739.118.
8. Weinberg, R. A. *The biology of cancer*. (Garland Science, Taylor & Francis Group, 2014).
9. Khurana, N. *et al.* Multimodal actions of the phytochemical sulforaphane suppress both AR and AR-V7 in 22Rv1 cells: Advocating a potent pharmaceutical combination against castration-resistant prostate cancer. *Oncol. Rep.* **38**, 2774–2786 (2017).
10. Wang, Z. *et al.* The characteristics of androgen receptor splice variant 7 in the treatment of hormonal sensitive prostate cancer: a systematic review and meta-analysis. *Cancer Cell Int.* **20**, 149 (2020).

11. Yu, Z., Zou, H., Wang, H., Li, Q. & Yu, D. Identification of Key Gene Signatures Associated With Bone Metastasis in Castration-Resistant Prostate Cancer Using Co-Expression Analysis. *Front. Oncol.* **10**, (2021).
12. Levenson, A. S., Kumar, A. & Zhang, X. MTA family of proteins in prostate cancer: biology, significance, and therapeutic opportunities. *Cancer Metastasis Rev.* **33**, 929–942 (2014).
13. Dhar, S. *et al.* Dietary pterostilbene is a novel MTA1-targeted chemopreventive and therapeutic agent in prostate cancer. *Oncotarget* **7**, 18469–18484 (2016).
14. Dias, S. J. *et al.* Nuclear MTA1 overexpression is associated with aggressive prostate cancer, recurrence and metastasis in African Americans. *Sci. Rep.* **3**, 2331 (2013).
15. Kumar, A. *et al.* MTA1 drives malignant progression and bone metastasis in prostate cancer. *Mol. Oncol.* **12**, 1596–1607 (2018).
16. Kumar, A., Dholakia, K., Sikorska, G., Martinez, L. A. & Levenson, A. S. MTA1-Dependent Anticancer Activity of Gnetin C in Prostate Cancer. *Nutrients* **11**, 2096 (2019).
17. Kai, L. *et al.* Targeting prostate cancer angiogenesis through metastasis-associated protein 1 (MTA1). *The Prostate* **71**, 268–280 (2011).
18. Dhar, S., Kumar, A., Li, K., Tzivion, G. & Levenson, A. S. Resveratrol regulates PTEN/Akt pathway through inhibition of MTA1/HDAC unit of the NuRD complex in prostate cancer. *Biochim. Biophys. Acta BBA - Mol. Cell Res.* **1853**, 265–275 (2015).
19. Schiewer, M. J., Augello, M. A. & Knudsen, K. E. The AR dependent cell cycle: Mechanisms and cancer relevance. *Mol. Cell. Endocrinol.* **352**, 34–45 (2012).
20. New Prostate Cancer Treatment Target - NCI. <https://www.cancer.gov/news-events/cancer-currents-blog/2016/prostate-ror-gamma-inhibitor> (2016).

21. Lonergan, P. E. & Tindall, D. J. Androgen receptor signaling in prostate cancer development and progression. *J. Carcinog.* **10**, 20 (2011).
22. Liao, X. *et al.* Androgen Stimulates Matrix Metalloproteinase-2 Expression in Human Prostate Cancer. *Endocrinology* **144**, 1656–1663 (2003).
23. Armstrong, A. J. *et al.* Five-year Survival Prediction and Safety Outcomes with Enzalutamide in Men with Chemotherapy-naïve Metastatic Castration-resistant Prostate Cancer from the PREVAIL Trial. *Eur. Urol.* **78**, 347–357 (2020).
24. Sanford, M. Enzalutamide: a review of its use in metastatic, castration-resistant prostate cancer. *Drugs* **73**, 1723–1732 (2013).
25. Kirby, M., Hirst, C. & Crawford, E. D. Characterising the castration-resistant prostate cancer population: a systematic review. *Int. J. Clin. Pract.* **65**, 1180–1192 (2011).
26. Dhar, S., Kumar, A., Rimando, A. M., Zhang, X. & Levenson, A. S. Resveratrol and pterostilbene epigenetically restore PTEN expression by targeting oncomiRs of the miR-17 family in prostate cancer. *Oncotarget* **6**, 27214–27226 (2015).
27. Kai, L. & Levenson, A. S. Combination of Resveratrol and Antiandrogen Flutamide Has Synergistic Effect on Androgen Receptor Inhibition in Prostate Cancer Cells. *Anticancer Res.* **31**, 3323–3330 (2011).
28. Li, K. *et al.* Pterostilbene acts through metastasis-associated protein 1 to inhibit tumor growth, progression and metastasis in prostate cancer. *PloS One* **8**, e57542 (2013).
29. Kai, L., Samuel, S. K. & Levenson, A. S. Resveratrol enhances p53 acetylation and apoptosis in prostate cancer by inhibiting MTA1/NuRD complex. *Int. J. Cancer* **126**, 1538–1548 (2010).

30. Dias, S. J. *et al.* Trimethoxy-Resveratrol and Piceatannol Administered Orally Suppress and Inhibit Tumor Formation and Growth in Prostate Cancer Xenografts. *The Prostate* **73**, 1135–1146 (2013).
31. Gadkari, K. *et al.* Therapeutic Potential of Gnetin C in Prostate Cancer: A Pre-Clinical Study. *Nutrients* **12**, 3631 (2020).
32. Iguchi, T. *et al.* Enzalutamide versus flutamide for castration-resistant prostate cancer after combined androgen blockade therapy with bicalutamide: study protocol for a multicenter randomized phase II trial (the OCUU-CRPC study). *BMC Cancer* **19**, 339 (2019).
33. Patel, N. K., Finianos, A., Whitaker, K. D. & Aragon-Ching, J. B. Advanced prostate cancer - patient survival and potential impact of enzalutamide and other emerging therapies. *Ther. Clin. Risk Manag.* **10**, 651–664 (2014).
34. Tucci, M. *et al.* Enzalutamide-resistant castration-resistant prostate cancer: challenges and solutions. *OncoTargets Ther.* **11**, 7353–7368 (2018).
35. Leary, M., Heerboth, S., Lapinska, K. & Sarkar, S. Sensitization of Drug Resistant Cancer Cells: A Matter of Combination Therapy. *Cancers* **10**, 483 (2018).
36. Levenson, A. S. & Kumar, A. Pterostilbene as a Potent Chemopreventive Agent in Cancer. in *Natural Products for Cancer Chemoprevention: Single Compounds and Combinations* (eds. Pezzuto, J. M. & Vang, O.) 49–108 (Springer International Publishing, 2020). doi:10.1007/978-3-030-39855-2_3.
37. Richmond, A. & Su, Y. Mouse xenograft models vs GEM models for human cancer therapeutics. *Dis. Model. Mech.* **1**, 78–82 (2008).
38. Wu, X. *et al.* Generation of a prostate epithelial cell-specific Cre transgenic mouse model for tissue-specific gene ablation. *Mech. Dev.* **101**, 61–69 (2001).

39. Kelmenson, P. Cre Lox Breeding for Beginners, Part 1. *The Jackson Laboratory*
<https://www.jax.org/news-and-insights/jax-blog/2011/September/cre-lox-breeding> (2011).
40. Understanding the Rosa26 Knock-in and Its Uses | ingenious.
<https://www.genetargeting.com/knockin/rosa26-knockin/> (2018).
41. Hemani, R. *et al.* Dietary pterostilbene for MTA1-targeted interception in high-risk premalignant prostate cancer. *Cancer Prev. Res. Phila. Pa* **15**, 87–100 (2022).
42. Butt, N. A. *et al.* Targeting MTA1/HIF-1 α signaling by pterostilbene in combination with histone deacetylase inhibitor attenuates prostate cancer progression. *Cancer Med.* **6**, 2673–2685 (2017).
43. 22Rv1 - CRL-2505 | ATCC. <https://www.atcc.org/products/crl-2505>.
44. Phansalkar, P. S., Zhang, Z., Verenich, S. & Gerck, P. M. Pharmacokinetics and Bioavailability Enhancement of Natural Products. in *Natural Products for Cancer Chemoprevention: Single Compounds and Combinations* (eds. Pezzuto, J. M. & Vang, O.) 109–141 (Springer International Publishing, 2020). doi:10.1007/978-3-030-39855-2_4.
45. Remsberg, C. M. *et al.* Pharmacometrics of pterostilbene: preclinical pharmacokinetics and metabolism, anticancer, antiinflammatory, antioxidant and analgesic activity. *Phytother. Res. PTR* **22**, 169–179 (2008).
46. Themes, U. F. O. Pharmacokinetics. *Basicmedical Key*
<https://basicmedicalkey.com/pharmacokinetics-6/> (2016).
47. Bhalani, D. V., Nutan, B., Kumar, A. & Singh Chandel, A. K. Bioavailability Enhancement Techniques for Poorly Aqueous Soluble Drugs and Therapeutics. *Biomedicines* **10**, 2055 (2022).

48. Tani, H. *et al.* Pharmacokinetics and safety of resveratrol derivatives in humans after oral administration of melinjo (*Gnetum gnemon* L.) seed extract powder. *J. Agric. Food Chem.* **62**, 1999–2007 (2014).
49. Azzolini, M. *et al.* Pharmacokinetics and tissue distribution of pterostilbene in the rat. *Mol. Nutr. Food Res.* **58**, 2122–2132 (2014).
50. Nakagami, Y. *et al.* Immunomodulatory and Metabolic Changes after Gnetin-C Supplementation in Humans. *Nutrients* **11**, 1403 (2019).
51. Mohler, J. L. *et al.* Prostate cancer, version 2.2014. *J. Natl. Compr. Cancer Netw. JNCCN* **12**, 686–718 (2014).
52. PC-3 - CRL-1435 | ATCC. <https://www.atcc.org/products/crl-1435>.
53. Riss, T. L. *et al.* Cell Viability Assays. in *Assay Guidance Manual* (eds. Markossian, S. *et al.*) (Eli Lilly & Company and the National Center for Advancing Translational Sciences, 2004).
54. Nair, A. & Jacob, S. A simple practice guide for dose conversion between animals and human. *J. Basic Clin. Pharm.* **7**, 27 (2016).
55. Riche, D. M. *et al.* Analysis of safety from a human clinical trial with pterostilbene. *J. Toxicol.* **2013**, 463595 (2013).
56. Guo, L. *et al.* Ilicicolin A Exerts Antitumor Effect in Castration-Resistant Prostate Cancer Via Suppressing EZH2 Signaling Pathway. *Front. Pharmacol.* **12**, (2021).
57. Dang, Q. *et al.* Anti-androgen enzalutamide enhances prostate cancer neuroendocrine (NE) differentiation via altering the infiltrated mast cells → androgen receptor (AR) → miRNA32 signals. *Mol. Oncol.* **9**, 1241–1251 (2015).
58. Ittmann, M. Anatomy and Histology of the Human and Murine Prostate. *Cold Spring Harb. Perspect. Med.* **8**, a030346 (2018).

59. Valkenburg, K. C. & Williams, B. O. Mouse Models of Prostate Cancer. *Prostate Cancer* **2011**, 895238 (2011).
60. Bouayed, J. & Bohn, T. Exogenous antioxidants--Double-edged swords in cellular redox state: Health beneficial effects at physiologic doses versus deleterious effects at high doses. *Oxid. Med. Cell. Longev.* **3**, 228–237 (2010).
61. Narisawa, T. *et al.* Prevention of N-methylnitrosourea-induced colon carcinogenesis in rats by oxygenated carotenoid capsanthin and capsanthin-rich paprika juice. *Proc. Soc. Exp. Biol. Med. Soc. Exp. Biol. Med. N. Y. N* **224**, 116–122 (2000).
62. Peiffer, D. S. *et al.* Chemoprevention of esophageal cancer with black raspberries, their component anthocyanins, and a major anthocyanin metabolite, protocatechuic acid. *Cancer Prev. Res. Phila. Pa* **7**, 574–584 (2014).
63. Shen, Y. T. *et al.* Potential Limitations of Bioluminescent Xenograft Mouse Models: A Systematic Review. *J. Pharm. Pharm. Sci. Publ. Can. Soc. Pharm. Sci. Soc. Can. Sci. Pharm.* **23**, 177–199 (2020).
64. Pecyna, P., Wargula, J., Murias, M. & Kucinska, M. More Than Resveratrol: New Insights into Stilbene-Based Compounds. *Biomolecules* **10**, 1111 (2020).
65. Mutlu, E. *et al.* Comparative toxicokinetics of Trans-resveratrol and its major metabolites in Harlan Sprague Dawley rats and B6C3F1/N mice following oral and intravenous administration. *Toxicol. Appl. Pharmacol.* **394**, 114962 (2020).
66. Puca, L., Vlachostergios, P. J. & Beltran, H. Neuroendocrine Differentiation in Prostate Cancer: Emerging Biology, Models, and Therapies. *Cold Spring Harb. Perspect. Med.* **9**, a030593 (2019).

67. Yuan, T.-C., Veeramani, S. & Lin, M.-F. Neuroendocrine-like prostate cancer cells: neuroendocrine transdifferentiation of prostate adenocarcinoma cells. *Endocr. Relat. Cancer* **14**, 531–547 (2007).

CHAPTER VIII. APPENDICES

APPENDIX A: Publications

In Preparation

Campanelli G, Al Deabel R, Paur A, Parupath P, Devarakonda L, Kumar A, and Levenson AS 2023, 'Efficacy of Gnetin C in a murine model of castrate-resistant prostate cancer'.

Published

Parupathi P[#], **Campanelli G**[#], Al Deabel R, Puaar A, Devarakonda LS, Kumar A, and Levenson AS 2022, 'Gnetin C intercepts MTA1-associated neoplastic progression in prostate cancer', *Cancers*, 14, 1638.

#The first and second authors contributed equally to this work

Hemani R, Patel I, Inamdar N, **Campanelli G**, Donovan V, Kumar A, and Levenson AS 2021, 'Dietary pterostilbene for MTA1-targeted interception in high-risk premalignant prostate cancer', *Cancer Prevention Research*, DOI: 10.1158/1940-6207.CAPR-21-0242.

Gadkari K, Kolhatkar U, Hemani R, **Campanelli G**, Cai Q, Kumar A, and Levenson AS 2020, 'Therapeutic potential of Gnetin C in prostate cancer: a pre-clinical study', *Nutrients*, 26;12(12):3631.

Kumar A, Dhar S, **Campanelli G**, Butt NA, Schallheim JM, Gomez CR, and Levenson AS 2018, 'MTA1 drives malignant progression and bone metastasis in prostate cancer', *Molecular Oncology*, 12(9):1596-1607.

APPENDIX B: Posters and Presentations

AACR Conference 2022

Gnetin C for Chemoprevention and Chemotherapy of Prostate Cancer



Gisella Campanelli¹, Rabab Al Deabel², Prashanth Parupathi¹, Ameer Adhvaryu¹, Avinash Kumar¹, and Anait S Levenson³

¹Arnold & Marie Schwartz College of Pharmacy and Health Sciences, Long Island University, Brooklyn, NY
²School of Health Sciences and Nursing, Long Island University, Brookville, NY 11548, USA
³College of Veterinary Medicine, Long Island University, Brookville, NY 11548, USA



Abstract# 5945

Introduction

- Prostate cancer (PCa) is one of the most commonly occurring cancers in American men¹.
- Despite current treatment, PCa continues to be a lethal disease.
- A need, therefore, exists for more effective treatment options.
- According to current treatment guidelines, active surveillance is all that is indicated for intermediate- and high-risk patients².
- However, targeted nutritional interception may prove to be the most appropriate chemoprevention for these patients.
- Our recent studies have demonstrated that Gnetin C, a resveratrol-dimer found abundantly in melinjo (*Gnetum gnetum*) plant, can reduce the tumor promoting genes, MTA1 and AR, and reduce prostate cancer progression in mouse models of PCa^{2, 4}.
- Gnetin C is also characterized with improved pharmacokinetics compared to other stilbenes³.

Results

Gnetin C as dietary-supplemented chemoprevention

A Control diet, Phenol-free diet, Gnetin C low-dose, Gnetin C high-dose

B PIN foci quantification, CD31 QUANTIFICATION

C Weight gain

D Diet Consumption

Gnetin C as treatment for PCa

E PC3 cell viability

Compound	IC ₅₀ (µM)	R ²
RES	39.36	0.94
PTE	33.10	0.90
GNET C	12.18	0.97

F Western blot for MTA1, AR, β-actin

G MTA1 and AR protein expression quantification

Conclusions

- Gnetin C-supplemented diet reduces progression of PIN.
- Gnetin C reduces progression of PCa.
- Gnetin C improves histopathology, reduces proliferation and angiogenesis, and reduces expression of MTA1 and AR in vivo.

Future Plans

- Collect further prostate tissues - complete WB and run qRT-PCR looking for expression of MTA1, AR, and apoptotic markers.
- Analyze selected inflammatory cytokines in serum using ELISA.

References

- Centers for Disease Control and Prevention. <<https://www.cdc.gov/cancer/prostate/>>.
- Gadkari K, et al., *Nutrients*, 2020, 12(12):E3631.
- Hemani R, et al., *Cancer Prevention Research*, 2021.
- Kumar A, et al., *Nutrients*, 2019, 11(9):2096.

Acknowledgements

- Supported: NCI/NIH #R15CA216970 to ASL.
- Gnetin C was a gift from Hosoda SHC Co., Ltd (Fukui, Japan).

Objectives

- To study the efficacy of Gnetin C as a dietary-supplemented chemopreventive agent in a transgenic mouse model for prostatic intraepithelial neoplasia (PIN) overexpressing MTA1 on a background of Pten heterozygosity.
- To study the efficacy of Gnetin C as a therapeutic agent in a transgenic mouse model for prostate cancer overexpressing MTA1 on a background of Pten loss.

Method

- Cell viability assay:** PCa cells were treated with natural and synthetic stilbenes. Viable cells were detected using MTT and quantitated by measuring absorbance.
- Western blot:** Lysates were prepared from prostate tissue. Proteins separated by 10% SDS-PAGE. Blots were developed and captured by Amersham Imager.
- H&E and IHC:** 4-µm-thick sections of mouse prostate tissue were stained for protein expression and visualized using EVOS XLCore microscope. The ImageJ 1.50i software was used to quantify three randomly selected fields.
- Experiment design (1):** Chemopreventive Gnetin C-supplemented diet
- Experiment design (2):** Therapeutic Gnetin C by daily i.p. injection

Conclusions

- Gnetin C-treated tumors display favorable histopathology, reduced proliferation, reduced expression of AR and MTA1, and reduced angiogenesis (Figs. H and I).

*p < 0.05; **p < 0.01; ***p < 0.001; ****p < 0.0001 (One-way ANOVA)

Contacts

Email: gisella.campanelli@my.liu.edu
anait.levenson@liu.edu



Gnetin C as a therapeutic agent for the treatment of Prostate Cancer

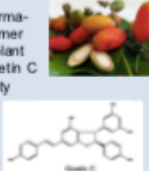
Gisella Campanelli¹, Prashanth Parupathi¹, Lakshmi Sirisha Devarakonda¹, Avinash Kumar¹, and Anait S Levenson²

¹Arnold & Marie Schwartz College of Pharmacy and Health Sciences, Long Island University, Brooklyn, NY
²College of Veterinary Medicine, Long Island University, Brookville, NY 11548, USA



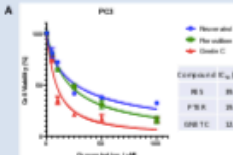
Introduction

- Prostate cancer (PCa) is a commonly diagnosed cancer among American men¹.
- Despite current treatments, PCa continues to be a leading cause of cancer-related death.
- Therefore, a need exists for more effective treatment options.
- Our lab has worked extensively with natural dietary stilbenes, such as Resveratrol and Pterostilbene.
- We have demonstrated their ability to reduce the severity and metastatic potential of PCa through their inhibition of metastasis associated protein 1 (MTA1) and androgen receptor (AR), which are key molecular players in the progression of PCa².
- Recently, the lab has been investigating the pharmacological properties of Gnetin C, a resveratrol-dimer found abundantly in melonjo (*Gnetum gnetum*) plant
- Compared to other stilbenes, we have found Gnetin C to more potently inhibit MTA1 and AR, cell viability and features of metastatic potential^{3, 4}.
- The greater efficacy of Gnetin C may be due, at least in part, to its superior bioavailability and pharmacokinetic profile compared to other stilbenes⁵.



Results

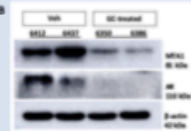
A



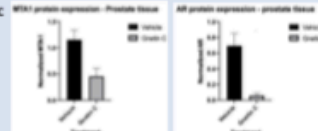
Compound	IC ₅₀ (µM)	IR
Resv	39.76	0.004
Pter	39.30	0.002
Gnetin C	12.38	0.017

- Gnetin C shows greater reduction in cell viability compared to other natural stilbenes in PC3 cells (Fig. A).
- Gnetin C reduces expression of MTA1 and AR in prostate tissue (Figs. B and C).

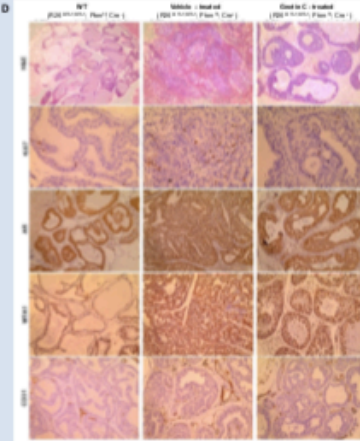
B



C

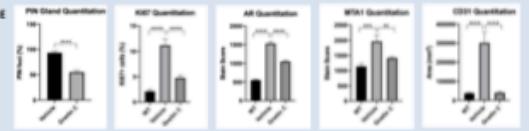


D



- Gnetin C-treated tumors display favorable histopathology, reduced proliferation, reduced expression of AR and MTA1, and reduced angiogenesis (Figs. D and E).

E



*p < 0.05; **p < 0.01; ***p < 0.001; ****p < 0.0001 (One-way ANOVA)

Discussion and Conclusion

- Gnetin C shows greater cytotoxicity against PC3 PCa cells compared to Resveratrol and Pterostilbene.
- Gnetin C improves histopathology by reducing the number of PIN foci in prostate tumor tissue.
- Gnetin C reduces proliferation and angiogenesis in prostate tumor tissue.
- Gnetin C reduces the expression of key tumor-promoting biomarkers, MTA1 and AR
- Overall, Gnetin C reduces the severity of PCa and progression of the disease.
- Its mechanism of action is believed to be largely due to its inhibitory action on MTA1 and AR signaling pathways.
- Overall, Gnetin C offers us an effective therapeutic option for PCa.
- In addition, as a naturally derived compound, Gnetin C may be associated with less toxicity when compared to other traditional cytotoxic agents.
- Fewer side effects corresponds to improved compliance, which in turn, leads to better patient outcomes.

Objectives

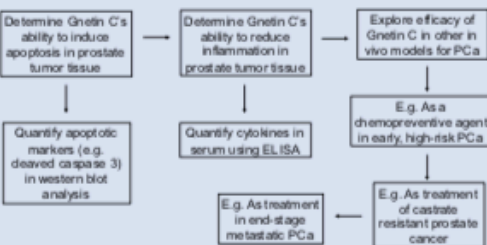
- To study the therapeutic efficacy of Gnetin C in reducing the severity of PCa in a prostate-specific transgenic mouse model overexpressing MTA1 on a background of Pten loss (R26^{MTA1}; Pten⁰; Probasin-Cre⁺).

Method

- Cell culture:** PC3 cells were grown in RPMI 1640 containing 10% FBS and antibiotics.
- Cell viability assay:** PC3 cells were seeded and treated with Resveratrol and Pterostilbene in concentrations of 5 µM, 10 µM, 25 µM, 50 µM, 100 µM, along with vehicle control. Treatment was replenished daily for three days. Metabolically viable cells were detected using MTT and analyzed quantitatively by measuring absorbance.
- Western blot:** Lysates were prepared from tissue in RIPA buffer. Samples containing 50 µg of protein were loaded on 10% SDS-PAGE and transferred onto PVDF membranes, blocked with 5% non-fat dry milk for an hour and then probed with the respective primary antibodies at 4°C overnight. The membranes were then probed with the desired secondary antibody for 1 hour and developed using the Supersignal west dura chemiluminescent substrate.
- H&E and IHC:** 4-µm-thick sections of mouse prostate tissue were stained for protein expression and visualized using EVOS XL Core microscope. The ImageJ 1.50 software was used to quantify three randomly selected fields.
- Experiment design:** Gnetin C administered by intraperitoneal injection daily for 3 months.



Future Direction



References

1. Centers for Disease Control and Prevention, 'Prostate Cancer', <<https://www.cdc.gov/cancer/prostate/>>.
2. Gadkari K, Kaihaikar U, Hemani R, Campanelli G, Cai Q, Kumar A, and Levenson AS 2020, 'Therapeutic potential of Gnetin C in prostate cancer: pre-clinical study', *Nutrients*, 12(12):E3631.
3. Hemani R, Patel I, Inamdar N, Campanelli G, Donovan V, Kumar A, and Levenson AS 2021, 'Dietary Pterostilbene for MTA1-targeted interception in high-risk premalignant prostate cancer', *Cancer Prevention Research*, DOI: 10.1158/1940-6207.CAPR-21-0242.
4. Kumar A, Dhakia K, Sikorska G, Martinez LA, and Levenson AS 2019, 'MTA1-dependent anticancer activity of Gnetin C in prostate cancer', *Nutrients* 11(9):2096.

Acknowledgements

- Supported: NCI/NIH #R15CA216970 to ASL.
- Gnetin C was a gift from Hosoda SHC Co., Ltd (Fuku, Japan).

Contacts

Email: gisella.campanelli@ny.liu.edu
anait.levenson@liu.edu

ACMAP Conference 2022

<p>LONG ISLAND UNIVERSITY</p> <h2>Chemopreventive activity of Gnetin C in murine tumor models of prostate cancer</h2> <p>Presenter: Giabella Campanelli</p> <p>Authors: G. Campanelli, P. Paragathi, Q. Cai, A. Kumar, AS Luvemont, Arnold & Marie Schwartz College of Pharmacy and Health Sciences, Long Island University, Brooklyn, NY 11203, USA; College of Veterinary Medicine, Long Island University, Brookville, NY 11548, USA.</p> <p>ACMAP Hybrid Conference, June 28 - July 2, 2022</p>	<h3>Introduction</h3> <p>Epidemiology</p> <ul style="list-style-type: none"> Prostate cancer (PCa) is the most common cancer in men Risk factors: age, race, family history, high-fat diet, obesity <p>Progression of Prostate Cancer</p> <p>Current Management</p> <ul style="list-style-type: none"> Observation → Surgery → ADT → Androgen ablation → Chemotherapy Despite current treatment, PCa remains a lethal disease Need to identify novel molecular targets 	<h3>Introduction</h3> <p>Pharmacological targets:</p> <p>Metastasis-associated protein 1 (MTA1)</p> <ul style="list-style-type: none"> Master transcription co-regulator Overexpression of MTA1 leads to PCa progression <p>Androgen Receptor (AR)</p> <ul style="list-style-type: none"> Ligand-dependent transcription factor 	<h3>Introduction</h3> <p>Pharmacological inhibition of PCa</p> <p>Dietary polyphenols:</p> <ul style="list-style-type: none"> Resveratrol and Pterostilbene Grapes and blueberries <p>Gnetin C</p> <ul style="list-style-type: none"> Resveratrol dimer Mitoxy seeds <p>Mechanism of action</p> <ul style="list-style-type: none"> MTA1 and AR inhibition Gnetin C demonstrates superiority Greater inhibition of MTA1 and AR
<h3>Gnetin C In Vitro Investigations</h3> <p>Results: Gnetin C shows low IC₅₀ values in PC1 and MDA-MB-231.</p> <p>Conclusions: Gnetin C shows greater apoptosis compared to Resveratrol and Pterostilbene.</p>	<h3>Study Aims</h3> <p>To study the efficacy of Gnetin C in various stages of PCa using ad equate PCa transgenic mouse models</p> <ol style="list-style-type: none"> Dietary supplemented chemoprevention Clinical chemoprevention by intervention in high-risk mouse models 	<h3>Dietary Chemoprevention by Gnetin C</h3> <p>Aim</p> <ul style="list-style-type: none"> Study the efficacy of oral Gnetin C as dietary supplemented intervention Mice: B26^{Cre}; Pten^{f/f}; Cre⁺ This model develops low-risk precancerous stage of PCa <p>Experiment design</p>	<h3>Gnetin C Effect on Prostate Anatomy</h3> <p>Results/Conclusions: Gnetin C diet is associated with smaller prostate compared to control.</p>
<h3>Effect of Gnetin C In Vivo</h3> <p>Results: Mice fed Gnetin C diets display favorable histopathology with lower PIN foci and reduced angiogenesis.</p> <p>Conclusions: Gnetin C diet reduces progression of PIN.</p>	<h3>Effect of Gnetin C on MTA1 and PTEN</h3> <p>Results/Conclusions: Gnetin C diet inhibits MTA1 and up regulates PTEN compared to control.</p>	<h3>Diet Consumption and Weight Gain</h3> <p>Results/Conclusions: Gnetin C diet does not have an effect on diet consumption or weight gain compared to control.</p>	<h3>Gnetin C (i.p.) Treatment of PCa</h3> <p>Aim</p> <ul style="list-style-type: none"> Study the efficacy of Gnetin C as a therapeutic agent Mice: B26^{Cre}; Pten^{f/f}; Cre⁺ This model develops high-risk, high-grade PIN <p>Experiment design</p>
<h3>Gnetin C reduces expression of MTA1 and AR</h3> <p>Results/Conclusions: Gnetin C reduces expression of MTA1 and AR in prostate tissue.</p>	<h3>Discussion</h3> <p>Study outcomes</p> <ul style="list-style-type: none"> Gnetin C shows greater cytotoxicity against PCa cells Improves histopathology by reducing proliferation, angiogenesis, and PIN foci Reduces the expression of key tumor-promoting biomarkers, MTA1 and AR <p>Conclusions</p> <ul style="list-style-type: none"> Gnetin C-supplemented diet reduces progression of PIN Gnetin C treatment reduces severity of high-risk/high-grade PIN progression to PCa <p>Overall: Gnetin C offers an effective chemopreventive and therapeutic option for PCa.</p>	<h3>Future Direction</h3> <ul style="list-style-type: none"> Determine other pharmacological benefits of Gnetin C <ul style="list-style-type: none"> Apoptosis in prostate tumor tissue Anti-inflammatory effects in prostate tumor tissue Explore efficacy of Gnetin C in other in vivo models for PCa <ul style="list-style-type: none"> As treatment of castrate resistant prostate cancer AR-V7 inhibition → Gnetin C plays role in CRPC To study the pharmacokinetics of Gnetin C <ul style="list-style-type: none"> Compare against other dietary stilbenes 	<h3>Acknowledgements</h3> <ul style="list-style-type: none"> Levens on Lab members Gnetin C was a generous gift from Hasoda SHC Co., Ltd (Fukui, Japan) Supported by NCI/NIH R15CA216970 to AS Luvemont



Targeting SREBP-dependent lipogenesis to combat metastatic prostate cancer

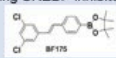
LIU Pharmacy

Gisella Campanelli¹, Nitesh K Nandwana¹, Bhaskar C Das¹, Avinash Kumar¹

¹Arnold & Marie Schwartz College of Pharmacy and Health Sciences, Long Island University, Brooklyn, NY

Introduction

- The five-year survival rate for metastatic prostate cancer (PCa) is about 30%.¹
- Despite current treatment, PCa continues to be a lethal disease.
- Sterol regulatory element binding proteins (SREBPs) are transcription factors that regulate lipid homeostasis.
- SREBP-1 predominantly regulates the expression of enzymes involved in fatty acid synthesis whereas SREBP-2 regulates the expression of enzymes involved in cholesterol synthesis.³
- SREBPs are key players in altered lipid metabolism, and their overexpression is associated with progression and metastasis of PCa.²
- BF-175 is a new stilbene-derivative, boron-containing SREBP inhibitor synthesized in-house.⁴
- The role of BF-175 in PCa is yet to be explored.



Objectives

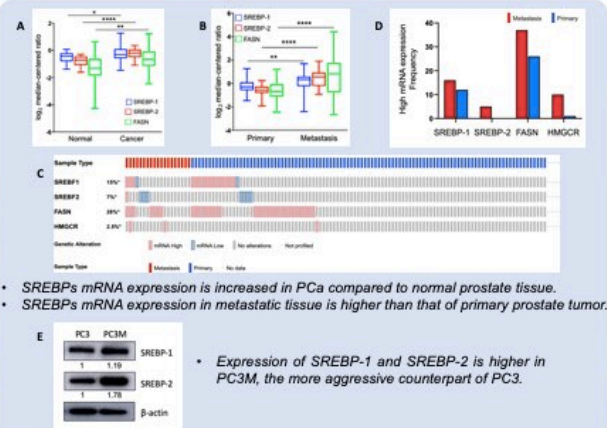
- To evaluate the expression of SREBPs in primary prostate tumors and metastatic samples.
- To determine the anticancer efficacy of BF-175 against PCa.

Method

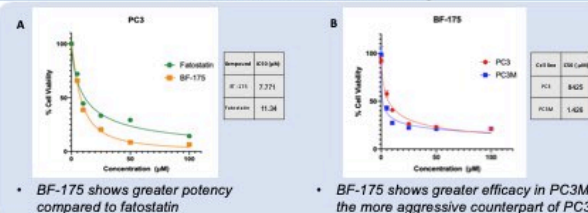
- Cell culture:** PC3 and PC3M cells were grown in RPMI 1640 containing 10% FBS and antibiotics.
- Patient datasets analysis:** Publicly available genomic data repositories, such as GEO (Gene Expression Omnibus), OncoPrint, cBioPortal, etc. were analyzed for mRNA expression of SREBP-1 and SREBP-2 in healthy prostate, primary tumor, and metastatic tissue.
- Western blot:** Lysates were prepared from cells in RIPA buffer. Samples containing 50 µg of protein were loaded on 10% SDS-PAGE and transferred onto PVDF membranes, blocked with 5% non-fat dry milk for an hour and then probed with the respective primary antibodies at 4 °C overnight. The membranes were then probed with the desired secondary antibody for 1 hour and developed using the Supersignal west dura chemiluminescent substrate.
- Cell viability assay:** PC3 and PC3M cells were seeded and treated with BF-175 in concentrations of 5 µM, 10 µM, 25 µM, 50 µM, 100 µM, along with vehicle control. Treatment was replenished daily for three days. Metabolically viable cells were detected using Alamar Blue and analyzed quantitatively by measuring fluorescence.

Results

SREBP Expression in Prostate Cancer



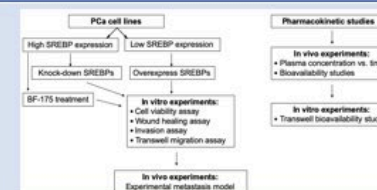
Effect of BF-175 on Cell Viability



Conclusions

- SREBPs are overexpressed in PCa compared to normal prostate tissue, and are overexpressed in metastatic samples compared to primary prostate tumors.
- SREBP protein expression is higher in PC3M, the more aggressive counterpart of PC3.
- BF-175 shows greater cytotoxic effects compared to fatostatatin.
- BF-175 shows greater cytotoxicity in the PC3M cell line, the more aggressive counterpart of PC3.

Future Plans



References

- Centers for Disease Control and Prevention 2020, 'Prostate Cancer Statistics'.
- Ettinger SL et al., 2004, 'Dysregulation of sterol response element-binding proteins and downstream effectors in prostate cancer during progression to androgen independence', *Cancer Research*, 64(6): 2212-21.
- Guo D, et al., 2014, 'Targeting SREBP-1-driven lipid metabolism to treat cancer', *Current Therapeutic Design*, 20(15): 2619-26.
- Zhao X, et al., 2014, 'Inhibition of SREBP transcriptional activity by a boron-containing compound improves lipid homeostasis in diet-induced obesity', *Diabetes*, 63: 2464-73.

Contacts

Email: gisella.campanelli@my.liu.edu
avinash.kumar@liu.edu

Discovery Day (LIU) 2021

LONG ISLAND UNIVERSITY

Evaluation of synthetic stilbene derivatives for targeted therapeutic options in prostate cancer

Gisela Campanelli, Nilesh K. Nandwana, Bhaskar Das, and Anat S. Levinson¹
¹Arnold & Marie Schwartz College of Pharmacy and Health Sciences, Long Island University, Brooklyn, NY 11201, USA; ²College of Veterinary Medicine, Long Island University, Greenvale, NY 11548, USA

LIU Pharmacy
LIUCVM

Discovery Day April 28, 2021

Introduction

Epidemiology

- Prostate cancer (PCa) is the most common cancer in men
- Second leading cause of cancer-related death
- Risk factors: age, race, obesity, diet, genetic factors

Molecular basis of PCa

- Metastasis-associated protein 1 (MTA1)
- Transcription regulator of oncogenes and tumor suppressor genes
- Overexpression of MTA1 leads to PCa progression and metastasis
- MTA1 is a suitable pharmacological target

Introduction



- Natural dietary stilbenes inhibit MTA1-mediated cell proliferation, invasion, migration, and angiogenesis in PCa, *in vitro* and *in vivo*

Introduction

Boron-containing stilbenes (BCSs)

- Newly synthesized BCSs: BT-546 and BT-547
- These are boron-containing stilbene derivatives
- Boron is included in the structure to improve binding capacity to targets

BT-546 and BT-547

- Yet to be studied in PCa
- Novel personalized treatment for advanced PCa

Study Aims

- To determine the *in vitro* anticancer efficacy of BT-546 and BT-547 against PCa
- To compare the anticancer efficacy of BT-546 and BT-547 with other stilbenes, such as Resveratrol, Pterostilbene, and Gnetin C

Effect of BT-546 and BT-547 on MTA1

A Western blot analysis of MTA1 and β-actin in PCa cells treated with Control, Resveratrol, Pterostilbene, BT-546, BT-547, and Gnetin C.

B Bar graph showing MTA1 protein expression levels normalized to β-actin. BT-546 shows a reduction in MTA1 expression comparable to Gnetin C.

BT-546 reduces MTA1 protein expression comparable to Gnetin C

BT-546 and BT-547 Effects on Cell Viability

A Dose-response curves for PCa cell viability. BT-546 and BT-547 show greater potency than Resveratrol and Pterostilbene.

B IC50 values for PCa cell viability.

Compound	IC50 (μM)
Res	21.76
PTer	12.67
BT-546	21.32
BT-547	31.76

BT-546 and BT-547 are capable of inhibiting PCa cell proliferation. BT-546 demonstrates greater potency.

BT-546 and BT-547 Effects on Cell Viability

A Dose-response curves for ZR75.1 cell viability. BT-546 and BT-547 show greater potency than Resveratrol and Pterostilbene.

B IC50 values for ZR75.1 cell viability.

Compound	IC50 (μM)
Res	35.76
PTer	19.1
BT-546	35.43
BT-547	36.46

BT-546 and BT-547 are capable of inhibiting ZR75.1 cell proliferation. BT-546 demonstrates greater potency.

Summary

- BT-546 and BT-547 demonstrate cytotoxic effects in PC3 and ZR75.1 PCa cells with BT-546 being more potent
- BT-546 and BT-547 downregulate MTA1 expression more potently than Resveratrol and Pterostilbene
- BT-546 reduces MTA1 expression in a manner comparable to Gnetin C
- BT-546 will be chosen for future experiments

Future Direction

- Further investigate the effects of BT-546 and BT-547 *in vitro*:
 - Cell viability assays, Western blot, Real time PCR, and assays for metastatic potential of cells
- Investigate the effects of BT-546 and BT-547 *in vivo*:
 - Bioluminescence assays and histological staining
 - Toxicity studies
 - Pharmacokinetic studies

Acknowledgements

- Supported: NCI/NIH #R15CA216970 to ASL
- Gnetin C was a generous gift from Hosoda SHC Co., Ltd (Fukuji, Japan)
- Dr. Cindy Yue Yin and Ms. Rabab Al Deabel for WB analysis
- Dr. Avinash Kumar

References

- Centers for Disease Control and Prevention 2020. Prostate Cancer Statistics. <https://www.cdc.gov/cancer/prostate/statistics/index.htm>.
- Dhar S, Kumar A, Zhang L, Fernando AM, Lajo JM, Levin JR, Ali A, Zhang X, and Levinson AS 2016. Dietary pterostilbene is a novel MTA1-targeted chemopreventive and therapeutic agent in prostate cancer. *Oncotarget*, 7, 59629-59.
- Levinson AS 2020. Metastasis-associated protein 1-mediated anti-tumor and anti-cancer activity of dietary stilbenes for prostate cancer chemoprevention and therapy. *Seminars in Cancer Biology*, <https://www.sciencedirect.com/science/article/abs/pii/S1044579X20300456?via=ih.org>
- Sotgiu-Lupu IA, Das BC, and Trujillo-Fernandez JG 2014. Boron-containing compounds: chemical, biological properties and expanding medical potential in prevention, diagnosis and therapy. *Expert Opinion on Therapeutic Patents*, 24(5): 485-500.

Discovery Day (LIU) 2021

LONG ISLAND UNIVERSITY

Targeting SREBP-dependent lipogenesis to combat metastatic prostate cancer

Gisella Campanelli¹, Nitesh K.Nandwana¹, Bhaskar C Das¹, Avinash Kumar¹
¹Arnold and Marie Schwartz College of Pharmacy and Health Sciences, Long Island University, Brooklyn, NY

LIU Pharmacy

Discovery Day April 29, 2021

Study Aims

- To demonstrate that an overexpression of SREBPs exists in primary prostate tumors
- To demonstrate that a higher expression of SREBPs exists in metastatic prostate tumors
- To determine the in vitro anticancer efficacy of BF-175 against PCa

BF-175 Effect on Cell Viability

A

BF-175 shows greater potency compared to fatostatin

B

BF-175 shows greater efficacy in the more aggressive PC3M cell line

Future Direction

```

    graph TD
      A[PCa cell lines] --> B[High SREBP expression]
      A --> C[Low SREBP expression]
      B --> D[Produce own SREBPs]
      C --> E[Overexpress SREBPs]
      D --> F[BF-175 treatment]
      E --> F
      F --> G[In vitro experiments: Cell viability assay, Wound healing assay, Invasion assay, Transwell assay]
      G --> H[In vivo experiments: Pharmacokinetic studies]
  
```

Introduction

Statistics

- Prostate cancer (PCa) is one of the most commonly diagnosed cancers in men
- In metastatic PCa, the five-year survival rate is about 30%

Treatment

- Despite current treatment, PCa continues to be a lethal disease
- Need to identify novel molecular players as pharmacological targets

New pharmacological target

- Altered lipid metabolism is associated with cancer progression and metastasis
- Sterol regulatory element binding proteins (SREBPs) are key molecular players in lipid metabolism and cancer progression

SREBP Expression in Prostate Cancer

SREBP's mRNA expression is increased in PCa, and is further increased in metastasis

References

- Centers for Disease Control and Prevention 2020. "Prostate Cancer Statistics". <https://www.cdc.gov/cancer/prostate/statistics/index.htm>.
- Eberle D, Hegarty B, Bossard P, Ferme P, and Foufelle F. "SREBP transcription factors master regulators of lipid homeostasis". *Biochimie*, 80(7): 633-63.
- Etlinger SL, Sabal R, Williams TG, Akbari M, Bradley DR, Greene HE, and Nelson CC 2004. "Dysregulation of steroid response element-binding proteins and downstream effectors in prostate cancer during progression to androgen independence". *Cancer Research*, 64(5): 2212-21.
- Guo D, Bei CH, Mischak P, and Chakravart A 2014. "Targeting SREB-1-driven lipid metabolism in test cancer". *Current Therapeutic Design*, 20(15): 2619-26.
- Soriano-Lucas MR, Das BC, and Trujillo-Fernandez JG 2014. "Boron-containing compounds: chemobiological properties and expanding medicinal potential in prevention, diagnosis and therapy". *Expert Opinion on Therapeutic Patents*, 24(5): 485-503.

Introduction

SREBP1 and SREBP2

- Transcription factors that regulate expression of enzymes involved in fatty acid and cholesterol synthesis
- SREBPs overexpression leads to progression and metastasis of PCa
- SREBPs could serve as a pharmacological target

SREBP inhibitors

- Newly synthesized boron-containing SREBP inhibitor: BF-175
- Its role in PCa has not been explored

SREBP Expression in Prostate Cancer

Expression of SREBP1 and SREBP2 are higher in PC3M

Summary

- SREBPs are overexpressed in PCa compared to normal prostate tissue
- SREBPs expression is higher in PC3M compared to PC3 cells
- BF-175 shows greater cytotoxic effects compared to fatostatin
- BF-175 shows greater cytotoxicity in the more aggressive PC3M cell line

THANK YOU!

MTA-1 POSITIVELY REGULATES CTSB TO PROMOTE TUMOR PROGRESSION AND BONE METASTASIS IN PROSTATE CANCER

Gisella Campanelli¹, Avinash Kumar¹, Swati Dhar^{2,3}, Nasir A. Butt^{2,4}, Christian R. Gomez^{2,3,4}, Jason M. Schallheim⁴ and Anait S. Levenson¹

¹Arnold and Marie Schwartz College of Pharmacy, Long Island University, Brooklyn, NY 11201, USA; ²Cancer Institute, University of Mississippi Medical Center, Jackson, MS 39216, USA; ³Department of Radiation Oncology, University of Mississippi Medical Center, Jackson, MS 39216, USA; ⁴Department of Pathology, University of Mississippi Medical Center, Jackson, MS 39216, USA.

Introduction

As prostate cancer progresses and becomes invasive, cells metastasize to the bone and other tissues. Through previous gene expression profiling, metastasis-associated protein 1 (MTA-1) was identified as a component of the bone metastasis signature in aggressive prostate cancer. MTA-1 is an epigenetic reader protein, which regulates the transcription of specific genes as part of multi-protein complexes [Zhi et al., 1994].

To investigate the functional relevance of MTA-1 in promoting tumor progression and metastasis, subcutaneous and intracardiac xenografts generated from PC3M aggressive cancer cells depleted for MTA-1 demonstrated reduced tumor progression and decreased metastasis to the bone, respectively, compared to xenografts generated from PC3M cells that expressed MTA-1. This was demonstrated by decreased colony-forming ability, invasiveness and migratory properties of PC3M cells depleted for MTA-1.

When the bone metastasis signature data was analyzed alongside MTA-1 ChIP-Seq data, it was revealed that Cathepsin B (CTSB) was a strong candidate responsible for MTA-1-driven invasiveness in prostate cancer. CTSB is a proteolytic enzyme, which plays an important role in the proteolysis of the extracellular matrix leading to tumor progression, invasiveness, and metastasis of prostate cancer cells.

Further investigation would be required to understand the direct relationship between MTA-1 and CTSB at the molecular level. Ongoing experiments will aim to identify the role of CTSB in MTA-1-driven bone metastasis of prostate cancer. The information learned from this study may eventually inform the development of novel, targeted anticancer therapy, or enable these proteins to be used as biomarkers for prostate cancer screening or disease staging.

Hypothesis

To establish that MTA-1 plays an active role in the metastasis of prostate cancer cells to the bone, and that MTA-1 positively regulates CTSB to promote prostate cancer progression and metastasis.

Methods

Cell culture: PC3M cells were grown in RPMI 1640 containing 10% FBS and antibiotics. To establish PC3M cells expressing luciferase (PC3M-Luc), the cells were transfected with the lentiviral-luciferase (Luc) construct and stable clones were selected using G418. We then established stable PC3M-Luc shMTA1 cells by transducing PC3M cells with the three GIPZ MTA1 lentiviral shRNAs, GIPZ GAPDH lentiviral shRNA as positive control and GIPZ Non-silencing lentiviral shRNA as negative control. The GIPZ lentiviral shRNA system (GE Healthcare Dharmacon) contains puromycin resistant gene for selection of transfected cells and TurboGFP for monitoring the selection under the fluorescence microscope. For preparation of the viral particles, we used the pCMV-DR8.91 packaging plasmid and the pMD2-G envelope plasmid (Addgene). Cells were transfected using RPMI medium (Life Technologies) which contained 4 µg/ml polybrene (Sigma-Aldrich) with lentiviral particles at multiplicity of infection (MOI) = 8. On day 2 post-transduction, selection was initiated with 200 µg/ml puromycin (Sigma-Aldrich) and GFP-positive clones were selected and propagated.

Prostate cancer xenografts: Four-week-old male mice were randomly divided into two groups of 6 mice each for both PC3M-Luc NS and PC3M-Luc shMTA1 tails. 0.5 x 10⁶ PC3M-Luc NS or PC3M-Luc shMTA1 cells in 100 µl of 50% matrigel (Corning) were inoculated subcutaneously (s.c.) on the dorsal right flank of mice. For generation of intracardiac xenografts, same number of cells as above were injected into the left ventricle of mice heart. The mice were sacrificed at day 20 and tumor, rib, maxilla and mandible bones or the tumors were harvested and placed in 10% formalin for histological analysis. Total RNA and protein were also isolated from a part of the tumor. Blood was also collected at sacrifice, and serum samples were stored at -20°C until further analysis.

H&E and IHC: Tumor samples from mice were formalin-fixed and paraffin-embedded, and 4-µm-thick sections were made. Standard protocol for staining was used to evaluate the desired protein expression.

Western Blot: Lysates were prepared from cells or homogenized prostate tissues in the RIPA buffer. Samples containing 70 µg of protein were loaded on 10% SDS-PAGE and transferred onto PVDF membranes, blocked with 5% non-fat dry milk for an hour and then probed with respective primary antibodies at 4°C overnight. The membranes were then probed with the desired secondary antibody for 1 hour and then developed using the SuperSignal West Dura chemiluminescent substrate.

Colony formation assay: 2 x 10⁴ cells were seeded in a 35 mm cell culture dish. The media was replaced with fresh media every other day during the 2-weeks observation time. After 2 weeks of incubation at 37 °C, when colonies were freely visible (>50 cells/colony), cells were fixed with formaldehyde and stained with 0.01% crystal violet solution for 30 min at room temperature and then destained with water.

Invasion assay: Invasion assay was performed using Corning Transwell Permeable Support Coated with Cultrex Basement Membrane Extract for Cell Invasion Assay as per manufacturer's instructions.

Wound healing assay: Cells were cultured to about 80% confluence in 6 well dishes, then starved in low serum media (0.1% serum in 2 ml RPMI) overnight. A line with a marker was drawn on the bottom of the dish. Using a sterile 200 µl pipet tip, three separate wounds were scratched through the cells moving perpendicular to the line drawn with the marker. The cells were then rinsed and replenished with the low serum media. The wound area was then imaged under the Olympus COAX microscope at 4x magnification above and below the marker line to help orient the measurements and the imaging was repeated at 6, 12, 24 and 48 hours.

Results

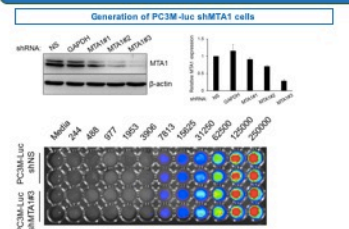


FIGURE 1 Top: Immunoblot (left) and qPCR (right) showing shRNA-mediated knockdown efficiency of MTA1 in PC3M-Luc cells. NS shRNA and GIPZ (GFP) shRNAs were used as controls. shMTA1 shRNAs demonstrated the most effective MTA1 silencing, and are thus selected for the experiments that followed. Bottom: In vivo bioluminescence luciferase imaging of PC3M-Luc NS and PC3M-Luc shMTA1 cells, showing equivalent luciferase intensity in both the cells.

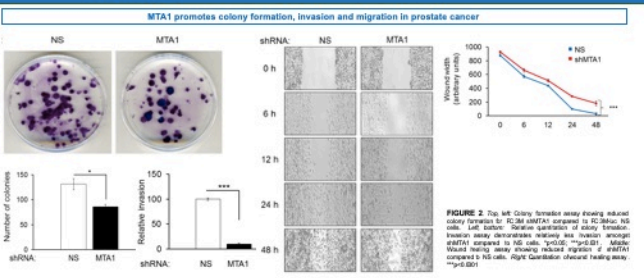


FIGURE 2 Top left: Colony formation assay showing reduced colony formation for PC3M shMTA1 compared to PC3M-Luc NS cells. Left: Bottom: Relative quantification of colony formation. Invasion assay demonstrated reduced area fraction amongst shMTA1 compared to NS cells. Middle: Wound healing assay showing reduced migration of shMTA1 compared to NS cells. Right: Quantitation of wound healing assay. *p<0.05.

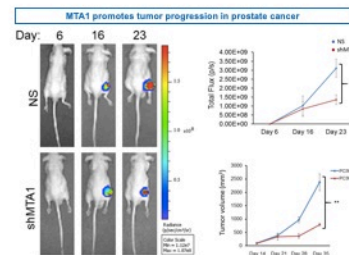


FIGURE 3 Left to right: Bioluminescence imaging of subcutaneous xenografts generated from PC3M-Luc NS and PC3M-Luc shMTA1 cells. shMTA1 tumor development was significantly slower (p<0.001) compared to the NS group. Top right: Quantitation of total luciferase activity in NS and shMTA1 tumors. Bottom right: Tumor volume by color measurement of all groups with NS and shMTA1 tumors. Results shown represent tumor growth in shMTA1 tumors compared to NS tumors. *p<0.05, **p<0.01.

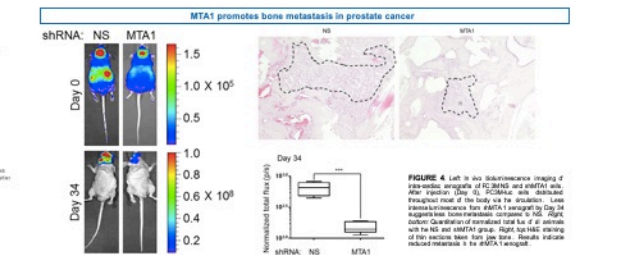


FIGURE 4 Left to right: Bioluminescence imaging of bone metastases of PC3M-Luc NS and shMTA1 cells after injection (Day 0). CTScan was conducted throughout most of the study to monitor the progression of bone metastases. Left: H&E stained histology images of bone metastases compared to NS. Right: Quantitation of normalized total luciferase activity in the NS and shMTA1 groups. Right top: H&E staining of this section from Day 34. Results indicate reduced metastasis in the shMTA1 group.

Conclusions

- MTA1 promotes progression of invasive prostate cancer and bone metastasis.
- MTA1 regulates CTSB expression at the transcriptional level.
- MTA1 promotes prostate cancer progression possibly through regulation of CTSB expression and CTSB-associated tumor promoting pathways.

Future Plans

- Establish correlation between invasiveness and reduced expression of CTSB in MTA-1-depleted PC3M cells and xenografts.
- Characterization of molecular and functional consequences of artificially upregulated CTSB in MTA1 depleted PC3M cells and xenografts.
- Development of novel dietary targeted therapies against the MTA1-CTSB axis for treatment and prevention of prostate cancer.

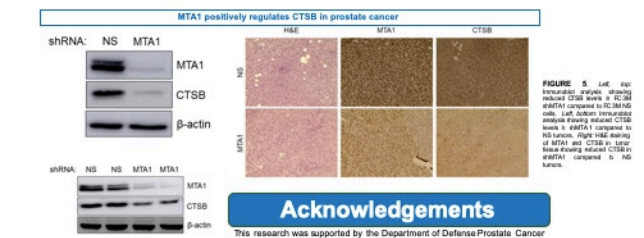


FIGURE 5 Left: Top: Immunoblot analysis showing reduced CTSB levels in PC3M shMTA1 compared to PC3M-Luc cells. Left: Bottom: Immunoblot analysis showing reduced CTSB levels in shMTA1 compared to NS tumors. Right: H&E staining of this section from Day 34. Results indicate reduced metastasis in the shMTA1 group.

Acknowledgements

This research was supported by the Department of Defense Prostate Cancer Research Program under award # W81XWH-13-1-0370 to ASL. Authors are thankful to Dr. R. Summers, Vice Chancellor of Research (UMMC) and to Dr. He (Histology core, UMMC).

This page intentionally left blank